ELAV(L1)ating Insight into Dynamic mRNA-Protein Interactions in Innate Immunity

By

Katherine Rothamel

Dissertation

Submitted to the Faculty of the

Graduate School of Vanderbilt University

in partial fulfillment of the requirements

for the degree of

DOCTOR OF PHILOSOPHY

in

Biochemistry

May 31st, 2021

Nashville, Tennessee

Approved:

Manuel Ascano, Ph.D

Kevin Schey, Ph.D

Scott Hiebert, Ph.D

Emily Hodges, Ph.D

Steve Townsend, Ph.D

"But the task of all tasks is to transform what is insignificant into greatness, what is inconspicuous into radiance; to present a speck of dust in a way that shows to be part of the whole so that one cannot see it without also instantly seeing all of the stars and heavens' deep coherence to which it intimately belongs."

– Rainer Maria Rilke

To Eric
for loving me with aloha

ACKNOWLEDGMENTS

I would like to thank my mentor, Dr. Manny Ascano, for sharing his unwavering enthusiasm, knowledge, and creativity. I appreciate his dedication to my training and for always challenging me to strive to greater depths and understandings. He has instilled in me the needed confidence and humility to continue in science – a feat not lightly achieved. I would also like to thank my thesis committee for their instrumental feedback and patience over the years.

I owe a deep sense of gratitude to all the Ascano Lab members, who have taught me to be a better scientist. Dr. Byungil Kim, the combination of your work ethic and patience is unparalleled, and I strive to become more like you every day. Dr. Sarah Arcos, my partner in science for many years, I want to thank you for all your help. You have intellectually challenged me and been a great teacher on all things computational. Caroline Wiser, your humor and honesty are something to be admired. Thank you for always making me laugh. Sam Lisy, your tenacity is infectious, and I thank you for inspiring me to be a courageous yet meticulous scientist. Robert Mann, thank you for your creativity and kindness, and Jeff Jian, thank you for all the epiphany walks and your friendship.

I would like to profusely thank the members of the Hodges' lab, Dr. Kelly Barnett, Bob Chen, Tyler Hansen, and Lindsey Guerin for being generous colleagues with their reagents, insight, and time. Hodgescano forever.

I would also like to thank Dr. John York, Jen Smith, and the Biochemistry Department for housing many creative and kind scientists. They have generated an inspiring and supportive environment to share science and friendships.

I would like to thank the Vanderbilt VANTAGE and FLOW core for their timely help and expertise. A special thanks for the financial support of the Chemistry-Biology Interface training grant 5T32GM065086-14.

I would like to thank my friends and family. Thank you to Monica Bomber, Dr. Andrea Browne, and Dr. Aviva Vincent for their endless support and friendship. Thank you to my parents for the home-cooked meals and the encouragement. Lastly, thank you to my infinitely patience husband, Eric Prazinko. He has been my constant through this wayward storm of graduate school.

TABLE OF CONTENTS

LIST OF TABLES

Table

LIST OF FIGURES

Figure

CHAPTER I: INTRODUCTION

Gene expression is a collective term used to describe the highly complex and coordinated production of proteins through the transcription and translation of messenger (m)RNAs. Prokaryotes lack a nuclear envelope, allowing for mRNAs to be simultaneously transcribed and translated. Whereas eukaryotes contain a nuclear envelope and their mRNAs undergo numerous post-transcriptional processing steps in the nucleus before exiting the nuclear pore into the cytoplasm (Moore, 2005). Once exported, eukaryotic mRNAs encounter quality control steps before being shuttled to specific subcellular locations to *only* then be either translated, stored, and/or degraded. Although energy-intensive, the decoupling of eukaryotic mRNA transcription and translation across the nuclear envelope provides i) an opportunity to proofread mRNAs for potential mistakes that encodes for mutant proteins, ii) temporal coordination of gene expression that can rapidly change the transcriptome and translatome, and iii) an intrinsic defense strategy to inhibit viruses and transposable elements from co-opting cellular machinery (Madhani, 2013). Together, these diverse sets of RNA processes, termed post-transcriptional gene regulation (PTGR), act on RNAs across a majority of eukaryotic cell types. The sum of these processes ultimately determines the protein levels and locations within a cell, thereby mediating complex biological processes from neural plasticity to immunity.

A significant piece of evidence in support of the hypothesis that PTGR determines gene expression is found when comparing the number of protein molecules to mRNA molecules from the same gene in a population of cells. The correlations between mRNAs and proteins, calculated via next-generation RNA-sequencing and quantitative mass spectrometry, are notably weak (*H.*

sapiens $r^2 = 0.13$) even when accounting for changes in protein degradation rates (Ingolia et al., 2009; McManus et al., 2015). Therefore, the rate of mRNA transcription is a poor predictor of protein levels within the cell, indicating a layer of regulation at the RNA level shaping the proteome. Another strong piece of evidence of the importance of PTGR is that there are numerous mutations in RBPs that lead to aberrant RNA metabolism giving rise to a gamut of complex human diseases (Gebauer et al., 2020; Lukong et al., 2008) (Table 1.1). As an example, Fragile X Syndrome (FXS), a heritable neurodevelopmental disease, is caused by an expansion (> 200) of CGG repeats in the 5' untranslated region (UTR) of *FMR1,* leading to the transcriptional silencing of the *FMR1* gene. *FMR1* encodes for the RBP Fragile-X Mental Retardation Protein (FMRP), and the loss of FMRP expression leads to profound intellectual disabilities, seizures, and macroorchidism in males (Vaerkerk et al. 1991).

In Chapter I of this dissertation, I will present background knowledge of the major players in PTGR, RNA-binding proteins (RBPs) and micro-RNAs (miRNAs), and how they drive mechanisms of gene regulation. I will then dive into how PTGR governs transcriptional programs during cellular signaling events, such as an innate immune response, a subject that is just only recently beginning to be investigated. The central questions of my thesis are how changes in an RBP's target RNAs and how changes in an RBP's binding distribution functionally contribute to an efficient innate immune response. RBPs are subject to signaling events and to the dynamic levels and sequences of their RNA substrates– thus, during an innate immune response, an RBP's role in gene expression might differ from its steady-state function. This is especially true when an RBP's substrate is an RNA virus, which I will also discuss and expand upon in the upcoming chapter.

Table 1.1 Conserved RNA-binding domains

Overview of the known RNA-binding domains, their RNA substrates, and examples of human RBPs containing the listed domains. Also, listed are the diseases associated with RBPs that contain each domain type.

mRNA-binding domain	RNA substrate	RBPs	Human Diseases	References
RNA recognition motif (RRM)	2-8 nt, ssRNA	(predicted to be found in > 500 proteins) ELAVL1, CELF, TIAL1, TDP-43, FUS	autoimmunity, cancer, myotonic dystrophy, amyotrophic lateral sclerosis	Auweter et al., 2006, Clery et al., 2009, Clery and Allain, 2012, Brinegar et al., 2016
K Homology (KH)	4 nt, ssRNA/DNA	MEX-3C, FMR1, QKI	Fragile-X mental retardation, schizophrenia	Zorn andKrieg., 1997. *Genes & Development*
Zinc Finger	3 nt repeats, ssRNA/DNA	TTP	autoimmunity	Font and Mackay, 2010
Pumillio (PUF)	8-10 nt ssRNA	PUM1, PUM2	autoimmunity, hypo-inflammation	Zhao et al., 2018
YT521-B Homology (YTH)	m6A modified RNA	YTHDFs	tumor growth, cancer	Xu et al. 2014, Shuiping Liu et al., 2020
Double Stranded RNA-binding domain (dsRBD)	A-form helix, 2'-OH phosphate backbone of dsRNA	ADARs, DICER1	Aicardi-Goutières Syndrome	Clery and Allain 2012, Ahmad, S. et al., 2018 *Cell*
Helicase	nucleic-acid binding region	SF1, RIG-I	inflammation, cancer, amyotrophic lateral sclerosis	Steimer and Klostermeier, 2012. *RNA Biology*
Cold Shock Domains	3-4 nts ssRNA/DNA	YB-1, CHSP1	inflammation, sepsis, liver disease	Lindquist and Mertens, 2018
La Motif	UUU-OH elements 3'UTR	LARP	rheumatic diseases	Liu Q and Dreyfuss 1997, Alspaugh and Tan 1976
Piwi-Argonaut-Zwillie (PAZ)	2 nt overhand, miRNAs	Argonauts (AGO2)	autoimmunity, cancer, anti-viral immunity	Gebauer et al., 2020, Nature *Reviews Genetics*

This dissertation's hero is the RBP Embryonic lethal vision like protein 1 (ELAVL1), and although ELAVL1 is well-studied, the majority of investigations have focused on its steady-state activities in non-immune cells. Thus, in Chapter II, I will present an in-depth examination using multiple high-throughput analyses of how ELAVL1 changes its target repertoire, binding affinity, and function on those targets during an innate immune response. The novelty of comparing an RBP's binding dynamics across cellular conditions presented in this work provides a general framework for studying other RBPs during analogous changes to a dynamic transcriptome or signaling transduction event. In Chapter III, I will discuss my work on another RBP important in innate immunity, Interferon-induced tetratricopeptide repeat protein 1 (IFIT1). IFIT1 binds the most 5' end of mRNA; therefore, its targets cannot be captured through canonical cloning methods that allow for high-throughput sequencing. I will present the development of an amendment of an RNA cloning method and how this method allows for the identification of cellular mRNA targets. Importantly, this method can be applied to other RBPs with similar binding properties as IFIT1. In Chapter IV, I will discuss conclusions and future directions of the post-transcriptional field with an emphasis on how cellular context shapes not only the RNA substrates of RBPs but also how RBPs themselves are subject to modifications mediating their function and binding properties.

Post-transcriptional gene regulation

Post-transcriptional gene regulation (PTGR) controls the mRNA levels of the cell through the mediation of RNA processing events, such as splicing, subcellular localization, nuclear export, stability, and/or translation. RBPs and miRNAs constitute major classes of PTGR effectors that

directly associate with target RNAs to facilitate regulation. Within the nucleus, RBPs can edit, modify, or splice mRNAs, dictating not only the protein-coding sequence but also determining the regulatory features of mRNAs, such as alternative 3'UTR usage. In the cytoplasm, RBPs shuttle mRNAs to certain subcellular locations determining if the message should be translated, stored, and/or degraded. Thus, RBPs mediate every stage of mRNA maturation (Figure 1.1). The human genome encodes for ~2,000 RBPs, nearly 10% of all proteins, and due to new proteomic methods of discovering RBPs, the number of RBPs continues to rise (Gerstberger et al., 2014; Hentze et al., 2018). For example, in recent years, > 20 metabolic enzymes (including GAPDH, FASN, and ENO1) have been shown to have RNA-binding activity. These discoveries have sparked the new RNA-enzyme metabolite hypothesis, which proposes that RNA-binding regulates the enzymatic function of these proteins (Castello et al., 2015).

RBPs are composed of different types of RNA-binding domains (RBDs) (average 4 per protein), where each RBD acts as a modular unit that binds RNA (Lunde et al., 2007). Individually, RBDs have a weak binding affinity (micromolar) and only bind to a few bases conferring low sequence binding specificity. Therefore, through the combination of numerous and diverse types of RBDs, an RBP can increase its binding specificity and affinity to its target (Corley et al., 2020). There are over ten well-characterized and highly conserved RBDs (Table 1.1). However, with the increase of new methods to discover RBPs on a transcriptome-wide scale (RBDmap, RNA-interactome capture), there are estimations of over a hundred different types of RBDs that have not yet been characterized (Corley et al., 2020; Perez-Perri et al., 2018). With the discovery of new domains and the use of interdomains linkers that can vary in size, the diversity and the modularity of RBPs are only just beginning to be understood.

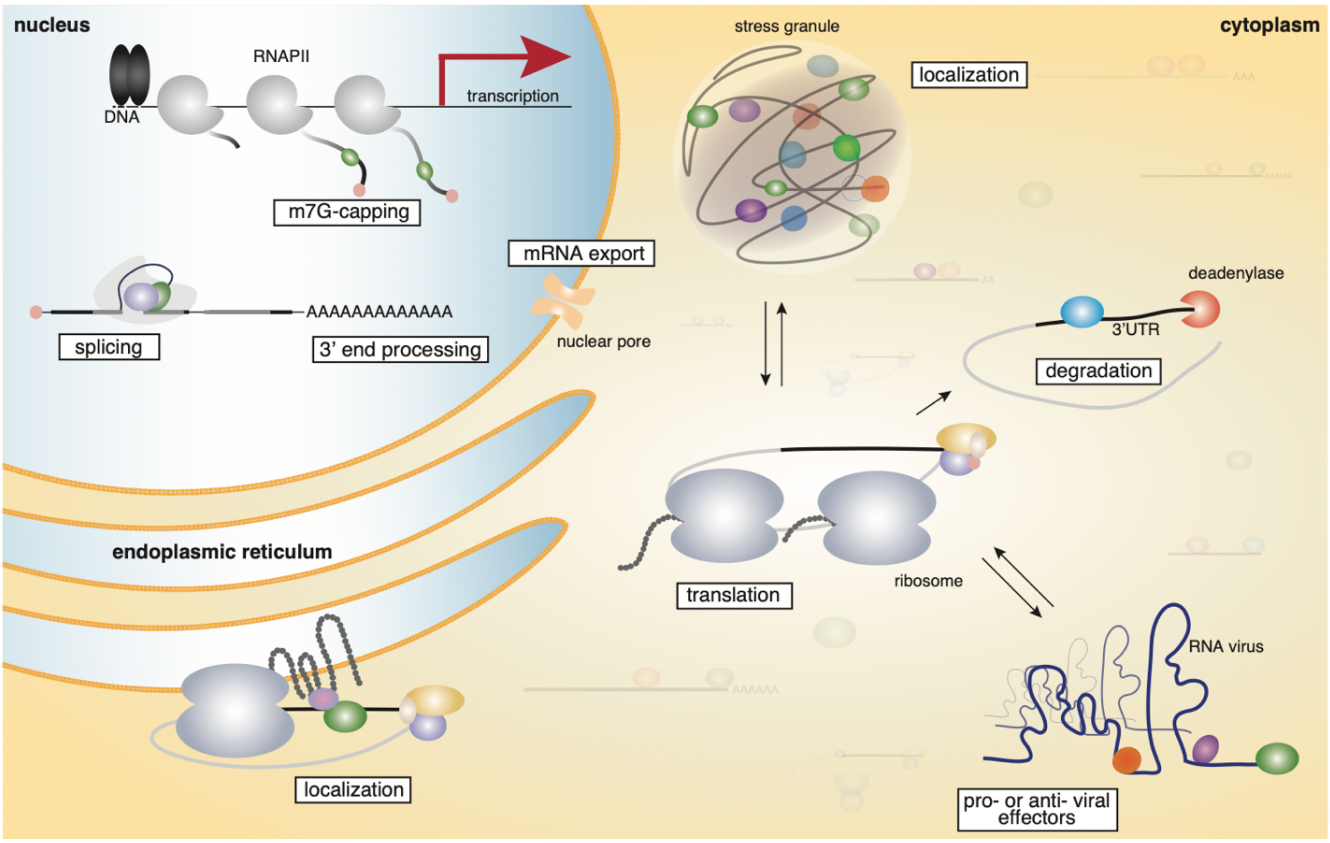

Figure 1.1 RNA-binding proteins regulate every stage of mRNA metabolism.
The nuclear (capping, splicing, 3' end processing, and mRNA export) and cytoplasmic (localization, translation, degradation, and viral effectors) stages of mRNA metabolism at depicted. RNA-binding proteins even affect the ability of viral RNA to replicate and can play either a pro- or anti-viral effect.

miRNAs are small, non-coding RNA molecules consisting of 21-24 nucleotides that associate and direct ARGONAUTS (AGO 1 - 4) to sequence-specific sites along transcripts to inhibit translation or degrade mRNAs (Bartel, 2018; Treiber et al., 2019). miRNAs are first transcribed by polymerase II (Pol II) as longer primary miRNAs (pri-mRNAs) from genes that are encoded either within protein-coding sequence or introns or as an independent non-coding transcript. pri-miRNAs (70 nts) are cleaved by the RNase complex DROSHA and its co-factor, DiGeorge Syndrome Critical Region Gene 8 (DGCR8), within the nucleus resulting in pre-microRNA (~60 nts). pre-microRNAs are then exported to the cytoplasm and bound by endonuclease Dicer and its partner protein, transactivation response element RNA-binding protein (TRBP), which further cuts the pre-miRNA creating a microRNA duplex. One of the microRNA strands is then loaded into AGO2, forming the RNA Induced Silencing Complex (RISC) that is then guided by the miRNA through its complementarity to its target RNA. The first 8 nucleotides of the 5' end of the miRNA create the "seed sequence" with can form Watson-Crick base-pairing to target mRNA. Loaded and bound RISC can then regulate mRNA through post-transcriptional repression.

miRNAs are used to titrate the magnitude of gene expression through mRNA destabilization and translation inhibition. Titration of gene expression is essential for the coordination of transcriptional programs and cellular processes (Momen-Heravi and Bala, 2018). As an example, during an innate immune response, pattern recognition receptors (PRRs), such as Toll-like receptors (TLRs), detect potential pathogens initiating a signaling cascade that turns on transcription of anti-microbial genes. Several different miRNAs, such as let-7i, miR-223, miR-146a, and miR-511, regulate this signaling cascade by targeting different levels of the pathway. Expression of let-7i downregulates the PRR, TLR4, and the miR-146 targets adaptors proteins,

TRAF6 and IRAK-1 that are responsible for the activation of the TLR-signaling pathway (Curtale et al., 2013). Expression of let-7i led to a decrease in the extracellular levels of TLR4 and facilitates the resolution of cytokine expression after an LPS challenged in epithelial cells (Y. Li and Shi, 2019). Whereas, expression of miR-511 upregulates the protein levels of TLR4, increasing the ability of a cell to detect a potential pathogen (Kleaveland et al., 2018). Thus, depending on the miRNAs expressed, certain dials of a signaling pathway can be up or down-regulated, mediating the cellular response and environment of the cell.

Interactions between RBPs and miRNAs

RBPs often compete with each other and with miRNA-RISC complexes over the same specific structure and sequence, called *cis*-elements, in a transcript. The interaction between RBPs can either be co-operative, forming a functional ribonuclear-complex (RNPs) or antagonistic, employing opposing functions on the RNA (Dassi, 2017). For example, ELAVL1, which binds adenylated uridylated-rich elements (AREs) in the 3'UTR and intron, has been shown to act co-operatively with the miRNA let-7b/C. The binding of ELAVL1 to the 3'UTR of *cMYC* increases the binding-affinity of let-7b/c and RISC-complex to a downstream binding site, resulting in the decrease of the RNA and protein levels of cMYC (H. H. Kim et al., 2009). In contrast, during cellular stress, ELAVL1 physically competes with miR-122 obscuring its binding to the 3'UTR of *CAT-1* mRNA. Thus, ELAVL1 prevents miRNA-driven destabilization and positively regulates CAT-1 levels and the amino acid metabolism in hepatocytes (Bhattacharyya et al., 2006). Ultimately, the regulatory fate of a transcript is dependent on the combinatorial effect of specific and bound RBPs and miRNAs.

High throughput and unbiased methods, such as RNAcompete (Ray et al., 2017) and RNA bind-n-Seq (Lambert et al., 2014), show that most RBPs tested have convergent sequence binding specificity. For 27 different RBPs that have distinct RBDs, the preferred 6-mer binding site overlapped with the top-ranked 6-mer site of at least one other RBP (Dominguez et al., 2018a). This observation underscores that numerous RBPs have analogous binding-motifs and that the RBPs tested have a low-complexity (one or two distinct base types) and short motif (< 5 mers) binding preference (Dominguez et al., 2018a). As an example, the RBPs TIAL1 and ELAVL1 show a preference for U-rich binding motifs found in 65% of all mRNAs and a structural motif found in 68% of mRNA (Adinolfi et al., 2019; Mukherjee et al., 2018). The overlap of the primary sequence and secondary-structure binding preference of the two RBPs is found in 45% of RNA molecules. Furthermore, a comprehensive mapping of 116 RBPs binding sites on predicted pre-miRNA found that ~68% of RBP-miRNA interactions are cell line-specific (Nussbacher and Yeo, 2018). Therefore, relying on sequence motifs and predicted RNA structure is insufficient to delineate the specific binding sites and function RNA targets of RBPs in specific cells and contexts. Though these studies are valiant in discovering the primary and secondary sequence binding specificity of RBPs, these methods often look at a single RBP and do not include competitor RBPs and miRNAs that could influence the RNA-substrate structure or the availability of a particular RNA binding site.

mRNA stability and translation

During transcription, Pol II mRNAs are given two stabilizing and translational factors, the 5’ N7-methylguanosine cap (5’cap) and the 3’ poly(A) tail (Figure 1.2). The 5’ cap and poly(A) tail exist as mRNA modifications and are not directly encoded in the genome. Through the

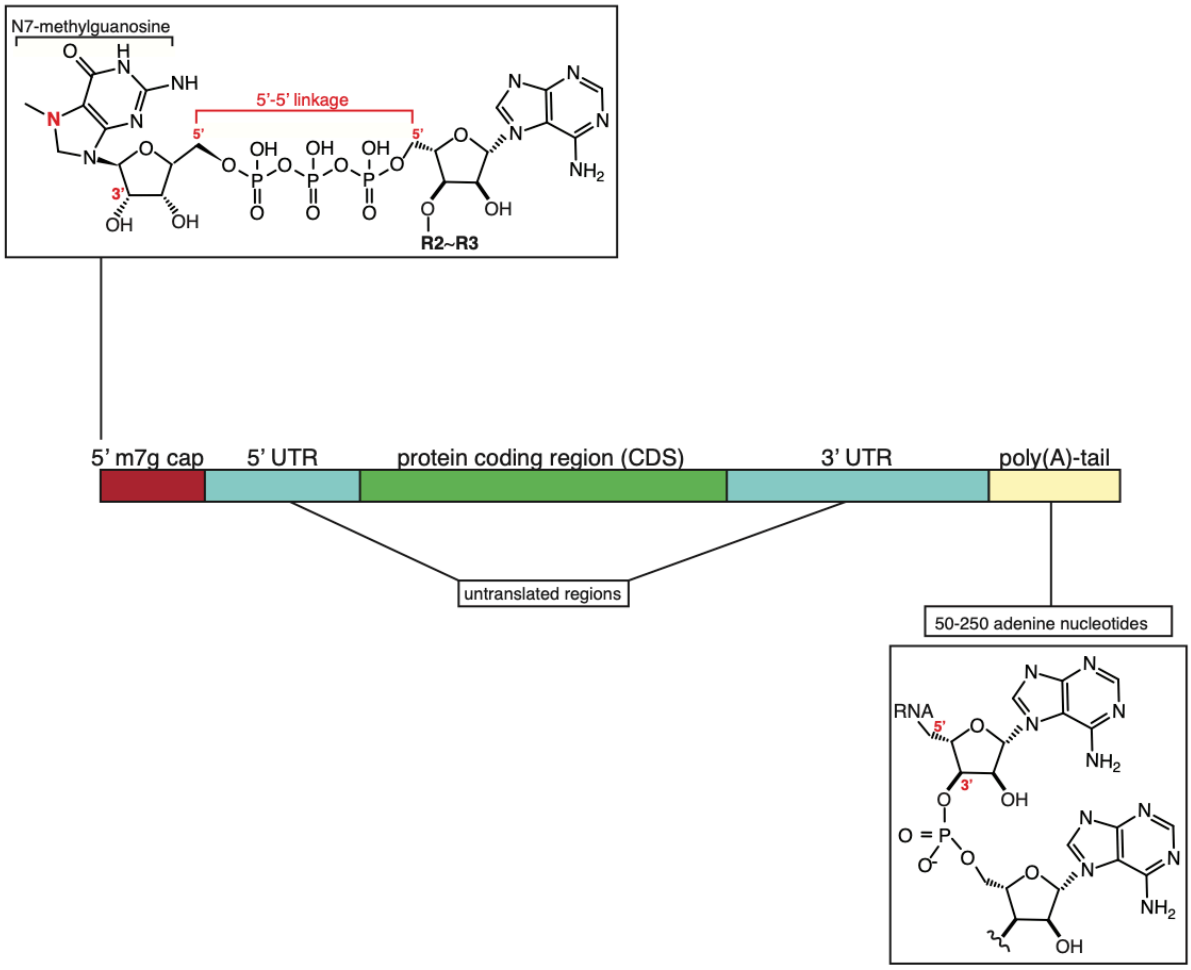

Figure 1.2 The functional units of a mature mRNA transcript.
The 5' end of the mRNA has a N7-methylguanosine cap that forms a 5'-5' phosphodiester bound to the first transcribed ribonucleotide. The 5'UTR is a highly structured region of the mRNA important in the recruitment of translation initiation factors. The 3'UTR is an active site of post-transcriptional gene regulation and the poly(A) is critical for the circularization of mRNA during active translation.

subsequent reactions of three enzymes (RNA triphosphatase, RNA guanylyltransferase, RNA guanine-7 methyltransferase), the 5' cap is added co-transcriptionally to the first transcribed ribonucleotide (Cowling, 2009). The addition of the 5' cap is critical for RNA stability and preventing RNA degradation by exoribonuclease activity through its unique 5'-5' phosphodiester linkage to the first encoded ribonucleotide (Shatkin, 1976). Meanwhile, the poly(A) tail is added at the end of transcription by the poly(A) polymerase and is necessary for efficient mRNA export and translation (Munroe et al., n.d.). The two structures act co-operatively to promote translation by recruiting the eukaryotic initiation factor 4E (EIF4E) and poly(A)-binding proteins (PABP). Interestingly, EIF4E and PABP interact with each other resulting in circularization of mRNA, which is has been shown to increase the translation rate of an mRNA (Moore, 2005).

Both RBPs and miRNAs have been reported to control gene expression by modulating RNA stability and translation rate of their target mRNA. Both effectors act in *trans* binding, *cis*-elements, often within the 3'UTR of mRNA. The majority of RBPs that target the 3'UTR of mRNAs do not have known enzymatic activity. Therefore, the function on their target RNA operates through the recruitment of large enzymatic complexes. For example, in the cytoplasm, Tristetraprolin (TTP) recognizes AU-rich stretches within the 3'UTR of RNA and recruits mRNA degradation machinery, the deadenylase complex CCR4-NOT and CAF1 (Fu and Blackshear, 2016). Deadenylation is the rate-limiting step in the mRNA decay process (Chen and Shyu, 2011). Thus, following deadenylation, mRNAs degrade through the continued shortening of the poly(A) tail, hydrolysis of the 5' cap structure, and degradation of the body of mRNA by a 5' to 3' exonuclease, such as XRN1. Other RBPs, such as AUF1, TIA1, and KSRP, contain an array of different RBDs, and yet they all bind the 3'UTR of target mRNA and recruit deadenylase machinery to promote destabilization.

RBPs are also necessary for translation regulation. La and Regulated Protein 1 (LARP1), a highly conserved RBP, has been shown to promote the translation of different subsets of mRNA. In human cells, LARP1's canonical function is to interact with PABP and the cap-binding proteins to facilitate translation. Interestingly, several studies have shown that LARP1 promotes the translation of 5' Terminal Oligo Pyrimidine (TOP) containing mRNAs, and this is mediated through mTORC1 signaling (Deragon and Bousquet-Antonelli, 2015). Specifically, mTOR-dependent phosphorylation of LARP1 promotes the binding of LARP1 to the 5'UTR of TOP-mRNAs, preventing mRNA decay and increasing TOP-mRNAs association with polysomes by promoting circularization of mRNAs (Tcherkezian et al., 2014). TOP-mRNAs encode for translation machinery and elongation factors that promote cellular growth in a context-dependent manner.

In all, these reports highlight both the ubiquitous regulation of mRNA stability and translation in eukaryotic cells and how subsets of mRNAs are regulated during specific cellular contexts like the TOP mRNAs. One RBP that is shown to mediate many RNA targets across numerous cellular processes and contexts is ELAVL1(Simone and Keene, 2013). Reconciling ELAVL1's multiple roles and zeroing in on the functional targets has been a challenge for the field. Below, I introduce ELAVL1 and what is known about its regulation in innate immunity. I also further explore the notion that during an innate immune response, RNA-substrates' levels and sequence are dynamic, and this can mediate the targeting and function of RBPs. Furthermore, there are numerous reports of ELAVL1 interacting with viral RNAs during an infection (Barnhart et al., 2013; Marceau et al., 2016; Shwetha et al., 2015). How these interactions affect viral replication and affect host mRNA metabolism is just starting to be investigated.

The RNA-binding protein ELAVL1

ELAVL1 is part of the ELAV/HuR family of RNA-binding proteins that are conserved across metazoans and ubiquitously expressed in most cell types (X. C. Fan and Steitz, 1998). ELAVL1 has three distinct and highly conserved RBDs belonging to the RRM (RNA-recognition motif) family (Figure 1.3). The first two RRM domains form a binding region that recognizes AREs within introns and 3' UTRs of mRNA. The third RRM is thought to stabilize RNA-protein interactions and form dimers with itself and other proteins via protein-protein interaction domains (Diaz-Quintana et al., 2015; Ripin et al., 2019). Between the RRM2 and RRM3 of ELAVL1 is a 63 amino acid hinge region that contains a nuclear shuttle (HNS) localization signal important for nucleocytoplasmic localization of ELAVL1 (X. C. Fan and Steitz, 1998). ELAVL1 is predominantly found in the nucleus during cellular steady-state. However, when the cell is under stress or in the presence of a pathogen, the HNS region of ELAVL1 can be post-translationally modified, promoting the translocation of ELAVL1 out of the nucleus and into the cytoplasm. The HNS region can be post-translational modified by many kinases, including but not limited to cyclin-dependent kinases (CDKs), checkpoint kinases (CHK), p38 mitogen-activated protein kinase (MAPK), and protein kinase C (PKC) (Grammatikakis et al., 2016). Thus, different post-translation modifications mediate the location of ELAVL1 within the cell and the location and expression of the mRNA targets of ELAVL1. For a comprehensive review of the post-translational modification of ELAVL1, see Grammatikakis et al., 2016.

ELAVL1 preferentially binds AREs, which are *cis*-elements composed of pentameric to nonameric adenine and uridine sequences often found in the 3'UTR of mRNAs. Nearly 4,000 transcripts that encode for proteins involved in cell growth, apoptosis, and immunity contain AREs (Bakheet et al., 2017). AREs mediate mRNA stability and translation rate through the recruitment

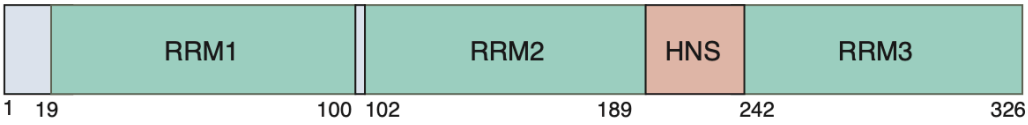

Figure 1.3 ELAVL1 has three RNA recognition domains
ELAVL1 contains 326 amino acids and has a molecular weight of 36 kDAs. The first two RRMs are important for recognition of its RNA substrates; whereas the third RRM facilitates protein-protein interactions. The hinge region contains the nuclear localization signal.

of protein machinery capable of poly-adenylation, decapping, and exonuclease activity. Furthermore, many (> 20) RBPs with different functions and RNA-binding domains, such as ELAVL1, TTP, CUGBP1, TIA1, and AUF1, target these AREs in the 3'UTR of mRNA (Carpenter et al., 2014; García-Mauriño et al., 2017). The majority of the well-studied ARE-RBPs (TTP, AUF1, KSRP) are negative regulators of cytokine expression and are important for the resolution of the inflammatory signal(Chen and Shyu, 1995). Mice lacking the ARE containing the 3'UTR of *TNF* developed inflammatory arthritis and inflammatory bowel disease due to overexpression of TNF (Katsanou et al., 2005a; Kontoyiannis et al., 1999). Therefore, the presence of the 3'UTR and the interacting RBPs are necessary to regulate the expression levels of TNF to prevent inflammatory disease progression.

Interestingly, during a type-I IFN immune response, *ELAVL1* transcript levels nor protein levels change; however, ELAVL1 is post-translationally modified, causing a change in its localization and possibly its RNA-binding preferences. This translocation and modification can affect what mRNA targets ELAVL1 binds and also determine the protein partners of ELAVL1. However, to date, no one has yet measured how the targeting of ELAVL1 changes in a whole transcriptome manner during immune activation in human cells. At steady-state in HEK293 cells, ELAVL1 binds many (4,000) mRNA targets (Lebedeva et al., 2011; Mukherjee et al., 2011) that have a diverse set of roles in cell cycle, proliferation, immune, and homeostatic functions. The 3'UTR binding function of ELAVL1 is well studied for its ability to regulate mRNA metabolism by promoting the stability of mRNA. Increased RNA stability is correlated with higher protein levels – thus, ELAVL1 is often described as a positive regulator of gene expression.

The role of ELAVL1 in innate immunity

To date, most of the reports that investigate ELAVL1's role in immunoregulation focus on a single mRNA target. Some of the known innate immune human transcripts ELAVL1 regulates are *CRP*, *COX-2, IL-8, TGFB, TNF, CCL2* (Table 1.2) (J. Fan et al., 2011; Nabors et al., 2001; Srikantan et al., 2012). C-reactive protein (*CRP*), the pro-inflammatory cytokine and inflammatory disease biomarker, was enriched in a RIP-Seq of ELAVL1 in hepatoma liver epithelial cells (H. H. Kim et al., 2009; Y. Kim et al., 2015). ELAVL1 knockdown by siRNA decreased CRP protein levels and the half-life of its mRNA. The decrease in ELAVL1 levels within the cell allowed for mir-637 to bind more readily to the 3'UTR of *CRP*, resulting in the transcripts destabilization and resulting decrease in *CRP* RNA levels (Figure 1.4). Therefore, during innate immune stimulation by IL-6, ELAVL1 binds CRP 3'UTR increasing stability and levels of CRP mRNA, leading to an increase in the inflammatory state of the cell. Furthermore, in the absence of ELAVL1, mir-637 binds the 3'UTR destabilizing the mRNA and decreasing the CRP levels of the cell.

Another well-studied immune target of ELAVL1 is the AREs within the 3' UTRs of *IFNB1*. Previous work has shown that the siRNA knockdown of ELAVL1 led to the significant reduction of IFNB1 levels (70% reduction in mRNA and 50% reduction of protein) in HeLaS3 cells compared to siRNA control, despite innate immune stimulation by polyinosinic: polycytidylic acid (poly I:C), a retinoic acid-inducible gene (RIG-I) and TLR3 ligand (Herdy et al., 2015; Takeuchi, 2015). Furthermore, investigators tested whether pharmacological inhibition of ELAVL1 affected IFNB1 during innate stimulation. MS-444 is a small molecule inhibitor that prevents the dimerization of ELAVL1, which is necessary for the function and the RNA-binding

Table 1.2 Known interactors of ELAVL1 in immunity

Overview of the known post-transcriptional interactors (RBPs or miRNAs) of ELAVL1 during an immune response. Table provides the consequences of the interaction and the cell type that the interaction between ELAVL1 and competitor occurred.

interactor	function	cell-type	mechanism	relevance	citation
~ 1,000 miRNAs	AGO2 PAR-CLIP, mapped miRNA overlapping sites in ELAVL1 KO	HEK293	75% of ELAVL1 binding sites in the 3'UTR overlap with AGO2 binding sites. Multiple models that ELAVL1 promotes or represses miRNA/AGO2 binding. Transcripts that had miRNA/ELAVL1 overlapping sites and non-overlapping sites had similar mRNA differential expression upon ELAVL1 KD.	*CXCR4, MAPK1, ITGA4, PDGF*	Lu et al., 2012 CellReports
miR-16	destabilizes mRNA	HeLA	Represses ELAVL1 3'UTR binding to *COX-2, TNFa, BCL2*	COX-2 is proinflammatory and overexpressed in my cancers	Young et al., 2012, Mol. Cancer Res
miR-4312	destabilizes *IL-8* mRNA	PDACs	the binding of ELAVL1 to IL-8 prevents the RISC from destabilizing mRNA.	*IL-8* mRNA stability increases PDAC metastasis	Li et al., 2018. Cell Death and Disease
CELF1	destabilizes *Myc* mRNA	intestinal epithelial cells	CELF sequesters *Myc* mRNA to p-bodies, ELAVL1 enhances its displacement	intestinal mucosal growth	Liu et al., 2015 MolBioCell
FXR1	decrease expression	hVSMCs	FXR1 is a binding partner of ELAVL1 in hVSMC during serum starvation and TNFa activation. siRNA KD of FXR1 lead to increase in proinflammatory gene expression (IL-1B, ICAM1, MCP-1). Addition of IL-19 decreases ELAVL1 expression in an FXR1 dependent manner. FXR1 negatively regulates the expression of ELAVL1 during IL-19 stimulation reducing inflammation in VSMC.	*IL19, TNFa*	Herman, A. B. et al. 2018, Cell Reports.
PARP1	parylation of ELAVL1 protein increases 3'UTR mediated stabilization	D226A	parylation of ELAVL1 leads to higher RNA levels of Cxcl2	*Cxcl2* expression levels	Ke et al., 2019 Nature Communications

TIA1	Stabilizes mRNA	MCF-7	ELAVL1 and TIA1 compete *PDCD4* mRNA	PDCD4 is a translation inhibitor and its expression is reduced in several cancers	Wigington et al. 2015. The Journal of Biological Chemistry
TIA1/TIAL	inhibits exon 8 exclusion leading to decrease levels of *SIRT1* mRNA	U251	differential splicing of exon 8 in *SIRT1* pre-mRNA (ELAVL1 promotes exon 8 exclusion)	SIRT1 role in stress response and inflammation. Exon 8 exclusion during ultraviolet light (stress condition)	Zhao, et al. 2014., International Journal of Molecular Sciences
TTP, ZFP36	destabilizes mRNA	BMDM	destabilizes mRNA by recruiting deadenylase and decapping complexes to 3' and 5' end of mRNA	binds ARE in 3'UTR of many LPS induced cytokines (*TNFa, IL-6, IL10. TTP. CXCL1, CSF2 IER3)*	Sedlyarov et al. 2016., Molecular Systems Biology

ability of the protein. When fibroblast and HeLa cells were treated for 8-16 hours with poly I:C in the presence of MS-444, there was a three-fold reduction of *IFNB1* mRNA levels. Additionally, conditioned cell-free media from ELAVL1 knockdown cells treated with poly I:C showed a tenfold decrease in protection against vesicular stomatitis virus (VSV) infection compared to media from cells expressing ELAVL1, indicating that released cytokine levels, including IFNB1, were lower in cells lacking ELAVL1. These reports collectively demonstrate that ELAVL1 association on the 3' UTR of *IFNB1* leads to its increased stabilization, and the genetic or pharmacologic disruption of ELAVL1 can lead to a compromised immune or inflammatory response during RIG-I and TLR3 activation. ELAVL1 was also shown to regulate IFNB1 expression levels in murine bone-marrow-derived macrophages (BMMs) by stabilizing the mRNA of the kinase, Polo-like kinase 2 (PLK2), that contributes to nuclearization of the transcription factor IRF3 during RIG-I stimulation (Sueyoshi et al., 2018). This study shows that in murine BMM and RAW264.7 cells, ELAVL1 stabilizes the mRNA of a signaling molecule that induces

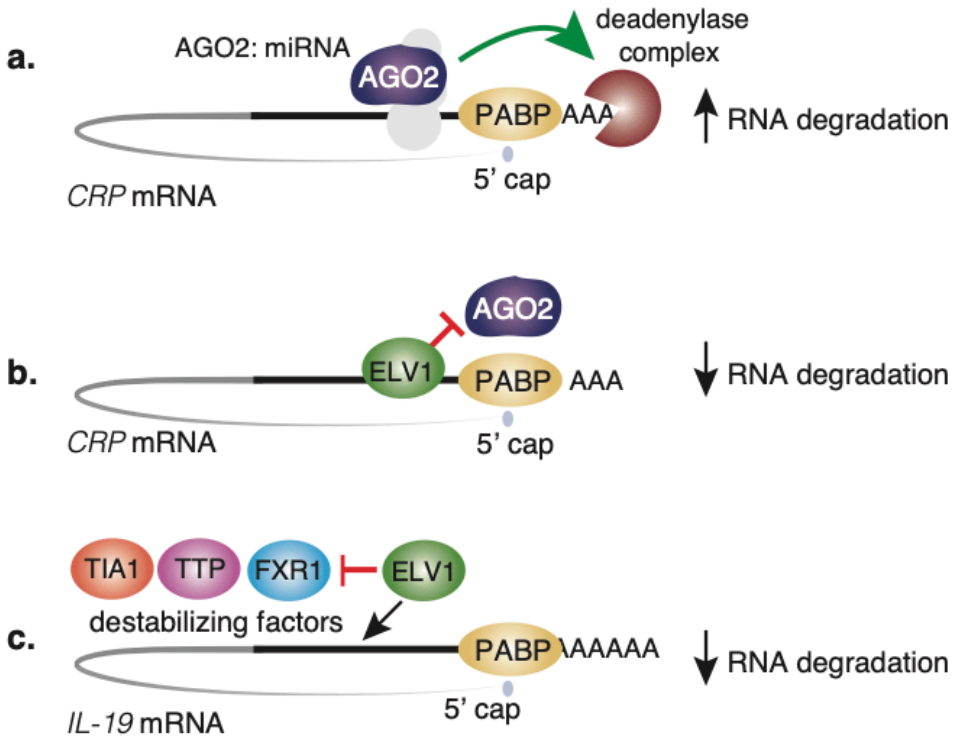

Figure 1.4 ELAVL1 binds the 3'UTR of mRNAs promoting mRNA stability
(**A**) Schematic of how miRNAs with the RISC complex can destabilizes mRNA transcripts thought the recruitment of mRNA degradation machinery. (**B**) ELAVL1 can prevent RISC complex from binding mRNA target preventing RNA degradation (**C**) ELAVL1 also competes with other RBPs that are negative regulators of RNA stability

the transcription of *Ifnb1*. Thus, loss of ELAVL1 during a RIG-I stimulation decreases the transcriptional output of *Ifnb1* through an indirect mechanism.

Not only is the stability of RNA affected in response to immune stimulation, but the translation kinetics of protein production is also affected (Piccirillo et al., 2014). Over 60% of transcripts that were upregulated by a fold-change > 2 during Influenza infection and IFNB exposure had an alternative translation-initiation start site from either upstream (u-) or downstream (d-) open reading frames (ORFs) (Machkovech et al., 2019). Alternative ORFs can act to either encode different protein isoforms or be used to regulate the translation initiation of the mRNA. For example, the mRNA of the apoptosis activator, Annexin II receptor (AXIIR), encodes two uORFs that, when bound by the RBPs ELAVL1 and hnRNPA2B1, inhibit the translation of the downstream canonical ORF. Cell types (RPMI8226 myeloma cell line) that have lower expression levels of ELAVL1 and hnRNPA2B1 express higher levels of AXIIR due to the lack of translation inhibition of *AXIIR* (Zhang et al., 2016). Thus, alternative ORFs can be bound ELAVL1, which regulates the translation efficiency of a particular mRNA. Together, these mechanisms show how RNA levels and protein production can be independent of transcription rates and regulate immune processes across different cell types.

Genetic experiments in mouse models have been disparate with regard to the role of ELAVL1 in immunity and inflammation (Christodoulou-Vafeiadou et al., 2018; Kafasla et al., 2014; Srikantan et al., 2012). In part, this speaks to the unknown direct RNA targets and roles RBPs play within the context of transcriptional activation. Knockout of intestinal ELAVL1 in mice increased epithelial degeneration due to infection, suggesting that ELAVL1 plays a protective role against infection and promotes pathogen clearance in the epithelial cells. However, mice deficient for ELAVL1 in myeloid (M-ELAVL1ko) cells have increased cytokine and exaggerated ISG

expression during LPS activation. The M-ELAVL1ko mice themselves were hypersensitive to LPS stimulation, leading to increased colitis and colitis-associated cancers. In this study, loss of ELAVL1 expression positively regulated key inflammatory transcripts (such as *Tnf*, *Tgfb*, *Il10,* and *Ccl2*), affecting myeloid cell migration and immune function (Kafasla et al., 2012). Although the prevailing model of ELAVL1 function is its ability to stabilize mRNA transcripts through its association with the 3' UTR, these observations are examples of notable exceptions. In consideration of the body of evidence that exists for ELAVL1, it appears clear that its presence is required for innate immune precision, although its exact mechanism of action is unclear. ELAVL1 knockdown in murine cells has opposing results depending on the cell type (epithelial vs. macrophage) and opposing phenotypes depending on the PRR agonist (LPS vs. RIG-I). The contrasting observations of its role as a pro-inflammatory RNA stabilizing factor versus its potential anti-inflammatory role may be explained by distinguishing between direct RNA binding targets and indirect effects. Future studies will need to be more precise in measuring the RNA-targets of RBPs during specific cellular contexts to delineate the functional role the RBP plays in gene expression.

Alternative 3'UTR usage in innate immunity

Though RBPs and miRNA are the main PTGR active constituents influencing gene expression, mRNAs are not just passive bystanders to this type of regulation. Greater than 50% of mRNAs encode for multiple polyadenylation sites (PAS) or have differential terminal exon splicing that dictates the length and sequence of 3' end of mRNAs. Thus, mRNAs, through alternative 3'UTR usage, can dictate which post-translational element will interact with it. The mRNA of lower phylogenetic species, such as worms, encode for only one 3'UTR isoform and, in

general, have shorter 3'UTRs (140 nts) compared to humans (1,200 nts), suggesting that alternative 3'UTR usage contributes to genetic and biological complexity. This hypothesis that alternative 3'UTRs contribute to "higher-level" gene regulation is supported by the evidence that miRNAs and RBPs can differentially bind and regulate mRNAs that contain the same protein-coding sequence but alternative 3'UTRs. Thus, specific transcripts undergo distinct post-transcriptional gene regulation resulting in "functional diversity to the proteome without changing the amino acid sequence" (Berkovits and Mayr, 2015). As an example, CD47, a cell surface protein important for distinguishing between self and non-self, expresses two 3'UTR isoforms. The longer 3'UTR is uniquely bound by ELAVL1. Knockdown of ELAVL1 does not affect the total CD47 protein levels; yet, the cell surface expression was significantly diminished [Mayr, 2015]. The longer 3'UTR isoforms (*lu*-CD47) functions as a scaffold for ELAVL1 mediating the cell surface expression of CD47. *lu*-CD47 bound ELAVL1 allows for the interaction of the mRNA with adaptor proteins that determines the subcellular localization of the translating protein. Furthermore, the cell surface expression of CD47 is critical for phagocytes to distinguish between pathogen and self; thus, the regulation of ELAVL1 on a transcript determined the immunophenotype of the cell. Another example of the functional importance of alternative 3'UTRs is that in response to bacterial infection, sequencing data from T-cells and macrophages showed a widespread shortening of the 3'UTRs of the newly transcribed mRNAs (Pai et al., 2016). Shorter 3'UTRs evade miRNAs that were expressed in response to cellular detection of bacteria [REF]. Thus, unique mRNA isoforms expressed during an immune response are targeted differentially by post-transcriptional effectors. Therefore, the cell transcriptional responded to bacterial infection while simultaneously coordinating alternative poly-adenylation to execute an anti-pathogen response.

ELAVL1-viral RNA interactions

Another active RNA constituent that can greatly influence PTGR effectors is viral (v)RNA. Over the past few years, due to an interest in investigating host factors that contribute to viral replication, there has been an increase in the number of reports of ELAVL1 directly or indirectly interacting and affecting vRNA replication (Table 1.3). One of the major genera of viruses that has many reports of ELAVL1 expression and interaction affect viral replication is Alphaviruses. Alphaviruses are part of the *Togaviridae* family and are enveloped, positive-sense, single-stranded RNA genome viruses (Fros and Pijlman, 2016). There are nearly 30 types of alphaviruses that can infect vertebrates, and transmission between species mainly occurs through mosquitoes. The RNA genome typically ranges between 11 and 12 kilobases and has both a 5' and 3' UTR. The genome has a 5' cap, contains a 3' poly(A) tail, and contains two ORFs encoding four non-structural proteins (nsP1-nsP4) and three structural proteins (C, E2, and E1) that are necessary for the nucleocapsid and envelope of the virion. Alphaviruses enter into host cells via endocytosis through an unknown cell surface receptor. The acidity of the endosome allows for the vRNA to be released into the cytosol, which is then directly translated into the polypeptide P1234. The polypeptide is then cleaved by nsP2, forming the subunits of the viral polymerase, which then transcribed negative-sense RNA and can transcribe template for genomic and subgenomic RNA (Figure 1.5) (J. H. STRAUSS and E. G. STRAUSS, n.d.).

Many alphaviruses, such as Sindbis (SINV), Chikungunya (CHKV), and Western Equine Encephalitis (WEE), induce a significant delocalization of ELAVL1 out of the nucleus into the cytoplasm 12-24 hours post-infection (Barnhart et al., 2013; Marceau et al., 2016). This translocation of ELAVL1 into the cytoplasm, either through retainment or recruitment, seems to

Table 1.3 ELAVL1 and RNA virus interactions

Overview of the viruses that are affected by expression of ELAVL1. Table provides whether the interaction between ELAVL1 and the virus is pro- or anti-viral and the mechanism if it is known

Family	Species	pro- or anti-viral	known interaction site	mechanisms	source
Adenoviridae	Adenovirus WT300	pro-viral	unknown	stabilizes ARE in vRNA. Increased half-life. Loss of ELAVL1 decreased viral titer	Higashino F et al., 2018
Flaviviridae	Hepatitis C (HCV)	pro-viral	3'UTR (in vitro)	Displaces vRNA destabilizing factors and promotes RNA circularization and polysome formation	Shweth and Das., 2015
Retroviridae	HIV-1	anti-viral	unknown	represses HIV-1 translation initiation. OE inhibit post-integration steps of HIV-1	Lopez-Lastra et al., 2009
Togaviridae Alpha	RiverRoss	unknown	3'UTR	Interacts with 3'UTR	Dickson and Wilusz, 2012
Togaviridae Alpha	Sinbis (SINV)	pro-viral	3'UTR	Loss of ELAVL1 decreased vRNA half-life. Increased rate of stability in the presence of ELAVL1 (deadenylation assay, in vitro)	Dickson and Wilusz, 2012
Togaviridae Alpha	Sinbis (SINV)	anti-viral	sfRNA (subgenomic)	sfRNA sponges ELAVL1 disrupting host gene expression	Barnhart and Wilusz, 2013
Rhabdoviridae	Vesicular stomatitis virus (VSV)	anti-viral	indirect interaction	Loss of ELAVL1 decreased expression of IFNB1 (anti-viral factors). Loss of ELAVL1 increased viral titer.	Superti-Furge et al., 2015
Togaviridae Alpha	Western Equine Encephalitis	Pro-viral	3'UTR	Unknown	Dickson and Wilusz, 2012
Flaviviridae	Zika	anti-viral	indirect interaction	ELAVL1 promotes expresses of anti-viral cytokines inhibiting viral replication	Pager et al., 2019
Flaviviridae	Zika	n/a	pre-replicated vRNA (primary)	unknown	Mariano Garcia-Blanco et al., 2019

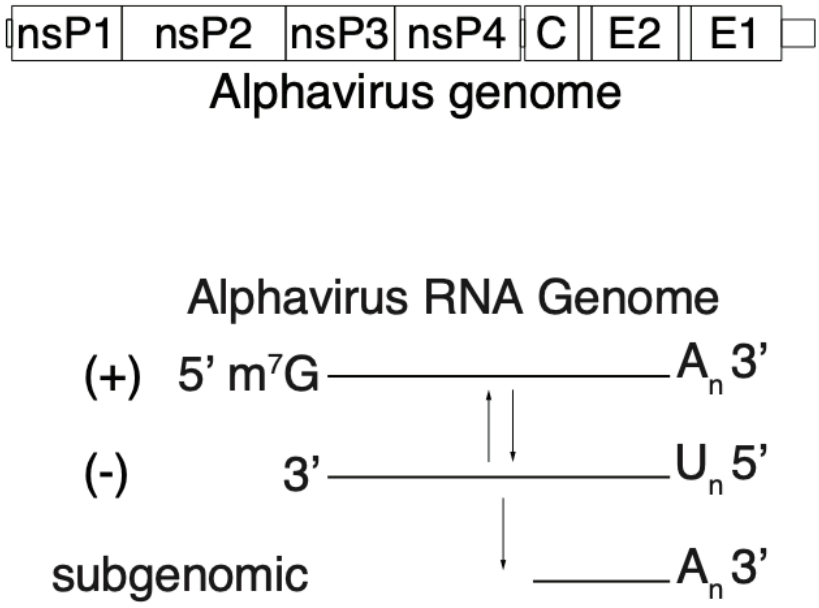

**Figure is adapted from Kim and Arcos, 2020 Molecular Cell*

Figure 1.5 Genome and replication of alphaviruses
Schematic of the (11-12 kb) alphaviruses genome and the nonstructural and structural proteins that it encodes for. Alphaviruses are capped and poly-adenylated and once in the cytoplasm are able to transcribe negative sense RNA to act as a template for genomic and subgenomic RNA.

be specific for certain alphaviruses and is not a part of a generic-RNA virus response. Using affinity purification, ELAVL1 was found to bind biotinylated 3'UTRs of CHIKV, SINV, RiverRoss, and WEE in HEK293T cells (Sokoloski et al., 2010). Knockdown of ELAVL1 caused a decrease in SINV viral titer and decrease vRNA half-life. For these observations, ELAVL1 is indicative of a pro-viral factor that positively regulates vRNA through the binding to the 3'UTR of certain alphaviruses and preventing the recruitment of mRNA decay machinery and subsequent vRNA degradation. Thus, it is reasoned that since the life-cycle of alphaviruses within a cell occurs primarily within the cytoplasm and that the translocation of ELAVL1 is thought to increase the amount of ELAVL1 that can interact with vRNA and promote its replication (Dickson et al., 2012).

Another study found that SINV transcribes non-coding viral RNA (sfRNA) can act as a "sponge" that can bind host miRNA and RBPs to circumvent the host immune response (Barnhart et al., 2013). Transfection of the 3'UTR of SINV into HEK293T cell type was sufficient to cause destabilizing of the immune relevant host-mRNAs (TUT1, RSPRY1, DDX58) (Barnhart et al., 2013). sfRNAs were shown to co-opt ELAVL1 from binding to and stabilizing these immune-relevant transcripts subverting the host's immune response. This is an example of how viral RNA-host protein interactions affect the post-transcriptional regulation of host mRNAs.

Hepatitis C virus (HCV), another positive-sense, single-stranded RNA virus part of the *Flaviviridae* family, is highly dependent on ELAVL1 binding to viral RNA. ELAVL1 binds the 3'UTR of HPC, displacing polypyrimidine tract-binding protein (PTB) and allowing for the La-mediated circularization of the viral genome. This circulation promotes rapid translation of viral proteins (Shwetha et al., 2015).

One example of the anti-viral activity of ELAVL1 is the function ELAVL1 plays in stress granules. During immune activation, translation rates are reduced, triggering non-translating

mRNPs to concentrate within the cytoplasm. High concentrations of stalled ribosomes on mRNAs induce liquid-liquid phase separation forming the dynamic, membrane-less organelles, such as stress granules (SG) and p-bodies (Protter and Parker, 2016). ELAVL1 is reported to be an important component of stress granules and is often used as a fluorescent marker of SGs (Buchan, 2014). Viral studies show that SG formation has anti-viral effects by sequestering needed translation machinery away from replicating RNA viruses and can also enhance host-mRNA interactions with translation factors (Buchan et al., 2008; Pager et al., 2013). Furthermore, stress granules have been shown to recruit and activate anti-viral PRRs, such as RIG-I, PKR, and OAS, amplifying the innate immune response. Many flaviviruses have evolved ways to inhibit SG formation through prevention of PRR detection or by inhibiting the phosphorylation eIF2alpha, which triggers SG formation (Bonenfant et al., 2019). ELAVL1 was shown to inhibit Zika replication by stabilizing key immune transcripts found in the SGs. Knockdown of ELAVL1 greatly increased Zika replication. Thus, as part of the SG, ELAVL1 is an anti-viral factor and promotes the expression of immune transcripts that negatively regulate viral replication.

Viruses have different strategies to subvert ELAVL1, either by directly using its function (stabilizing viral RNA) or misdirecting the cellular function of ELAVL1 by "soaking up" ELAVL1 with noncoding-RNAs. To better understand the effects of an RBP-viral RNA interactions, it is important to narrow down the window of time during the viral infection of when testing whether your RBP of interest is pro or anti-viral. ELAVL1 might have pro-viral effects early during the early stages of infection before ISG transcripts are made. But at later stages of infection, during a full-blown IFNB response, ELAVL1 might have an anti-viral effect stabilizing anti-viral cytokines.

One area of host-viral interactions that is not well understood is what host factors bind to the pre-replicated RNA genomes when a virus first enters the cell. These early interactions are extremely critical in determining if the virus will successfully replicate and produce progeny. From the host's perspective, these early encounters provide a small window of time where the cell can defend itself and prevent infection. It is easier for the cell to prevent a single RNA genome from replicating than hours later when the virus has replicated itself hundreds of times (Fros and Pijlman, 2016). To address these questions, the Ascano lab (we) developed a method called Viral Cross-Linking And Solid-phase Purification (VIR-CLASP) to probe these early virus and host interactions and capture host RBPs that directly bind to the viral genome (B. Kim et al., 2020a).

VIR-CLASP discovers host RBPs and pre-replicated RNA virus interactions

VIR-CLASP uses the uridine analog 4-thiourdine (4SU) to label RNA viruses which are then used to infect unlabeled host cells. Once the 4SU-labeled viruses enter the host, the cells are exposed to 365nm light, causing the covalent cross-linking of host RBPs to the incoming viral RNA genomes. RBPs will only crosslink to RNAs containing 4SU– so the only proteins that will be covalently bound are to the incoming labeled viral genome. Once RBPs are cross-linked to the viruses, the host cells undergo protein-denaturing lysis and sequence-independent RNA solid-phase purification. Proteins bound to the virus can then be identified using mass spectrometry or immunoblotting (B. Kim et al., 2020b). This method is amendable to most RNA viruses and can theoretically be used in most host cell lines.

Using VIR-CLASP, our lab discovered that ELAVL1, along with many other proteins, directly associates with the primary ssRNA genome of the emerging infectious pathogen, Chikungunya virus (CHIKV) (Figure 1.6). We then examined whether ELAVL1 could regulate

viral replication. Knockdown of ELAVL1 in U20S cells decreased intracellular levels of CHIKV RNA 3 hours post-infection (MOI= 10) (Figure 1.7). Furthermore, the knockdown of ELAVL1 affected luciferase activity (CHIKV-nLuc), indicating that ELAVL1 expression affects translation of CHIKV RNA (Figure 1.7). This line of investigation suggests that ELAVL1 regulates CHIKV replication. However, more experiments are needed to narrow if the decrease in RNA levels and translation rates are due to direct interactions of ELAVL1 to the vRNA or if knockdown is impacting the host and indirectly affecting CHIKV replication. Altogether, it is clear that ELAVL1 is important for the regulation of RNA viruses. However, a more in-depth investigation is needed to understand the mechanisms of how the binding of ELAVL1 to vRNA is affecting replication.

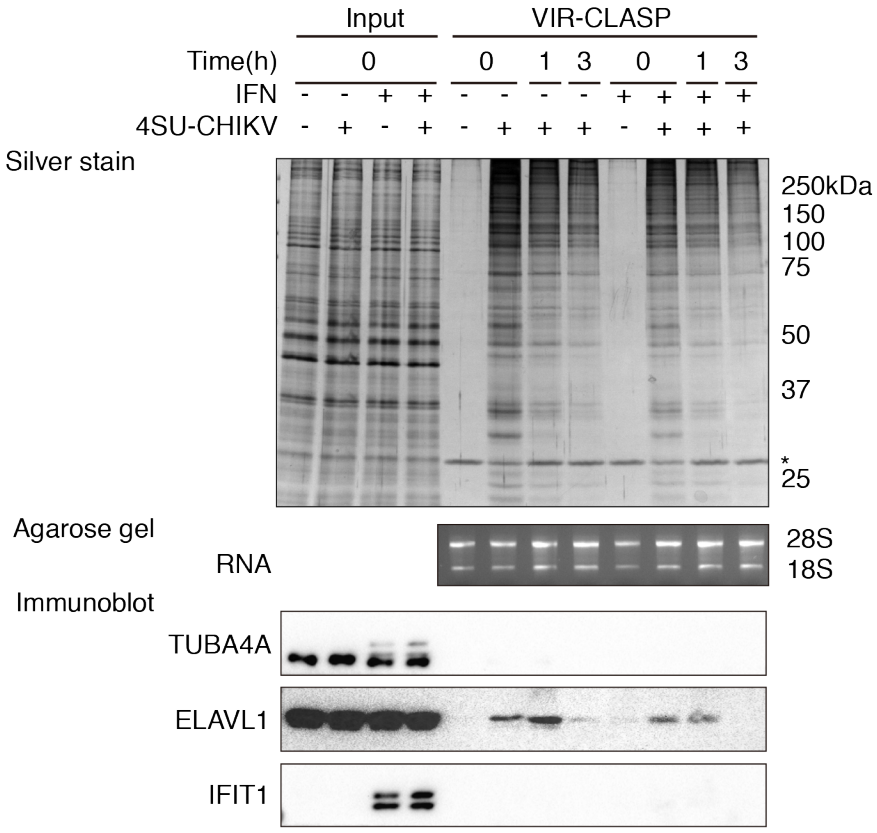

**Figure is adapted from Kim and Arcos., 2020 MolCell*

Figure 1.6 VIR-CLASP captures host protein and pre-replicated virus interactions

SDS-page and silver stain of 4SU labeled CHKV from cell culture in the presence or absence of 4SU or IFN. Immunoblot shows that ELAVL1 binds to the pre-replicated CHKV genome within 15 minutes of infection. ELAVL1 also binds in the presence of IFNB1. IFIT1 is another RNA binding protein that does now bind the CHKV genome.

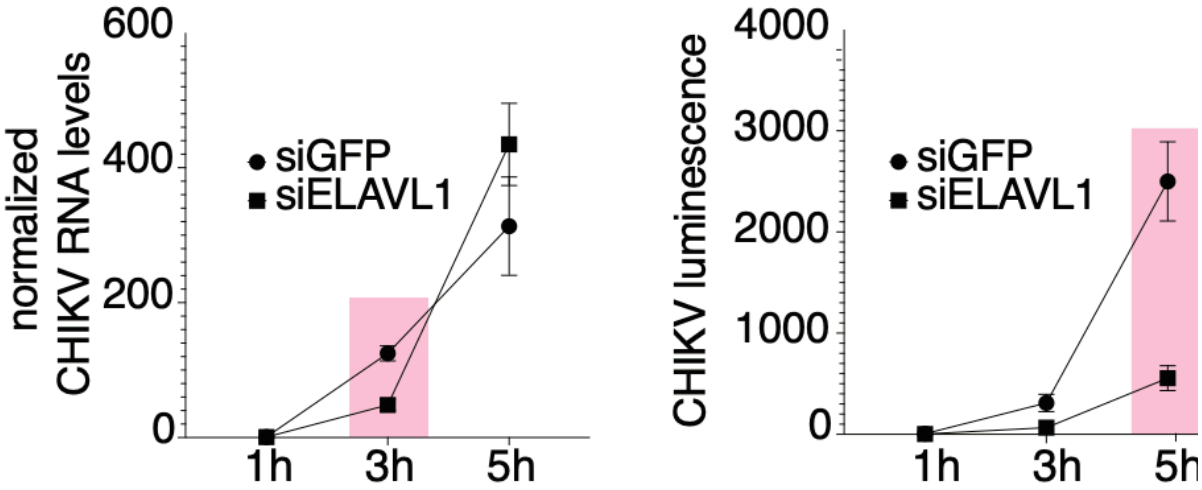

Figure 1.7 Knockdown of ELAVL1 expression reduces CHIKV RNA and protein reporter

Knockdown of ELAVL1 reduces CHIKV vRNA levels 3 hours after infection, and decreased protein expression of the CHIKV-nanoluciferase reporter 3 and 5 hours after infections.

Innate Immune Stimulation

cGAS-STING pathway

The innate immune system contains numerous PRRs that can detect foreign or aberrantly located nucleic acids. The sensing of pathogenic nucleic acids leads to a signaling transduction response resulting in transcriptional upregulation of hundreds of interferon stimulatory genes (ISGs). Cyclic-GMP-AMP synthase is the major dsDNA sensor located within the cytoplasm. Upon detection of dsDNA, the enzyme forms a cyclic dinucleotide called cyclic-GMP-AMP (cGAMP), forming an asymmetric phosphodiesterase (2',5'- and a 3',5') bond between GTP and ATP (Gao et al., 2013a; 2013b) (Figure 1.8). cGAMP is the endogenous agonist of the immune adaptor protein STIMULATOR OF INTERFERON GENES (STING) (Cai et al., 2014; Ishikawa and Barber, 2008; Sun et al., 2013; Wu et al., 2013). The activation of STING ultimately elicits an INTERFERON REGULATORY FACTOR-3 (IRF3)-dependent transcriptional response, which includes the upregulation of hundreds of ISGs (Cai et al., 2014; Ishikawa and Barber, 2008; Ishikawa et al., 2009; Sato et al., 1998; Shae et al., 2019). For my experiments, I used cGAMP to activated THP-1 cells to model innate immune stimulation. Exposing cells to cGAMP allows for precise and robust activation of cells via IRF3 – a major arm of the innate immune system, without confounding crosstalk effects through the stimulation of additional immune signaling pathways by other pathogen-associated molecular pattern molecules.

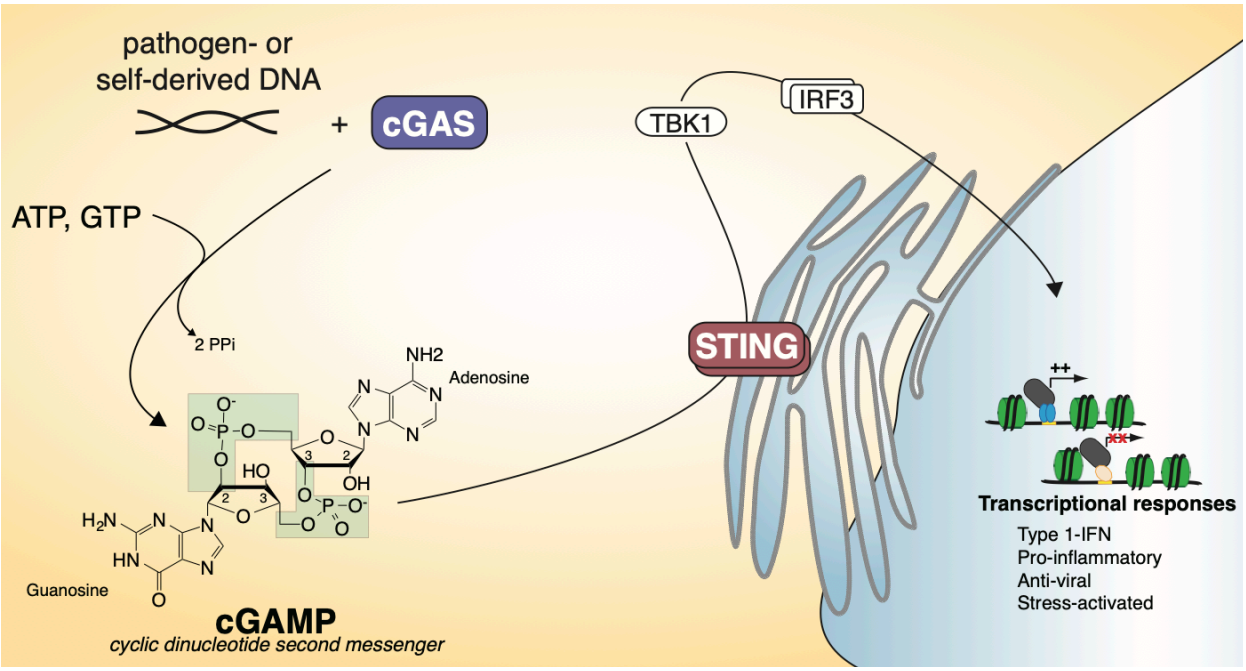

Figure 1.8 cGAS-STING pathway
When the cytosolic dsDNA sensor cGAS detects dsDNA, it forms the cyclic di-nucleotide cGAMP. cGAMP is a second messenger molecule that binds to the adaptor protein STING located in the ER membrane. STING activated TBK1 which phosphorylates the transcription factor IRF3. Once phosphorylated, IRF3 translocates into the nucleus driving gene expression of interferon stimulatory genes (ISGs).

The RBP and ISG IFIT1

One of the top upregulated genes in response to cGAMP stimulation in THP-1 cells is IFIT1 (Figure 1.9). IFIT1 is a member of the IFIT, interferon-induced protein with tetratricopeptide repeats, family and is a critical single-stranded RNA binding protein involved in restricting virus infection. The mRNA of higher eukaryotes and some viruses often contain a guanosine cap at the 5' most end of the transcript. The guanosine cap forms an unusual 5'-5' phosphodiester linkage with the first nucleotide of the mRNA preventing exonucleases from degrading the transcript. Additionally, the guanosine cap can be further modified with methyl groups, and these different modifications are thought to help a cell distinguish between self and foreign RNA. The proposed mechanism of IFIT1 is to sense different 5' terminals of RNA and bind viral RNA transcripts to prevent their translation in human cells (D. F. Young et al., 2016). How IFIT1 distinguishes viral RNA from host-encoded RNA remains a subject of intense study. Structural studies show that IFIT1 has different binding affinities for pathogenic viral RNA and cellular RNAs, potentially binding to 5'-triphosphorylated RNAs, non-methyl 7-guanosine-capped RNAs, and differentially 2'-O-methylated capped mRNAs (Fleith et al., 2018). Furthermore, the proposed antiviral activity of IFIT1 is due to its ability to outcompete host translation machinery, such as EIF3, from binding viral genomes. Given the observation that IFIT proteins can distinguish between different viral and cellular RNAs, yet these same RNAs bear sequence and chemical modifications that are known to exist in many 5' UTR, it remains unclear how IFIT proteins exert specific effects.

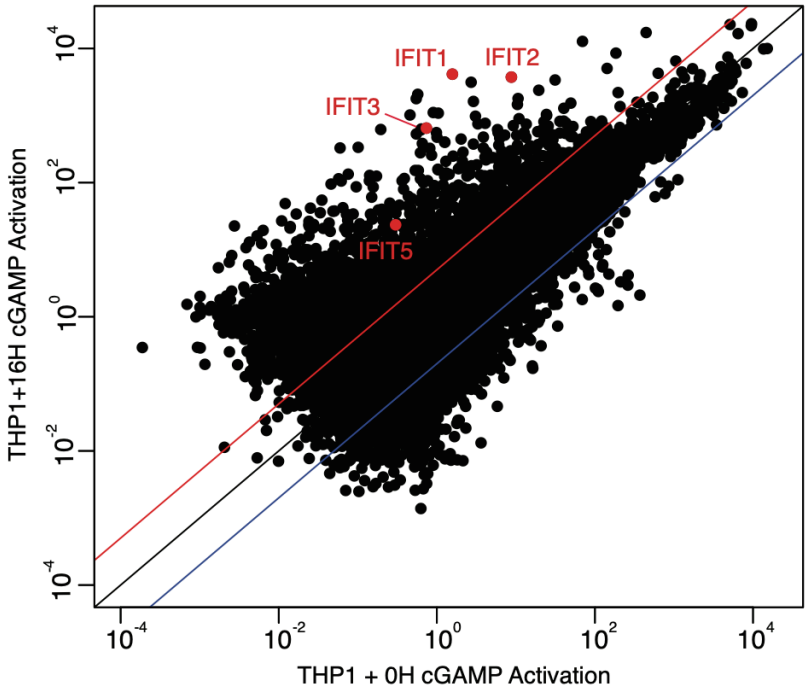

Figure 1.9 The IFITs are among the top upregulated mRNAs during cGAMP stimulation

When comparing the gene expression profiles from naïve THP-1 and 16 cGAMP activated THP-1 cells, numerous mRNA levels are differentially expressed. The family of IFIT mRNAs are greatly upregulated (> 100 foldchange).

To date, there has been a lack of research that has focused on the RNA targets of IFIT in vivo or in an unbiased fashion. All the studies that have examined the RNA binding affinities of IFIT1 have been structural and most notably do not exclude the ability of IFIT1 to bind to host mRNA. Therefore, I hypothesize that the anti-viral activity of IFIT1 extends beyond its interaction with viral RNA and that IFIT1 interacts with host RNA, and this interaction is vital to innate immune response. In support of this notion, Guo et al. found that the overexpression of IFIT1 in HT1080 cells decreased global translation rates by 40%. This suggests that the IFIT1 function of inhibiting translation is not exclusively on viral RNA. Moreover, IFIT1 expression has been observed to inhibit IFN production, suggesting that IFIT1 can also regulate the cellular innate immune response. To better understand how IFIT1 selects its targets, an essential step must be to identify those targets. In Chapter 3, I show my efforts towards identifying IFIT1 cellular targets, with the hypothesis that IFIT1 binds host RNA during an innate immune response and prevents these targets from being translated. This hypothesis will not only address the binding targets of IFIT1 but also address the mechanisms of the antiviral effects of IFIT1. This type of research will provide new insight into molecular mechanisms of host-virus interactions and their impact on RBP-mediated PTGR and viral replication.

CHAPTER II: ELAVL1 PRIMARILY COUPLES MRNA STABILITY WITH THE 3'UTRS OF INTERFERON STIMULATED GENES

Introduction

The need to rapidly control gene expression is of paramount importance to implement a robust but punctuated immune response. When a cell is exposed to an immunogenic stimulus, high levels of interferon-stimulated gene (ISG) transcripts are expressed, requiring the cell to orchestrate its translation while simultaneously preventing pathogenic (e.g., viral) RNA from using the same machinery (Liu and Qian, 2013; Piccirillo et al., 2014). ISGs encode for anti-viral, pro-inflammatory, and survival proteins, and their expression is essential in creating a heightened immunoreactive state (Hubel et al., 2019; Schneider et al., 2014). Just as crucial as the initiation of an inflammatory response are the processes that lead to its resolution; therefore, the cell must return to a basal state by limiting the activities of ISGs to prevent damage to the host tissue (Anderson, 2009; Khabar and H. A. Young, 2007; Rigby and Rehwinkel, 2015; Savan, 2014). Prolonged Interferon-Beta 1 (IFNB1) expression has been shown to increase susceptibility to many inflammatory diseases and is a hallmark of autoimmune diseases and cancer (Crow, 2015; Frangou et al., 2013; Reder, 2013). Emerging evidence indicates that RNA-binding proteins (RBPs) can affect the levels and translation rates of immune-specific transcripts to influence the intensity and duration of an innate immune response (Anderson, 2008; Hao and Baltimore, 2009; Kafasla et al., 2014; Mino and Takeuchi, 2013). RBPs facilitate RNA metabolism through the control of such processing events as splicing, subcellular localization, stability, and translation (Dreyfuss et al.,

2002; Gerstberger et al., 2014; Keene, 2007; Lunde et al., 2007). RBPs act *in trans* by binding specific structural and/or sequence *cis*-elements, often within the 3'UTR of mRNAs, a highly trafficked region that is essential to many modes of post-transcriptional gene regulation (Gebauer et al., 2012).

A major strategy by which RBPs function to regulate mRNAs during immune-activated states is through managing their stability. RBPs such as Tristetraprolin (TTP) and the cytotoxic granule-associated T-Cell-Restricted Intracellular Antigen 1 (TIA1) function as negative regulators of cytokines by leading to increased transcript decay, which is essential for the resolution of inflammation (Herman et al., 2018; Meyer et al., 2018; Tiedje et al., 2016). Conversely, Embryonic Lethal Vision-Like Protein 1 (ELAVL1) has been reported to play a role in immunoregulation by antagonizing the effects of RBPs such as TTP (Kafasla et al., 2014). ELAVL1, also known as HuR (Szabo et al., 1991), binds uridine- (U) and adenyl-uridine-rich elements (AREs) (Chen and Shyu, 1995; López de Silanes et al., 2004), a common low complexity *cis*-element found throughout the transcriptome. Yet, somewhat paradoxically, ELAVL1 binds almost exclusively to cellular mRNAs within introns and the 3'UTRs (Lebedeva et al., 2011; Mukherjee et al., 2011; Sedlyarov et al., 2016). ELAVL1 is ubiquitously expressed in most cell types and has three distinct and highly conserved RNA-binding domains belonging to the RNA-recognition motif (RRM) family. During steady-state conditions, ELAVL1 is predominantly found in the nucleus but can translocate to the cytoplasm via phosphorylation of Y200, S202, and S221, located in the hinge region of the protein between the second and third RRM. The phosphorylation of ELAVL1 at these residues is reported to occur as part of signal transduction events, including cellular response to immune agents and mitogen signal transduction events (X. C. Fan and Steitz, 1998; Grammatikakis et al., 2016).

Previous reports have shown that ELAVL1 is required to maintain the mRNA levels of AU-containing transcripts, including the immune-relevant transcripts *IFNB1, COX-2, IL-8,* and *TGFB*(J. Fan et al., 2011; C. Li et al., 2018; Louis and Bohjanen, 2016; Lourou et al., 2019). However, most of these studies do not examine if these effects on mRNA levels are due to the direct binding of ELAVL1. Additionally, many of these studies examine the regulatory impact of ELAVL1 on a singular target. Thus, how ELAVL1 prioritizes cellular targets and orchestrates its role in overall immunoregulation was not fully ascertained. Further complicating our understanding of the role of ELAVL1 in immunity and inflammation are the phenotypic outcomes reported in mouse models (Christodoulou-Vafeiadou et al., 2018; Katsanou et al., 2005b; Srikantan et al., 2012). ELAVL1 knockouts in murine cells have conflicting results depending on the cell-type (epithelial vs. myeloid) and opposing phenotypes depending on the pattern recognition receptor (PRR) agonist (LPS vs. RIG-I) (Yiakouvaki et al., 2012).

With the advent of high-throughput sophisticated RBP-crosslinking and immunoprecipitation (CLIP) methods, such as PhotoActivable Ribonucleoside-enhanced Cross-Linking and Immunoprecipitation (PAR-CLIP), the ability to precisely capture the binding sites of RBPs such as ELAVL1 in cells and study their direct effects have enabled a more molecular understanding of their function (Hafner et al., 2010). The targets and the regulatory impact of ELAVL1 on mRNA targets have been performed in HEK293 and HeLa cells (Lebedeva et al., 2011; Mukherjee et al., 2014). These landmark studies ushered in a broader appreciation for the post-transcriptional role that ELAVL1 can elicit on its targets – particularly for pre-mRNA processing. However, these earlier reports examined ELAVL1 regulation of targets under steady-state conditions in cell types that do not reflect more specific biological processes for which ELAVL1 is implicated – making it difficult to extrapolate whether the reported direct targets

contribute to the phenotypes associated with overexpression or knockout of ELAVL1 in murine models. This is especially true for an RBP that binds to commonly occurring ARE's, which obviates the effectiveness of using predictive analyses to identify its functional targets. Given its purported biological roles in development, cancers, and immunoregulation, what remains lacking is a deeper understanding of how the targeting and binding distribution of ELAVL1 to RNA changes in response to a cellular signaling event that substantively alters the transcriptome, and by virtue, substrate pool of ELAVL1.

Here, we report a multidisciplinary analysis of the targeting and functional outcomes of ELAVL1 during a nucleic acid-induced innate immune response in human THP-1 monocyte-like cells. We find that the mRNA targets of ELAVL1 in THP-1 cells only share 25% of the binding sites of previously published datasets. ELAVL1 largely transitions to binding the 3'UTRs of mRNA transcripts upon innate immune activation, and this 3'UTR shift is an absolute prerequisite for enrichment. The loss of ELAVL1 led to widespread destabilization of its enriched target transcripts. Specifically, we found that highly regulated targets had a three-fold average reduction in their stabilities, losing 30 to 80% of their original half-lives. Importantly, we found that among the most highly regulated targets were transcripts that encode for ISGs and their transcriptional regulators, suggesting that ELAVL1 contributes at multiple levels of a pro-inflammatory response. To date, this is the first report comparing how the binding properties and the targeting of an RBP change between steady-state and innate immune conditions, thus providing a general framework for investigating RBPs as they govern dynamic transcriptomes.

Results

Transcriptional landscape during an IRF3 innate immune response

To model a nucleic acid-induced innate immune transcriptional response, which would be analogous to viral infection and cellular detection of pathogenic nucleic acids, we stimulated THP-1 monocyte-like cells with cyclic GMP-AMP (cGAMP) - the endogenous agonist of the immune adaptor protein STIMULATOR OF INTERFERON GENES (STING) (Cai et al., 2014; Ishikawa and Barber, 2008; Sun et al., 2013; Wu et al., 2013). cGAMP is a second messenger molecule produced by the pattern recognition receptor cyclic GMP-AMP synthase upon the detection of cytoplasmic dsDNA in the cytoplasm (Gao et al., 2013a; 2013b); (Ablasser et al., 2013; Burdette et al., 2011). cGAMP's activation of STING ultimately elicits an INTERFERON REGULATORY FACTOR-3 (IRF3)-dependent transcriptional response, which includes the upregulation of hundreds of ISGs (Cai et al., 2014; Ishikawa and Barber, 2008; Ishikawa et al., 2009; Sato et al., 1998; Shae et al., 2019). Importantly, the activation of IRF3 integrates not only the detection of cytoplasmic dsDNA but also the upstream activities of the RIG-I family of RNA pattern recognition receptors (Honda et al., 2006). Thus, exposing THP-1 cells to cGAMP allows for precise and robust activation of cells via IRF3 – a major arm of the innate immune system, without confounding crosstalk effects through the stimulation of additional immune signaling pathways by other pathogen-associated molecular pattern molecules.

Against the transcriptomic background of an IRF3-driven innate immune response, we sought to characterize the post-transcriptional gene regulatory role of ELAVL1. As an overall experimental design, we integrated four independent high-throughput datasets (Figure 2.1A). Using RNA-Sequencing (RNA-Seq), we (i) performed gene expression analysis comparing the mRNA levels from naïve and cGAMP-stimulated THP-1 cells. We next (ii) identified the direct

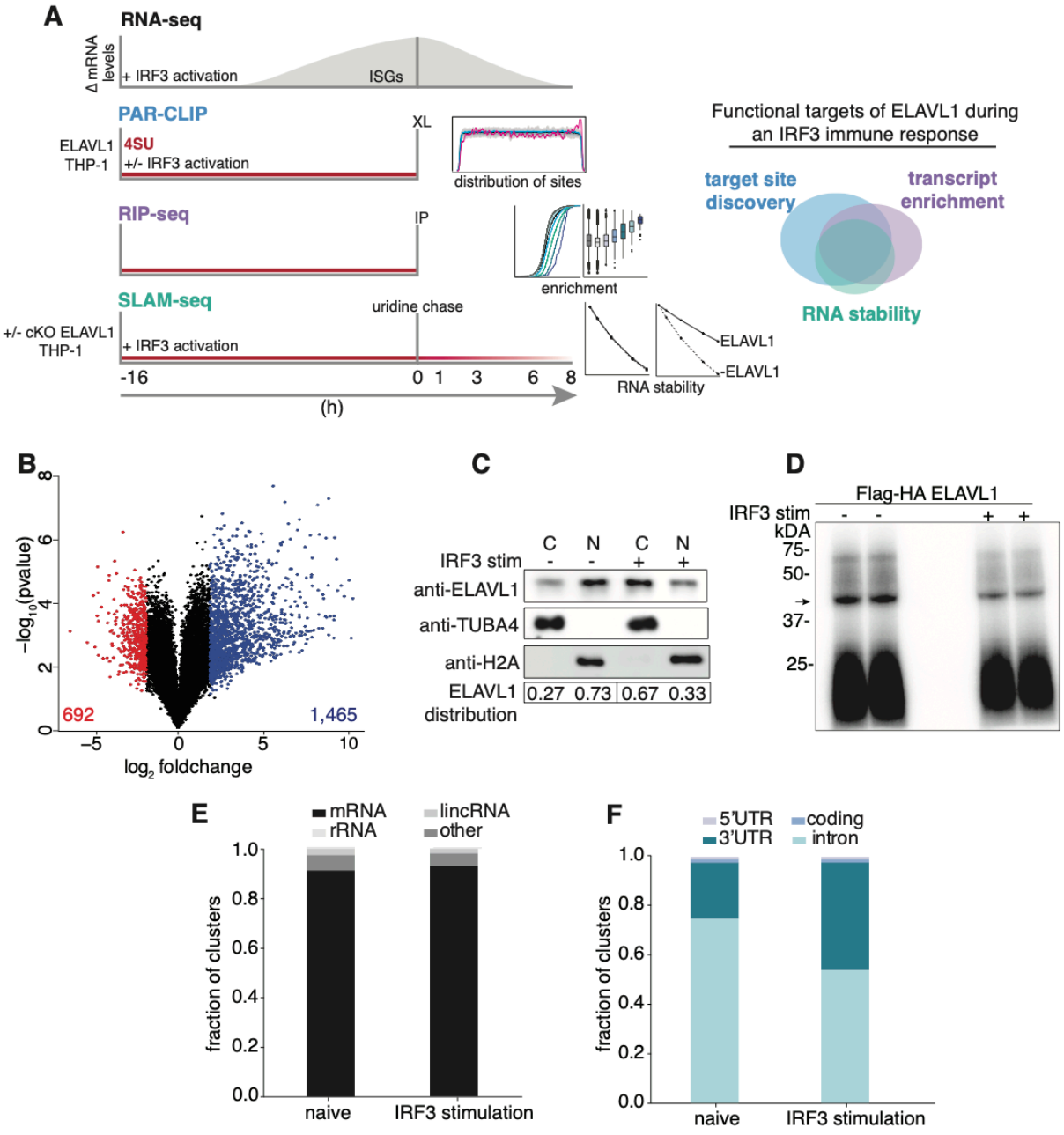

Figure 2.1 RNA-Seq and PAR-CLIP capture the context-dependent RNA substrates of ELAVL1

(**A**) Schematic of the overall experimental design used to define how ELAVL1 regulates its mRNA substrates during an innate immune response. In naïve and stimulated THP-1 cells, mRNA levels of potential ELAVL1 substrates were measured using RNA-Seq. Then condition-specific ELAVL1 binding site data were mapped at nucleotide resolution to RNA loci using PAR-CLIP. RIP-Seq was used to quantitatively measure the interaction ELAVL1 has to its RNA targets.

Lastly, ELAVL1 target stability was measured using SLAM-seq. The Venn diagram (right panel) illustrates how high throughput datasets will be used to assess the functional targets of ELAVL1. **(B**) Volcano plot comparing the differential mRNA levels between naïve and stimulated THP-1 cells. The red and blue represent the down- and upregulated transcripts in response to cGAMP stimulation. (**C**) Immunoblot showing the cellular distribution of ELAVL1 (nuclear or cytoplasmic) during a naïve and stimulated cellular state. Tubulin (TUBA4) and histone 2A (H2A) are shown as localization controls. The quantitation of the ELAVL1 bands is showing the percentage of total ELAVL1 in each cellular compartment. (**D**) Phosphorimage of ^{32}P-RNA bound to ELAVL1 in the naïve and stimulated THP-1 cells. 4SU crosslinked ELAVL1 was immunoprecipitated then separated by SDS-PAGE; arrow indicates ELAVL1 covalently-bound to radiolabeled RNAs. (**E**) Distribution of ELAVL1-binding sites across indicated RNA categories. (**F**) Distribution of binding sites across different mRNA transcript features for naïve and stimulated PAR-CLIP samples.

RNA targets of ELAVL1 in both cellular conditions using PAR-CLIP (Hafner et al., 2010). Using RNA Immunoprecipitation (RIP)-Sequencing, we (iii) quantified the relative enrichments of ELAVL1 targets (Keene et al., 2006; Ramanathan et al., 2019; Tenenbaum et al., 2000; Zhao et al., 2010). Finally, we (iv) assessed the regulatory impact of ELAVL1 by measuring the RNA half-lives of its target mRNAs with thiol (SH)-Linked Alkylation for Metabolic Sequencing of RNA (SLAM-Seq) upon the loss of its expression during an immune-stimulated transcriptional state (Herzog et al., 2017). Together, these datasets will enable the identification of high-confidence ELAVL1-regulated targets during an innate immune response and provide insight into how signaling events alter the mRNA targets of an RBP, like ELAVL1, during a changing substrate landscape.

To compare the mRNA levels that occur in THP-1 cells upon 16 h exposure to cGAMP, we performed gene expression profiling using RNA-Seq (Figure 2.1 B). The 16 h time point was selected based on our assessment of peak level expression of ISGs, including IFNB1, which was previously identified as a direct target of ELAVL1 (Figure 2.1.1 A) (Herdy et al., 2015; Takeuchi, 2015). We found that 2,157 (1,465 upregulated and 692 downregulated) genes were differentially regulated with two-fold or greater change (adjusted P-value $\leq .005$) upon stimulation (Figure 2.1B; Table 2.1). The changes in mRNA levels of several candidate genes were validated using RT-qPCR (Figure 2.1.1B). Pathway analysis of the top (25%) upregulated genes indicated that these mRNAs are involved in the regulation of the innate immune response, apoptosis, and hematopoiesis (not shown). Many of the upregulated genes (60%) are known ISGs, including the anti-viral effectors (*OAS, MX1*, *ISG15*), positive regulators of IFN response (*IRFs, STAT1, JAK*), and nucleic acid pattern recognition receptors (*TLR8, RIG-I, IFITs*) (Hubel et al., 2019; Rusinova et al., 2012; Schneider et al., 2014; Schoggins et al., 2011).

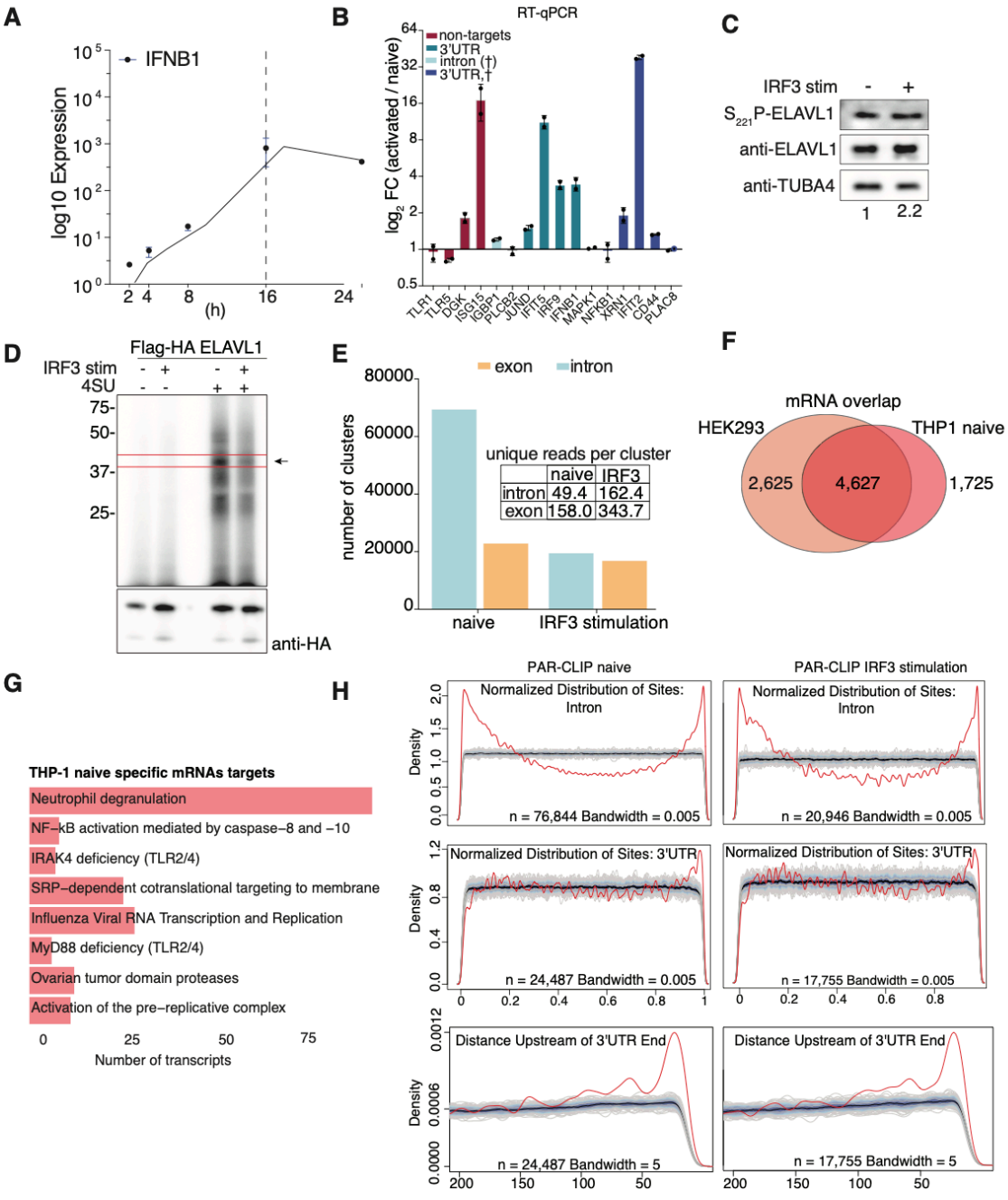

Figure 2.1.1 PAR-CLIP identifies and maps the cell-type-specific and condition-specific binding sites of ELAVL1

(**A**). THP-1 cells were stimulated with the STING agonist cGAMP (EC50), and RNA was collected at indicated time points. RT-qPCR was used to measure the mRNA levels of *IFNB1.* (**B**) Bar graph of the $\log_2$ foldchange of mRNA levels (RT-qPCR) in immune activated cells compared to naive.

(C) Immunoblot shows the whole-cell amount of phosphoserine (S221) ELAVL1 and ELAVL1 in both naive and immune activated cells. (**D**) Phosphoimage showing both the non-crosslinked (no 4SU) and crosslinked ELAVL1 to RNA samples of the IP for PAR-CLIP. Immunoblot shows that equal amounts of immunoprecipitated ELAVL1 from each condition. (**E**) Bar graph showing the number of clusters that mapped either to exons and introns across the two cellular conditions. Inset shows the average number of unique reads for each exonic- or intronic- cluster across the cellular states. (**F**) Venn diagram showing the overlap of target mRNAs from HEK293 (Mukherjee et al. 2011) and THP-1 naïve. (**G**) Reactome pathway analysis for the mRNAs that were uniquely bound in THP-1 cells compared to HEK293. (**H**) Metagene analysis showing the normalized distribution of binding sites across introns or the 3'UTR across both conditions.

Interestingly, ELAVL1 has been reported to translocate out of the nucleus into the cytoplasm by a mechanism that, at least in part, requires post-translational modification (Bidet and Garcia-Blanco, 2014; Grammatikakis et al., 2016; Lourou et al., 2019). To determine whether immune activation of THP-1 cells would lead to a change in ELAVL1 subcellular localization, we performed immunoblots on biochemically fractionated lysates. We observed an increase in the distribution of ELAVL1 in the cytoplasm upon IRF3 driven immune stimulation (Figure 2.1C). Furthermore, using an antibody that recognizes phosphorylated serine 221 on ELAVL1 (anti-phospho HuR Ser221), we observed a slight increase (two-fold) in the activated state (Figure 2.1.1 C). These data suggest that ELAVL1 in THP1 cells can be subject to signal transduction activity upon immune activation, leading to its post-translational modification and a marked change in its localization.

The binding site distribution and mRNA targets of ELAVL1 are cell-type and context-dependent

To identify the direct RNA-targets of ELAVL1 during a naïve-state (naïve) and an IRF3-driven innate immune state (stimulated), we performed PAR-CLIP in THP-1 cells conditionally expressing Flag and HA epitope-tagged ELAVL1 (Flag-HA ELAVL1) that were either stimulated with cGAMP for 16 h or mock-treated prior to crosslinking. A phosphorimage of the crosslinked and immunoprecipitated Flag-HA ELAVL1 revealed one major band migrating at approximately 40 kDa, the expected molecular mass of Flag-HA ELAVL1, in the presence and absence of an immune stimulus (Figure 2.1D and 2.1.1D). RNA from this band was recovered and processed for small RNA-Seq. Each cDNA library contained approximately 70 million reads with an average of ~10.7 and ~12.7 million *unique* reads for the naïve and stimulated samples, respectively (Table

2.2). ~91% of the reads mapped to (pre-)mRNA with an 86.4% average T-to-C fraction across all samples from naïve and stimulated conditions, altogether indicating high-quality recovery and crosslinking efficiencies of our PAR-CLIP procedure for isolating ELAVL1-bound RNA targets (Figure 2.1E). Using PARpipe, we identified 133,740 naive and 50,074 stimulated ELAVL1 distinct RNA-binding sites that have ≥ 2 unique T-to-C positions and > 20% T-to-C ratio (Corcoran et al., 2011). Although the greater than two-fold difference in the total number of RNA-binding sites between the two conditions was notable, this difference was not due to lower complexity libraries for the stimulated samples since these libraries contained more unique reads mapped per cluster (Figure 2.1.1E). 106,081 (79%) and 40,681 (81%) of the clusters identified by PAR-pipe have RNA-Seq expression data (> 5 counts per million, CPM) and RIP-Seq enrichment data (IgG normalized) for the RNA transcripts that correspond with the cluster (Table 2.3). Of those clusters, 98,689 (74%) and 38,607 (76%) of ELAVL1 binding sites map to (pre)-mRNA with high confidence in naïve and stimulated samples, respectively.

To test the hypothesis that ELAVL1 has a distinct binding site distribution due to cell-type, we compared the THP-1 naive binding sites to previously published PAR-CLIP data on ELAVL1 from HEK293 (Mukherjee et al., 2011). 29,820 clusters (30% of the THP-1 naïve clusters and 25% of the HEK293 clusters) overlapped by at least one nucleotide between the THP-1 and HEK293 datasets (Figure 2.1.1F). We find that ELAVL1 in naïve THP-1 cells uniquely binds to 1,725 mRNAs even though 1,007 (58%) of these transcripts are expressed in HEK293 based on RNA-Seq data (Mukherjee et al., 2011). Reactome pathway analysis revealed that the mRNAs bound by ELAVL1 in THP-1 cells are associated with NF-kB activation (R-HSA-933543), viral defense (R-HSA-168273), and toll-like receptor signaling (R-HSA-5603041) (Figure 2.1.1G).

We found that a substantial fraction of ELAVL1 binding sites (74%) in THP-1 cells were located within the introns of pre-mRNAs in the naïve state, as similarly observed in HEK293 cells (Mukherjee et al., 2011). However, upon immune stimulation, intronic binding was significantly depleted: only 52% of the clusters mapped to introns of target transcripts in the stimulated condition (Figure 2.1F; Table 2.2). Nonetheless, intron-located clusters were enriched near 5' and 3' splice sites in both conditions suggesting a consistent role for ELAVL1 in regulating splicing (Figure 2.1.1H). Nearly 96% of the exonic binding sites mapped to the 3'UTR in both naïve and immune-activated conditions. The 3'UTR-binding sites were depleted proximal to the stop codon (0 -150 nts after stop codon) and enriched toward the most distal region of the transcript near the polyadenylation site (40 nts before the poly(A) site) (Figure 2.1.1H). Interestingly, when we compared the distribution of the binding sites along the 3'UTR to previous ELAVL1 PAR-CLIPs (Lebedeva et al., 2011), we found that the enrichment of ELAVL1 sites towards the poly(A) tail is specific for our dataset. The 3'UTR binding site distribution for ELAVL1 in HeLa contains a similar depletion towards the stop-codon but does not include the distinct enrichment of binding towards the poly(A) tail. Per previous reports, the HeLa binding sites are equally distributed across the distal region of the 3'UTR (Lebedeva et al., 2011).

The most striking change observed between naïve and stimulated conditions was the increase in the percentage of exonic sites (from 26% to 48%), indicating a profound shift in the binding site distribution of ELAVL1 upon immune stimulation (Figure 2.1F). This divergence in the total number of sites and the change in binding site-specificity does not seem to be due to a subsampling issue as there was a greater number of unique and total reads per cluster in the stimulated condition samples (Wang et al., 2015).

From our PAR-CLIP data, we observed a major shift in not only the number of ELAVL1 binding sites between the naïve and stimulated states (~100,000 naïve to ~40,000 stimulated), but we also see a condition-specific difference in the proportion of sites that map to introns and the 3'UTR. The change in the distribution of ELAVL1 sites between the naïve and stimulated cellular states gives insight into the context-dependent mRNA-targeting of ELAVL1. From the RNA-Seq data, we observed that the mRNA levels (i.e., the potential ELAVL1 mRNA substrates) significantly change during an IRF3-driven immune response. Therefore, we wanted to understand how ELAVL1 mRNA targeting changes during a highly dynamic mRNA-substrate environment. Namely, we wanted to examine the proportion of ELAVL1 binding sites that are found on newly expressed stimulated specific transcripts. Furthermore, if ELAVL1 binds a target mRNA in both conditions, is the number and location of the ELAVL1 binding sites the same, and how do changes in binding site position affect the function of ELAVL1 on that transcript? We would predict that ELAVL1 would target upregulated transcripts in the 3'UTR to promote mRNA stabilization and gene expression.

The mRNA target spectra of ELAVL1 differ in immune cell type

To investigate how ELAVL1 differentially targets mRNAs due to cellular condition, we first determined the conservation of ELAVL1 binding sites between the naïve and stimulated states and found that 27,323 clusters overlapped by at least one nucleotide (Figure 2.2A). This overlap comprises 27% of the sites in the naïve state and 70% of the stimulated state sites. At the mRNA transcript level, we found that the majority (5,051) of targets were bound in both naïve and

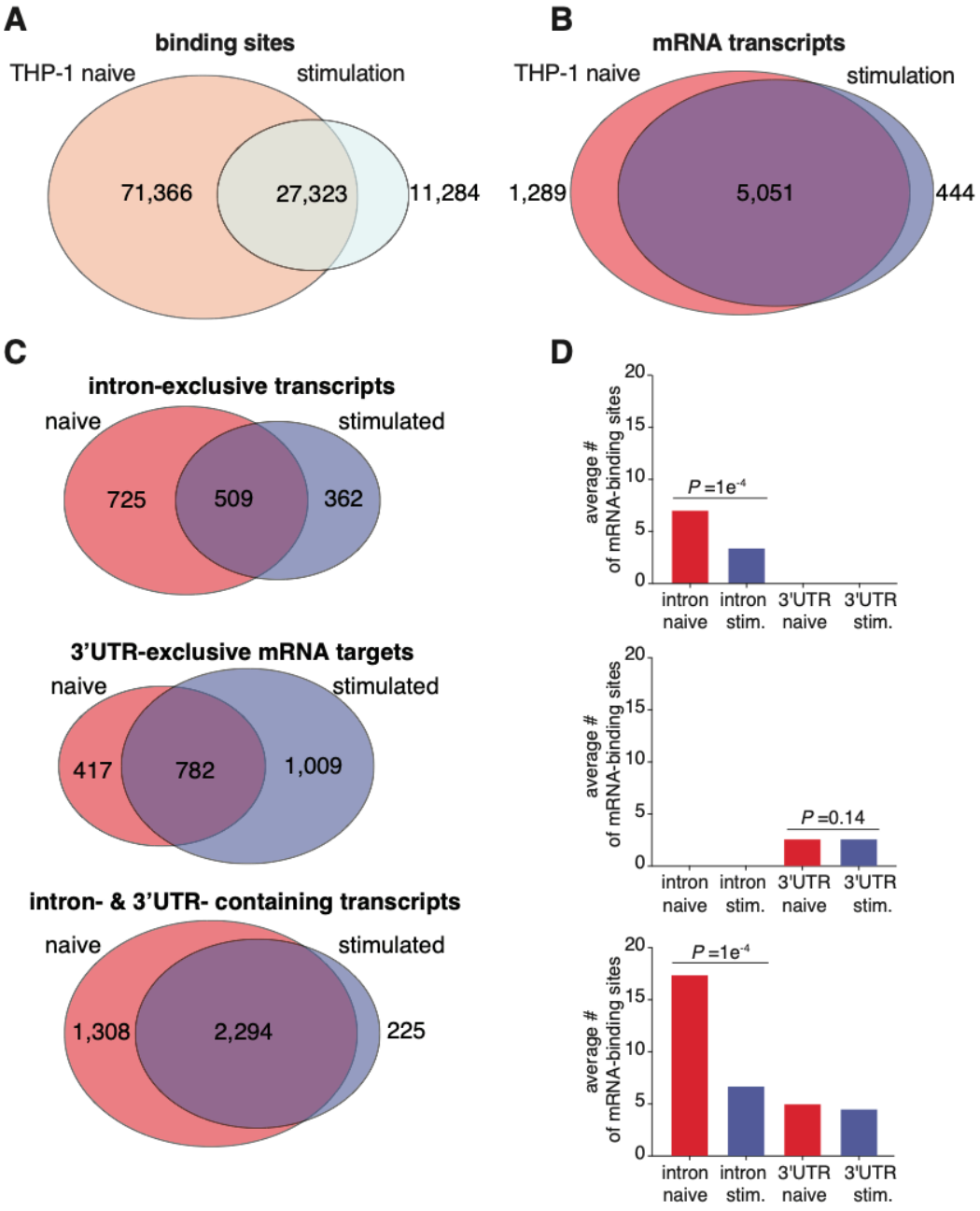

Figure 2.2 Innate immune stimulation pivots ELAVL1 binding towards 3'UTR sites

During immune stimulation, there is a significantly decreases in the total number of intronic binding sites transitioning the binding preference of ELAVL1 to the 3'UTR. (**A**) Venn diagrams showing the overlap of PAR-CLIP- defined ELAVL1 clusters between naïve and stimulated samples within mRNA or, (**B**), the overlap at the transcript level. (**C**) Venn diagrams indicating the number of transcripts in naïve and stimulated cells that are bound exclusively in the intron, 3'UTR, or both. (**D**) The average number of binding sites for the three mRNA location categories (intron-exclusive, 3'UTR-exclusive, or intron- and 3'UTR-containing transcripts) across conditions.

stimulated conditions, though a notable number were uniquely found in the naïve (1,289) or stimulated (444) states (Figure 2.2B; Table 2.4).

We wanted to parse this data further and investigate if the mRNAs that were shared or uniquely bound were differentially targeted by ELAVL1. Of the 6,340 mRNAs bound by ELAVL1 in the naïve state, > 94% of transcripts contained sites that mapped to intron-exclusive, 3'UTR-exclusive, or both; < 6% of transcripts contained sites within 5'UTR and/or CDS. A similar proportion was observed for the transcripts bound in the stimulated state. Consequently, we focused our analyses on transcripts that bore a distribution of intron and 3'UTR sites, which naturally divided into three populations: transcripts that contained ELAVL1 sites exclusively within: (1) introns, (2) the 3'UTR, or (3) both regions. In comparing the proportion and the absolute number of transcripts bound by ELAVL1 that were either intron- or 3' UTR-exclusive, we observed a significant shift in binding site distribution for the 3'UTR in the stimulated state. Conversely, the naïve state had nearly 50% more transcripts that were exclusively bound within introns (Figure 2.2C).

We next examined mRNAs that contained ELAVL1 binding sites within introns and the 3'UTR, as they represented the majority of ELAVL1 targets. Since these transcripts contained sites for both regions, we reasoned that a change in intra-transcript binding would give insight into how ELAVL1 targets RNA in a condition-specific manner. Previous work has shown that that the total number of ELAVL1 binding sites correlate with the extent of its regulation for that particular mRNA (Mukherjee et al., 2011). Therefore, we calculated the average number of ELAVL1 sites for each region, with the hypothesis that a change in intra-transcript binding site distribution would point to the region(s) of the mRNA that is relevant to its function during immune stimulation. In the stimulated state, we see a two- to three-fold reduction in the number of intronic binding sites

for intron-exclusive transcripts and those that contained both intron and 3'UTR sites (Figure 2.2D). Among the mRNA targets that contained both intron and 3'UTR sites, the ratio of intron sites to 3'UTR sites shifted from 3:1 to 1.3:1 upon stimulation. Corroborating the observation that the changes are due to the loss of intronic binding sites, we found no significant change in the average number of 3'UTR sites upon immune stimulation. Altogether, our data show that immune stimulation leads to a loss of mRNA targets exclusively bound within introns, as well as the total number of intronic sites across all other transcripts – resulting in a net increase in the proportion of 3'UTR bound ELAVL1 targets.

Given the condition-dependent shift in the distribution of the binding sites from intron to 3'UTR, we wanted to see if there was a change in motif usage by ELAVL1. Motif analysis (6-mer analysis) of the binding sites in both conditions located in 3'UTR and introns revealed a UUUUU and AUUUA rich RNA recognition element (RRE) (data not shown). Similar results were obtained from previous PAR-CLIPs from HeLa and HEK293, indicating that ELAVL1 does not change sequence-specific binding site preference in different cell types or conditions (Mukherjee et al., 2011). These data suggest that other factors, such as RNA secondary structure and competition with other RBPs, influence the ability of ELAVL1 to bind to its RNA targets.

PAR-CLIP and RIP-Seq define enrichment criteria for ELAVL1 during an innate immune response

We assessed the quantitative changes in substrate binding by ELAVL1 as cells transitioned from the naïve to the immune activated state, given the rapid changes to the transcriptome that we observed. ELAVL1 functions through its targeting of AREs within mRNAs. By quantifying its

association to targets, we can discern the salient binding properties that drive the relative enrichment differences caused by an IRF3-driven innate immune response. Therefore, we performed RIP-Seq for ELAVL1 (Keene et al., 2006; Tenenbaum et al., 2000; Zhao et al., 2010; 2008). Flag-HA ELAVL1 from THP-1 cells was immunoprecipitated in the same manner as with PAR-CLIP but without UV crosslinking and RNA digestion. RNAs that co-immunoprecipitated with ELAVL1 were recovered and sequenced. A total of 3,459 and 3,406 PAR-CLIP identified mRNA targets in naïve and stimulated samples, respectively, were enriched over the IgG background by RIP-Seq (Figure 2.3A-B and 2.2.1A; Table 2.4). Overlapping the enriched targets from both conditions, we found that 2,114 mRNAs were enriched in a context-independent manner; 1,345 mRNAs were specific to the naïve state, while 1,292 were specific to the stimulated state (Figure 2.2.1B). We next discerned whether the enriched targets in the stimulated specific state represented just the upregulated mRNAs. Surprisingly, we found that a majority (61%) of the 1,292 transcripts were already expressed in the naïve state, and their expression values did not significantly change (< two-fold change) upon immune stimulation. The mean expression value for these existing transcripts was 10.7 CPM (all transcripts mean = 9.2 CPM). This data indicates that the differences in the target repertoire between the two cellular states are not solely due to changes in the expression levels of mRNAs. ELAVL1 competes for binding sites with other post-transcriptional regulatory elements, including miRNAs or other RBPs, whose expression and activities are similarly dynamic and dependent on the cellular context (Dassi, 2017; Lu et al., 2014; Srikantan et al., 2012; L. E. Young et al., 2012).

Reactome pathway analysis on target genes that were either naive-specific or shared showed that they encoded for proteins involved in transcriptional regulation by TP53 (R-HSA-3700989), processing of capped-mRNAs (R-HSA-72203), and cell cycle checkpoints

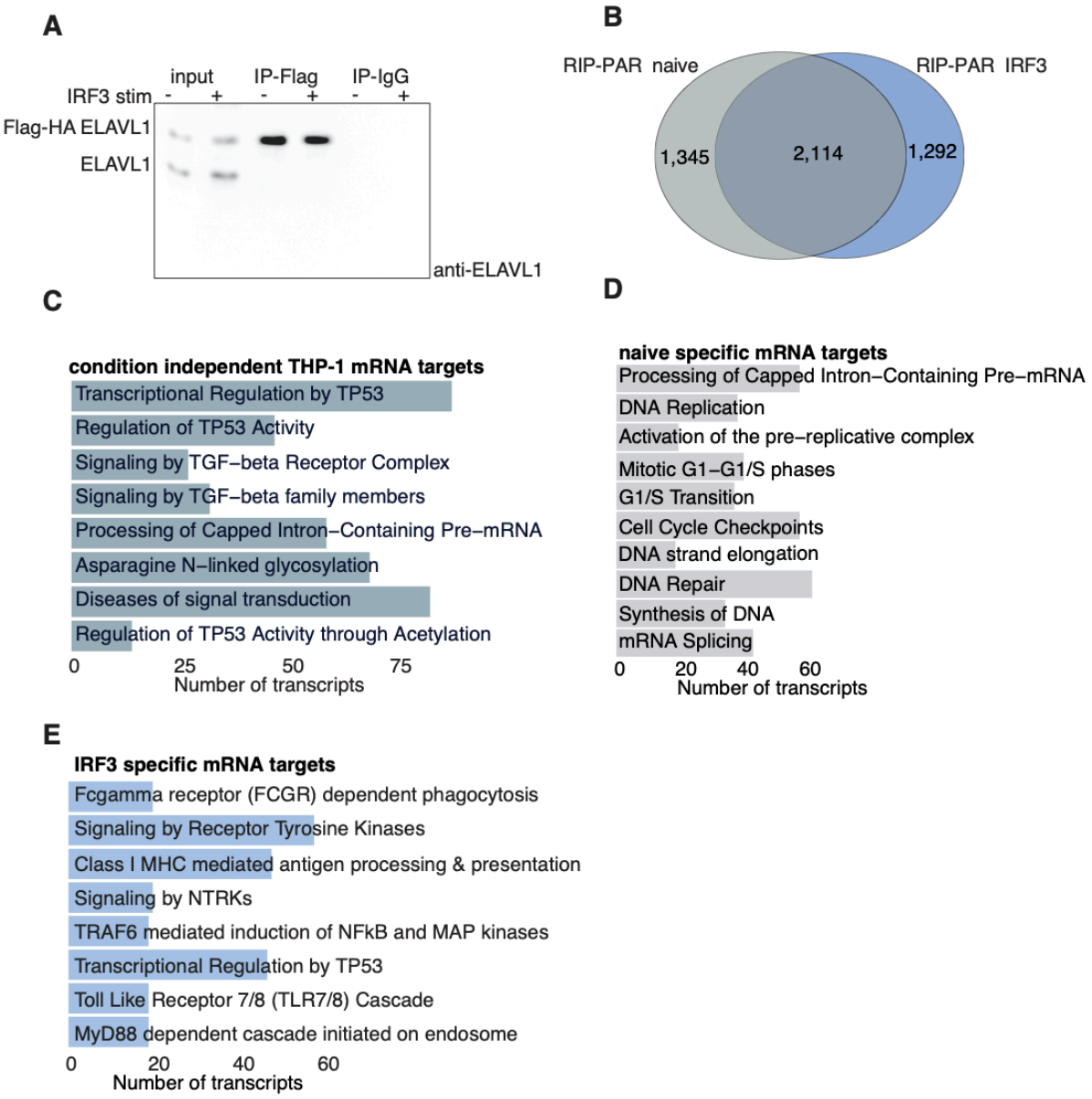

Figure 2.2.1 PAR-CLIP and RIP-Seq identify enriched transcripts that are condition independent or dependent

(**A**) ELAVL1 immunoblot from an IP (anti-Flag) of Flag-HA ELAVL1 in naïve and immune activated THP-1 cells. (**B**) Venn diagram showing the overlap between the bound (PAR-CLIP) and enriched (RIP-Seq) mRNA transcripts across conditions. (**C**) Bar graph of a Reactome pathway analysis for each group of transcripts that were either shared (from S2A) between the two conditions or unique bound and enriched in the naïve (**D**) or (**E**) the stimulated states.

(R-HSA-69620) (Figure 2.2.1C-D; Table 2.5) (Techasintana et al., 2015). These pathways comprise of more ubiquitous cellular processes that are generalizable across multiple cell types, often found as steady-state functions. By contrast, Reactome pathways enriched from targets specific to the stimulated state include toll-like receptor (TLR) signaling (R-HSA-168181), NF-kB (R-HSA-975183), and MAP kinase (MAPK) signaling (R-HSA-975138) (Figure 2.2.1E; Table 5). This observation is interesting because the majority of the targets that were enriched in the stimulated-specific state were expressed at similar levels in naïve cells but not enriched - thus suggesting that ELAVL1 associates with transcripts belonging to immune signaling pathways regardless of mRNA levels (transcriptional output). Consistent with our observation, 71% (918/1,292) of these stimulated-specific enriched targets were also found as PAR-CLIP bound transcripts in a HEK293 study, yet only 122 were enriched; pathway analysis of these 122 did not yield enrichment in the TLR, NF-kB, or MAPK signaling terms (Mukherjee et al., 2011).

3'UTR binding determines the level of enrichment to context-dependent mRNA targets

To test the hypothesis that the frequency and position of ELAVL1 binding sites influence levels of enrichment in THP-1 cells, we examined the cumulative distribution of ELAVL1 target enrichment (RIP-Seq) based on PAR-CLIP binding site data. Independent of cellular state, transcripts with ≥ 2 binding sites showed significant enrichment compared to transcripts with one or zero sites. Furthermore, an increase in the number of ELAVL1 binding sites showed a positive correlation with enrichment (Figure 2.3C and 2.3D). Interestingly, we saw that enrichment levels were more pronounced in the stimulated state. Overall, for transcripts that had ≥ 2 sites in the

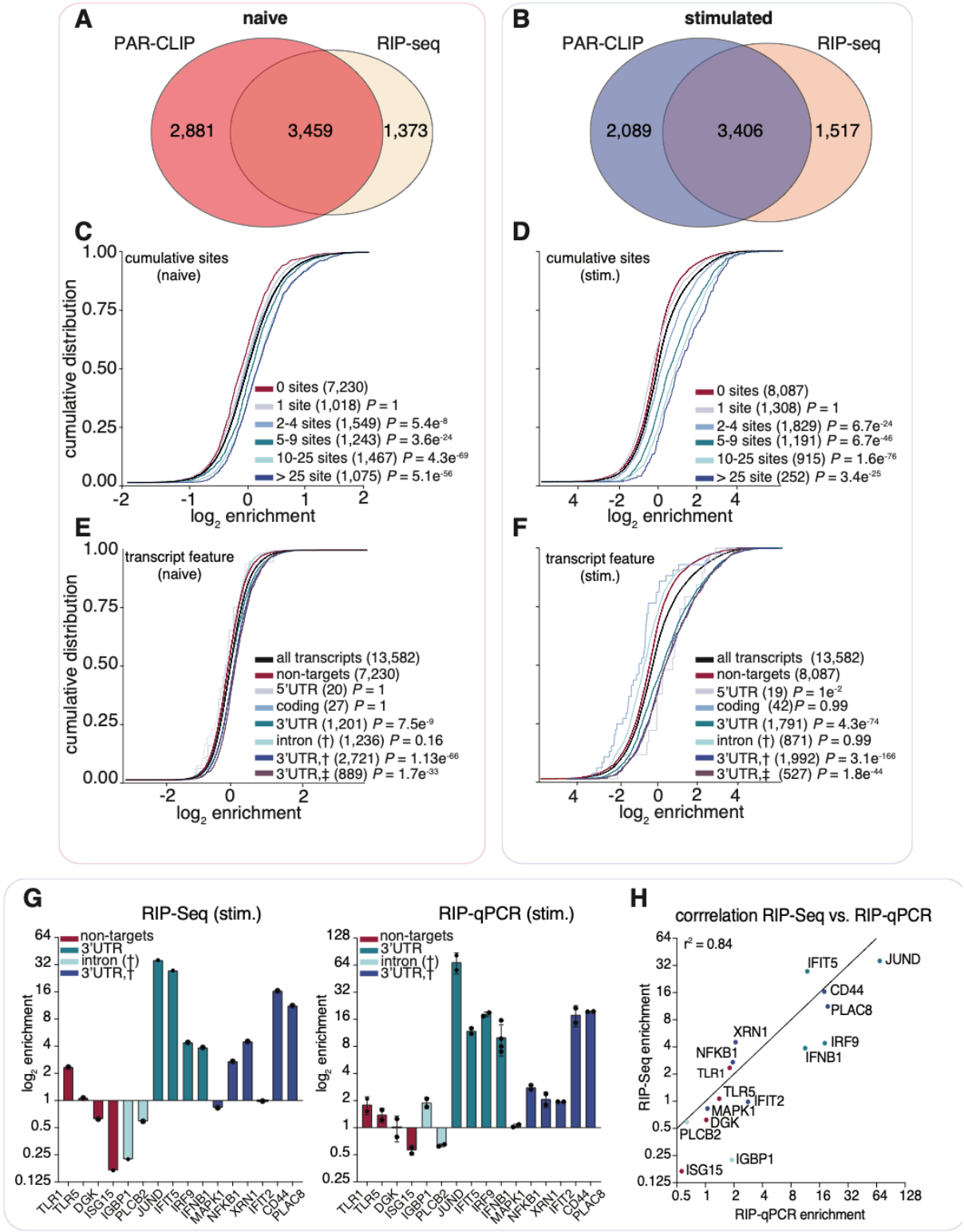

Figure 2.3 ELAVL1 RIP-Seq and PAR-CLIP define transcript enrichment criteria during immune stimulation

The total number of ELAVL1 binding sites confers greater enrichment, especially in the stimulated condition, and requires association at the 3'UTR.

(**A**) Venn diagram of the overlap between mRNA transcripts defined as targets using both PAR-CLIP and RIP-Seq data in the naïve and **B**) IRF3 stimulated state.
(**C**) To test the hypothesis that an increasing number of ELAVL1 sites lead to transcript enrichment, we performed cumulative distribution fraction analyses for the mRNA targets of ELAVL1 in naïve or (**D**) stimulated conditions on the basis of the number of total binding sites indicated. (**E**) To test the hypothesis that the location of the binding site contributes to enrichment, we performed cumulative distribution fraction analyses for ELAVL1 mRNA targets in naïve or (**F**) stimulated cells. Transcripts were binned based on the indicated location of the ELAVL1 binding sites. (**G**) Bar graphs of RIP-Seq and RIP RT-qPCR enrichment levels for transcripts listed. (**H**) Correlation plot of enrichment levels between RIP-Seq and RIP RT-qPCR.

stimulated state, there was nearly a 200% increase in fold-enrichment over non-targets, whereas targets (≥ two sites) in the naïve state were only nominally enriched (10%) over non-targets.

From our PAR-CLIP data, we observed a net decrease in the total number of binding sites per transcript in the stimulated state compared to naïve. However, we found that an increase in the number of sites per transcript correlated with greater enrichment – especially in the stimulated state. To reconcile these observations, we grouped transcripts based on the location of PAR-CLIP sites. We found that mRNA that contained at least one 3'UTR binding site had the highest levels of enrichment compared to binding sites in other transcript regions (Figure 2.3E and 3F). These results were further validated using RIP RT-qPCR on candidate target and non-target transcripts (Figure 2.3G). We found that the RIP-Seq and RIP RT-qPCR data were highly correlated (r^2 = 0.82) (Figure 2.3H).

A majority of 3'UTR-bound transcripts also contained additional intronic sites, and previous reports showed that intronic binding contributed to enrichment (Lebedeva et al., 2011; Mukherjee et al., 2011). Therefore, we tested whether increasing numbers of intron-bound sites led to greater enrichment but found no correlation (Figure 2.4A-B). Enrichment was dependent solely on the number of 3'UTR sites in both naïve and stimulated states. Of note, the 3'UTR-bound transcripts in the stimulated state were five times more enriched over non-3'UTR bound targets compared to the same populations in the naïve condition (Figure 2.4C-D). We also observed that the fractional occupancy of 3'UTR sites per transcript was significantly favored in the stimulated state (Figure 2.4E). This might explain the increase in the 3'UTR-specific enrichment in the stimulated state compared to the naïve.

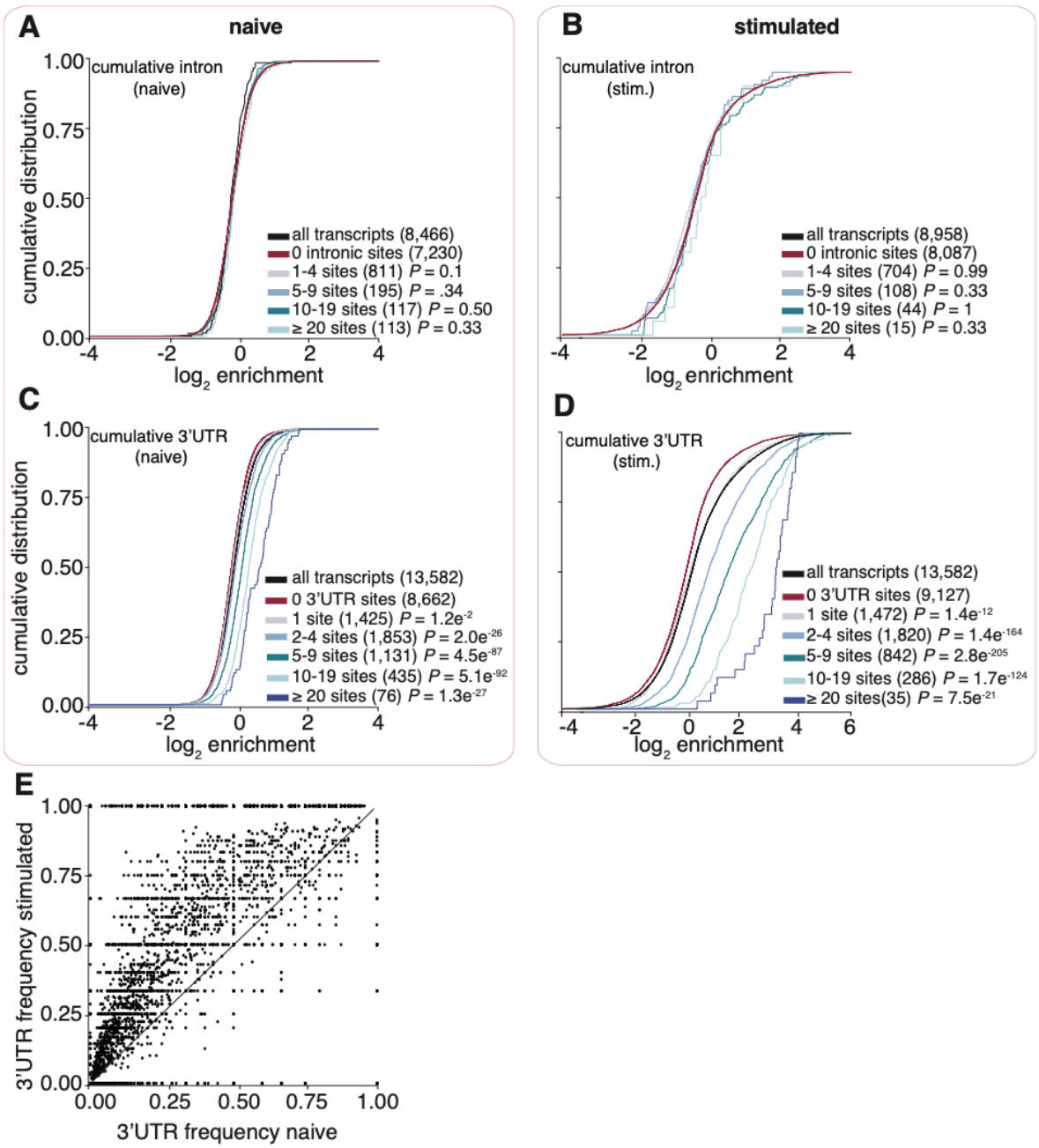

Figure 2.4 ELAVL1-mRNA enrichment is exclusively dependent on 3'UTR association and intensifies upon immune stimulation

The binding of ELAVL1 at 3'UTR sites drives the greatest levels and is sufficient for transcript enrichment when cells are immune activated.

(**A, B**) Cumulative distribution function analyses were used to determine whether intronic binding versus 3' UTR binding (**C**, **D**) confers greater transcript enrichment in naïve and stimulated states. (**E**) A scatterplot shows the bias of fractional occupancy, or frequency, of 3'UTR binding per given transcript for the stimulated state. The fraction of 3'UTR sites over the total number of binding sites was plotted wherein the x-axis represents the naïve state, and the y-axis indicates the stimulated state.

To assess whether the targets of ELAVL1 would be similarly enriched in other human monocyte-like lines, we examined the target spectra and protein localization of ELAVL1 in U937 cells. This cell line has been previously used to study how ELAVL1 regulates an inflammatory response (Sahlberg et al., 2013). We found that the expression of ISGs in response to cGAMP activation correlated well ($r^2 = 0.79$) in U937 and THP-1 cells (Figure 2.3.1A). However, when investigating the localization and protein expression levels of ELAVL1 across the two cell types, we unanticipatedly found that in U937 cells, the predominant form of ELAVL1 is approximately 12 kDa smaller than the full-length ELAVL1 (36 kDa) and that the majority of the protein was found to be cytoplasmic independent of IRF3 stimulation (Figure 2.3.1B). Interestingly, previous publications have reported the existence of a caspase-dependent cleaved form of ELAVL1 of similar mass (Sahlberg et al., 2013; Mazroui et al., 2008; Talwar et al., 2011; Roretz et al., 2019). The caspase-dependent cleaved form was reported to be missing its third RNA recognition motif and dimerization domain and that it largely localized to the cytoplasm. We next transiently transfected a Flag-HA epitope-tagged form of ELAVL1 to assess whether U937 cells were genetically expressing a truncated ELAVL1 or if the smaller molecular weight form of ELAVL1 is more consistent with that reported by previous investigators. Immunoblot analysis of the expression of FLAG- HA ELAVL1 in U937 cells indicated that the recombinant form was also truncated, despite encoding for a full-length protein (Figure 2.3.1C). We anticipated that the truncated form of ELAVL1 would not behave similarly to the full-length protein. Accordingly, immunoprecipitation of FLAG-HA ELAVL1 in U937 cells followed by RT-qPCR analysis showed no significant enrichment of highly enriched THP-1 validated targets (*IFIT2, IFNB1, IFIT5, IRF9, JUND*) (Figure 2.3.1D).

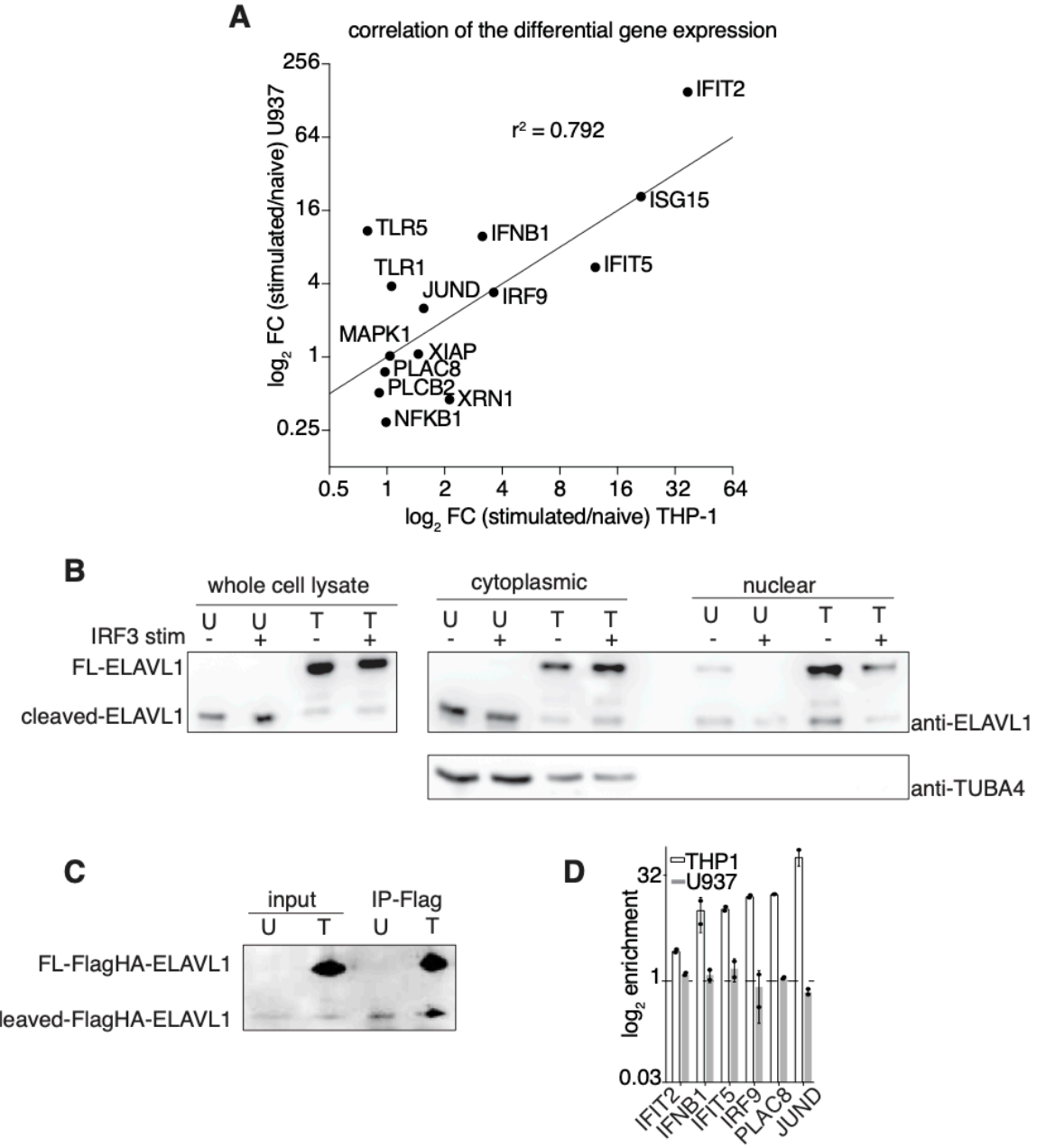

Figure 2.3.1 ELAVL1 in U973 cells is predominantly cleaved

(A) Correlation plot of gene expression foldchanges (activated /naïve) of the stated ISG transcripts between THP-1 and U937 cells. (**B**) Immunoblot against endogenous ELAVL1 on biochemically fractionated lysates in naïve and immune activated U937 (U) and THP-1 cells (T). The predominant form of ELAVL1 is a truncated form that is ~24 kDa, independent of the cellular state. (**C**) Anti-HA immunoblot from the input and IP (anti-Flag) of Flag-Ha ELAVL1 in U937 (U) and THP-1 cells (T). Based on molecular weight, the exogenous form of Flag-HA ELAVL1 appears cleaved in U937 compared to THP-1. (**D**) Bar graph comparing the RIP RT-qPCR enrichment levels of ISG transcripts in U937 cells and THP-1 cells. The transcripts were chosen because they were validated, highly enriched targets in THP-1 cells.

From the integration of RIP-Seq and PAR-CLIP datasets, we observed that an increasing number of 3'UTR sites correlates with greater enrichment with ELAVL1 in THP-1 cells. Importantly, mRNAs bound by ELAVL1 in the immune-stimulated state showed significantly higher enrichment levels, demonstrating a stronger association and potentially indicating a more profound level of post-transcriptional gene regulation. However, the binding and enrichment of a transcript with an RBP is not directly equivalent to its regulatory fate, given that any single mRNA is potentially subject to other post-transcriptional factors that may impose a stronger regulatory effect. In most reported cases, the primary function of ELAVL1 is through the stabilization of its target transcripts (Herdy et al., 2015; Srikantan et al., 2012; Takeuchi, 2015; Turner and Díaz-Muñoz, 2018). ELAVL1 competes over AREs on transcripts, opposing negative post-transcriptional regulators like RNA-induced silencing machinery or ZFP36 (TTP), which can recruit the CCR4-NOT1 deadenylase complex (Fu and Blackshear, 2016). Consequently, to best understand the functional impact of our enriched ELAVL1 targets, we utilized SLAM-Seq to quantitatively measure transcript decay rate (Herzog et al., 2017).

ELAVL1 stabilizes a subset of 3'UTR targets involved in innate immune signaling

By overlapping SLAM-Seq results with our RIP-Seq and PAR-CLIP datasets, we were able to precisely identify the consequences of ELAVL1 absence on the stabilities of its target transcripts during an innate immune response (Figure 2.5A-B). Slam-Seq uses 4SU to metabolically label nascent RNA transcripts, which is subsequently chased with unlabeled uridine. Thiol-alkylation of RNA generates chemical adducts that induce reverse transcriptase-dependent

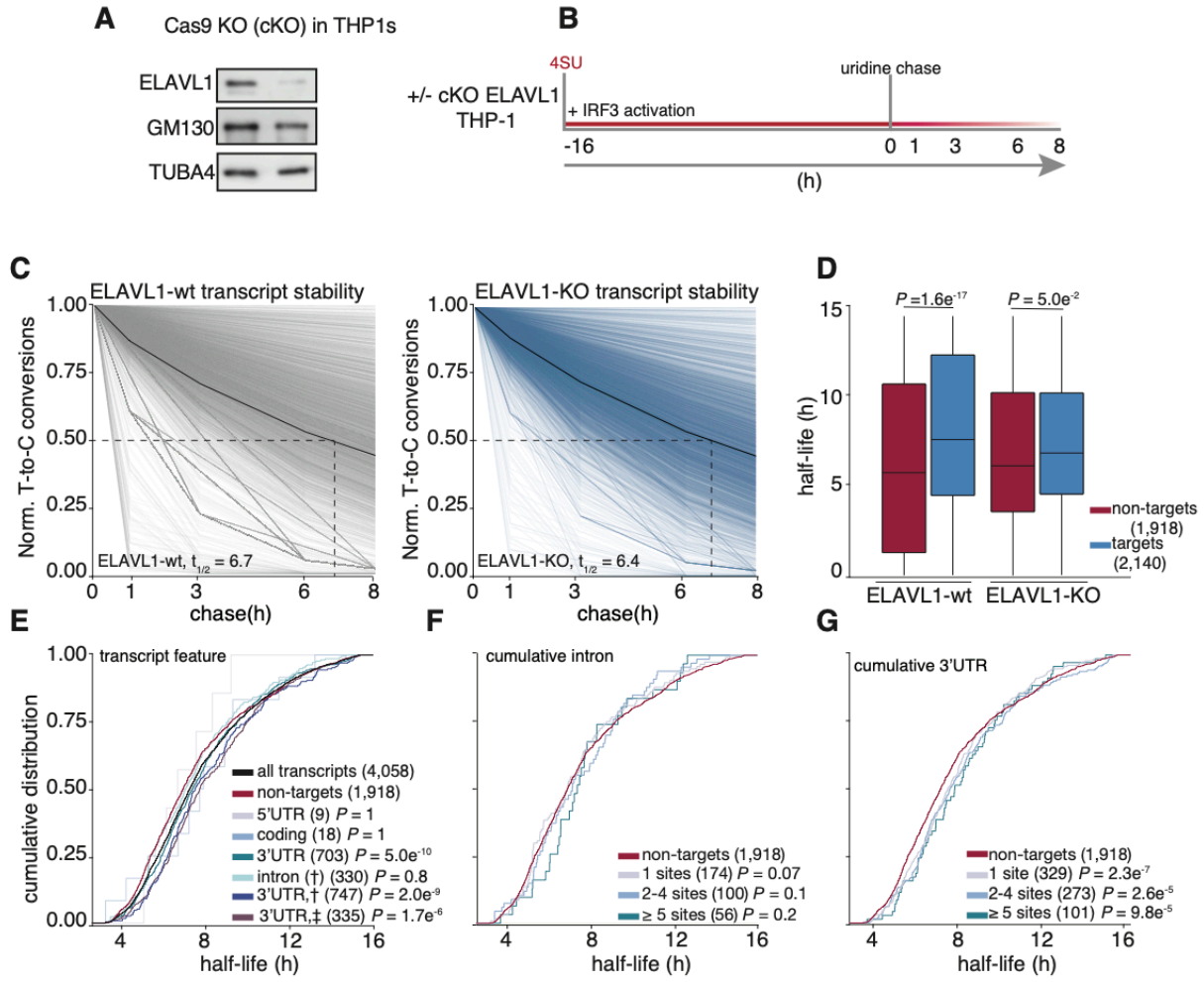

Figure 2.5 Analysis of transcriptome-wide mRNA stability in the absence of ELAVL1

Overlapping SLAM-Seq transcript stability data with RIP-Seq enrichment and PAR-CLIP binding site information defines which target transcripts are most affected by the loss of ELAVL1. (**A**) Immunoblot staining for the presence of endogenous ELAVL1-wt and ELAVL1-KO THP-1 cells. (**B**) Schematic of the SLAM-Seq experiment setup. THP-1 cells (+/-cKO) were stimulated, and 4SU labeled for 16 hours before wash and uridine chase. Timepoints for SLAM-Seq were 0, 1, 3, 6, and 8 hours after uridine chase. (**C**) The decay of T-to-C conversions after the uridine chase was determined by fitting the data to a single-exponential decay model to derive mRNA half-lives (dotted-line). Graphs show that the RNA stabilities over time. The solid black line indicates the median T-to-C conversion rate over time; the dotted black line denotes median half-life ($t_{1/2}$), as indicated per condition. (**D**) Box plots showing the median half-lives of non-targets (red) and targets (blue) in the ELAVL1-wt and ELAVL1-KO cells. (**E**) To test if the location of ELAVL1 binding sites contributes to increased RNA stability, we performed cumulative distribution fraction analyses of the RNA half-lives. Transcripts were grouped by the location of the ELAVL1 binding sites. (**F**) Cumulative distribution fraction analyses were used to determine whether the RNA half-lives of targets are affected by the number of intronic- or (**G**) 3'UTR-binding sites. Data not shown for CDS and 5'UTR targets because of too few targets.

deoxycytosine substitutions at 4SU positions during cDNA library preparation (T-to-C substitutions). The ratio of unlabeled to T-to-C containing reads across all the timepoints is used to calculate RNA half-life for each expressed transcript (Herzog et al., 2017; Neumann et al., 2019). Here, we performed SLAM-Seq during an IRF3-driven innate immune response. Parental and ELAVL1-KO THP-1 cells were labeled with 4SU for 16 h, followed by washout and chase using uridine. Cells were collected at various time points after the chase, and extracted RNAs were processed for high-throughput sequencing. We determined the half-lives of nearly ~5,000 transcripts that were shared across parental and ELAVL1-KO datasets and found their median half-lives to be 6.7 hours and 6.4 hours, respectively (Figure 2.5C; Table 2.6), indicating comparable global RNA stability independent of condition type. Importantly, the difference in the median half-lives between ELAVL1 targets and non-targets is greater when ELAVL1 is present (1.8 h), in comparison to the median half-life difference when it is knocked out (0.7 h) (Figure 2.5D). These data indicate that the half-lives of ELAVL1 target transcripts are more similar to non-targets upon its knockout.

In the parental THP-1 cells, we observed that transcripts with at least one 3'UTR binding site had statistically significant longer RNA half-lives ($t_{1/2}$ = 7.5 h) than non-targets ($t_{1/2}$ = 5.7 h); whereas, 5'UTR, coding-, or intronic-bound targets were not statistically significant (Figure 2.5E). We noticed that transcripts that have binding sites either in the intron and 3'UTR ($t_{1/2}$ = 7.6 h) or intron and 3'UTR plus another location ($t_{1/2}$ = 7.5 h) tended to have slightly longer RNA half-lives than transcripts bound exclusively in the 3'UTR ($t_{1/2}$ = 7.4 h). Similar to our analysis of transcript enrichment, of comparing the intron- or 3'UTR- exclusively bound transcripts, we found that only the presence and increase in the number of 3'UTR sites conferred greater stability (Figure 2.5F-G). Interestingly, targets with >10 3'UTR binding sites exhibited half-lives 3 hours longer than

non-targets ($t_{1/2}$ = 8.9 h versus 5.7 h). In looking at the change in target transcript half-lives between KO and wt, no feature other than 3'UTR conferred any significant stability effect (Figure 2.4.1A).

To assess whether target transcripts that were enriched based on 3'UTR content were specifically stabilized by ELAVL1, we examined their behaviors when ELAVL1 was knocked out. The half-lives of only the enriched 3'UTR-containing ELAVL1 transcripts were significantly reduced in the absence of ELAVL1 (Figure 2.6A). The half-lives of the non-enriched transcripts bound by ELAVL1 were not as affected by the absence of ELAVL1, suggesting that the decay rates of these transcripts are either partially or completely independent of ELAVL1 regulation, despite being bound. Moreover, transcripts with an increasing number of ELAVL1 sites have the greatest decrease in half-lives, further supporting this 3'UTR stability signature (Figure 2.6B). Among the most 3'UTR enriched targets (n=1,141), we noted that a substantial fraction (50%) are ISGs, and collectively they had a greater change in half-life in the knockout, compared to enriched transcripts that are not ISGs (Figure 2.6C). ISGs such as *NFKB1*, *IRF9*, *IFIT5*, and *MAPK1*, are less stable in the absence of ELAVL1, in contrast to ISGs for which we had zero evidence of ELAVL1 association or enrichment (Figure 2.6D). The change in the mRNA half-lives of targets and non-targets of ELAVL1 were confirmed by shutting off transcription (actinomycin D) and measuring mRNA decay using RT-qPCR. Transcription inhibition coupled with RT-qPCR validated the SLAM-seq data showing that the half-lives' of ISGs with 3'UTR binding were significantly affected due to the absence of ELAVL1 (Figure 2.6E and 2.4.1B-C).

To further establish a direct link between ELAVL1 binding and mRNA stability, we generated luciferase reporter plasmids expressing the luciferase ORF followed by the wt or the mutant 3'UTR of *IRF9* (Figure 2.4.1D). The *IRF9* 3'UTR was used because it contains two distinct 3'UTR binding sites and is an enriched, functional target that we validated through multiple

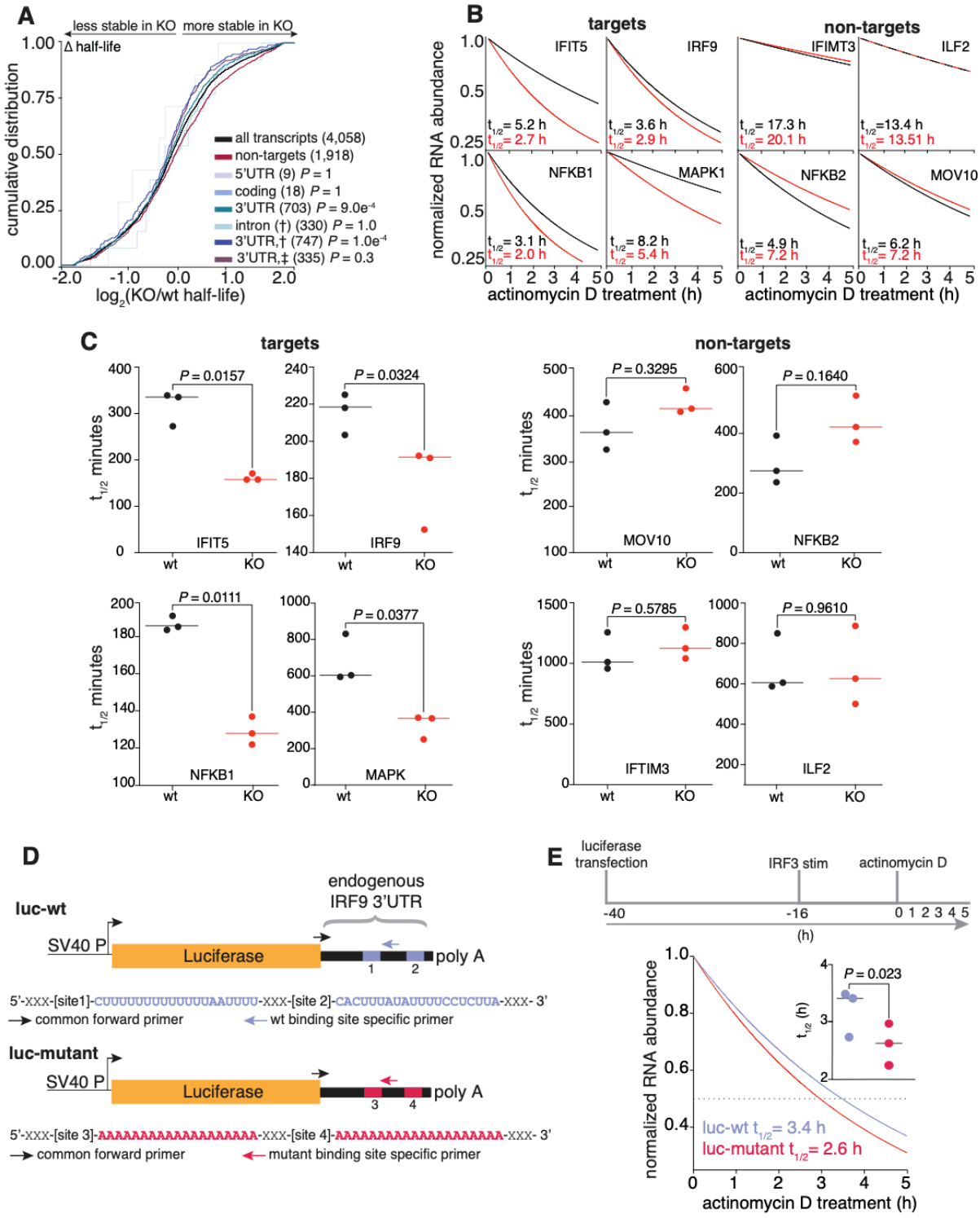

Figure 2.4.1 KO determines transcripts whose half-lives are dependent on the presence of ELAVL1

(**A**) Cumulative distribution plot of the $\log_2$ foldchange (KO/wt) in half-life showing the group of transcripts whose half-lives are most affected by the loss of ELAVL1. (**B**) The calculated RNA half-lives and stability plots of transcripts indicated. RNA half-lives were measured using actinomycin D and RT-qPCR.

(**C**) Pairwise comparisons of the RNA half-lives in the presence or absence of ELAVL1 for either non-target or target transcripts**. (D**) To test if an exogenous transcript can be stabilized in an ELAVL1 site-dependent manner, we constructed two gene reporters from the luciferase ORF and wt *IRF9* 3'UTR or mutant *IRF9* 3'UTR. Schematic shows luciferase ORF with either the wt *IRF9* 3'UTR or the mutant. (**E**) Schematic of luciferase reporter experiment. RNA-stability profiles and a pairwise comparison of the half-lives of an exogenous gene (ORF of luciferase) expressed with either the wt or mutant 3'UTR *IRF9.*

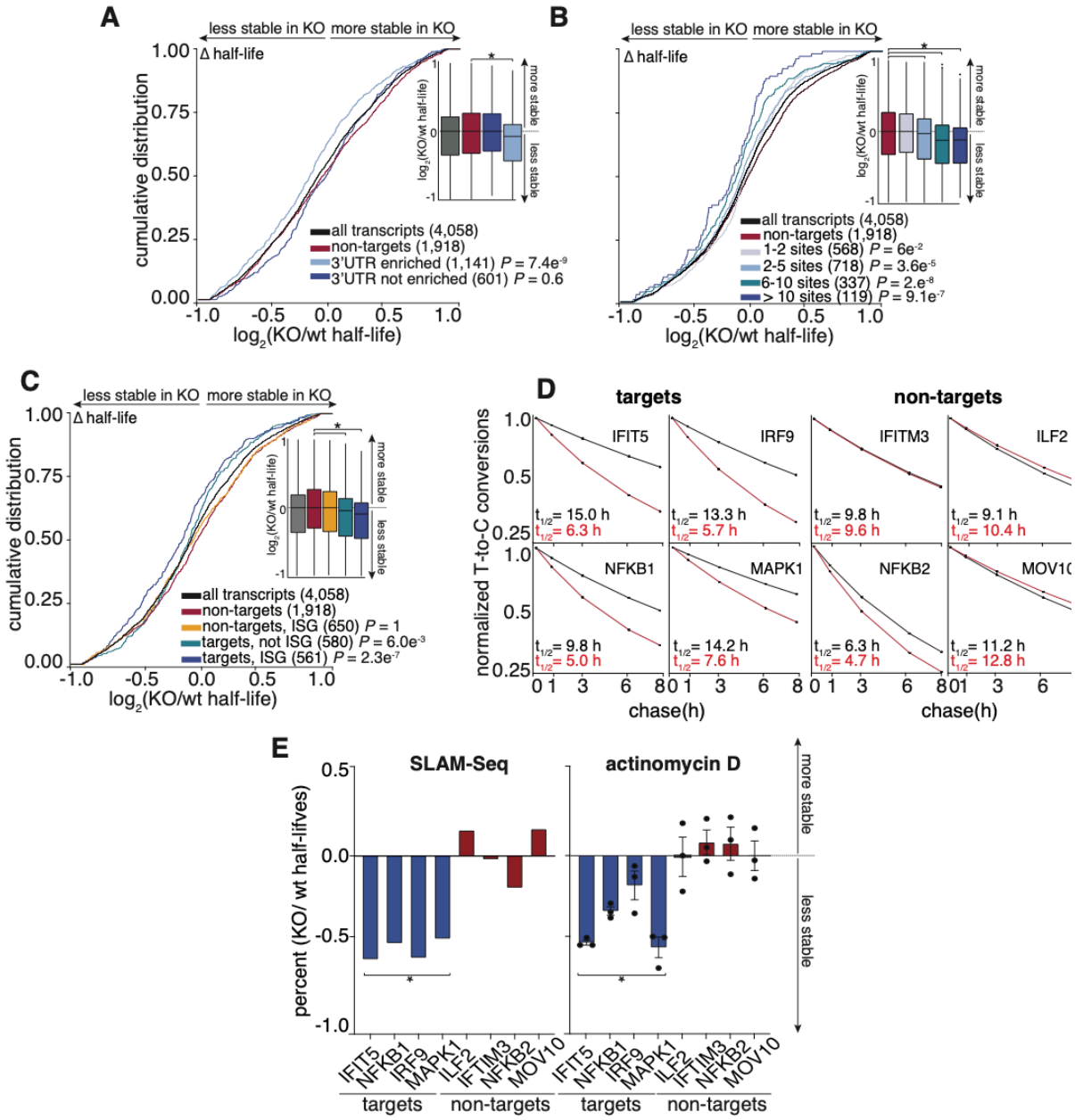

Figure 2.6 The RNA half-lives of highly enriched ELAVL1 target ISGs are the most affected by its loss.

(**A, B**) Cumulative distribution analyses of the $\log_2$ fold-change in half-life (KO/wt), binning transcripts based on enrichment. Insets show a box plot of the $\log_2$ fold-change (KO/wt) in half-life based on indicated groupings. (**C**) Cumulative distribution analysis of the $\log_2$ fold-change of half-life (KO/wt) to test if transcripts classified as ISGs are more affected by the loss of ELAVL1 than non-ISGs. (**D**) Transcript stability plots and the calculated RNA half-lives of the indicated ISG mRNA targets or non-targets are shown; ELAVL1-wt (black) or ELAVL1-KO THP-1 cells (red). (**E**) Bar plots validating the change in the half-lives (KO/wt) of the listed transcripts due to the loss of ELAVL1 measured by SLAM-Seq and actinomycin D experiments.

independent experiments (RIP-Seq, SLAM-Seq, RIP RT-qPCR with actinomycin D). THP-1 cells were transfected with both wt and mutant 3'UTR plasmids and 24 hours later stimulated with cGAMP. The transfected and activated cells were then treated with actinomycin D to inhibit transcription, followed by taking time-resolved samples to measure mRNA decay by RT-qPCR using primers that can distinguish between wt and mutant IRF9 3' UTRs. We found that the mRNA fused with the mutant IRF9 showed a statistically significant decrease in half-life from 3.4 to 2.6 hours (Figure 2.4.1E), a 24% drop in transcript stability that is consistent with our RT-qPCR analysis of the endogenous IRF9 transcript (Figure 2.4.1B).

Pathway analysis showed that the ELAVL1-regulated targets (n = 409), which we defined as 3'UTR enriched targets whose half-life decreased by 1.5-fold-change in the absence of ELAVL1, encode for proteins associated with endocytosis, transcriptional dysregulation in cancer, and multiple innate immune signaling pathways (Figure 2.7A; Table 2.7). Of the immune-relevant pathways, ELAVL1 regulated components of interleukin-17 (R-HSA-448424), TNF-pathway (R-HSA-75893), and Toll-like receptor signaling (R-HSA-168164). Other signaling pathways, such as MAPK (R-HSA-450294), and apoptosis (R-HSA-109606) terms, were also enriched. MAPK signaling, along with NF-kB and IRFs, are important for generating an immunoreactive state in the presence of a pathogen (Arthur and Ley, 2013). In the case of TLR signaling, ELAVL1 binds directly and stabilizes the adaptor protein (TRAF6), a kinase involved in integrating upstream PRR activity (TAK1) and the transcription factor itself (NF-kB) – which are all positive regulators of the pathway. Overall, we found that these innate immune pathways form a network containing regulators of ISG expression (STAT3, MAPK, IRF9, FOS, NF-kB, RIPK2) (Figure 2.7B)

(Gilchrist et al., 2012; Mostafavi et al., 2016). Thus, our data indicate that ELAVL1 stabilizes the transcripts of ISGs and ISG regulators critical for a cell to mount an immunoreactive state.

Of note, we found that a surprising number of the highly regulated transcripts were already bound by ELAVL1 in the THP-1 naïve state. However, their enrichment level (based on rank) were significantly higher upon immune stimulation. This increase in enrichment was concomitant with higher 3'UTR fractional occupancy - reinforcing the importance of a transition to 3'UTR binding. Only ~10% of our ELAVL1-regulated targets were found as enriched or even affected by the knockdown of ELAVL1 in HEK293 cells – underscoring the importance of examining ELAVL1 targets under changing transcriptomic contexts.

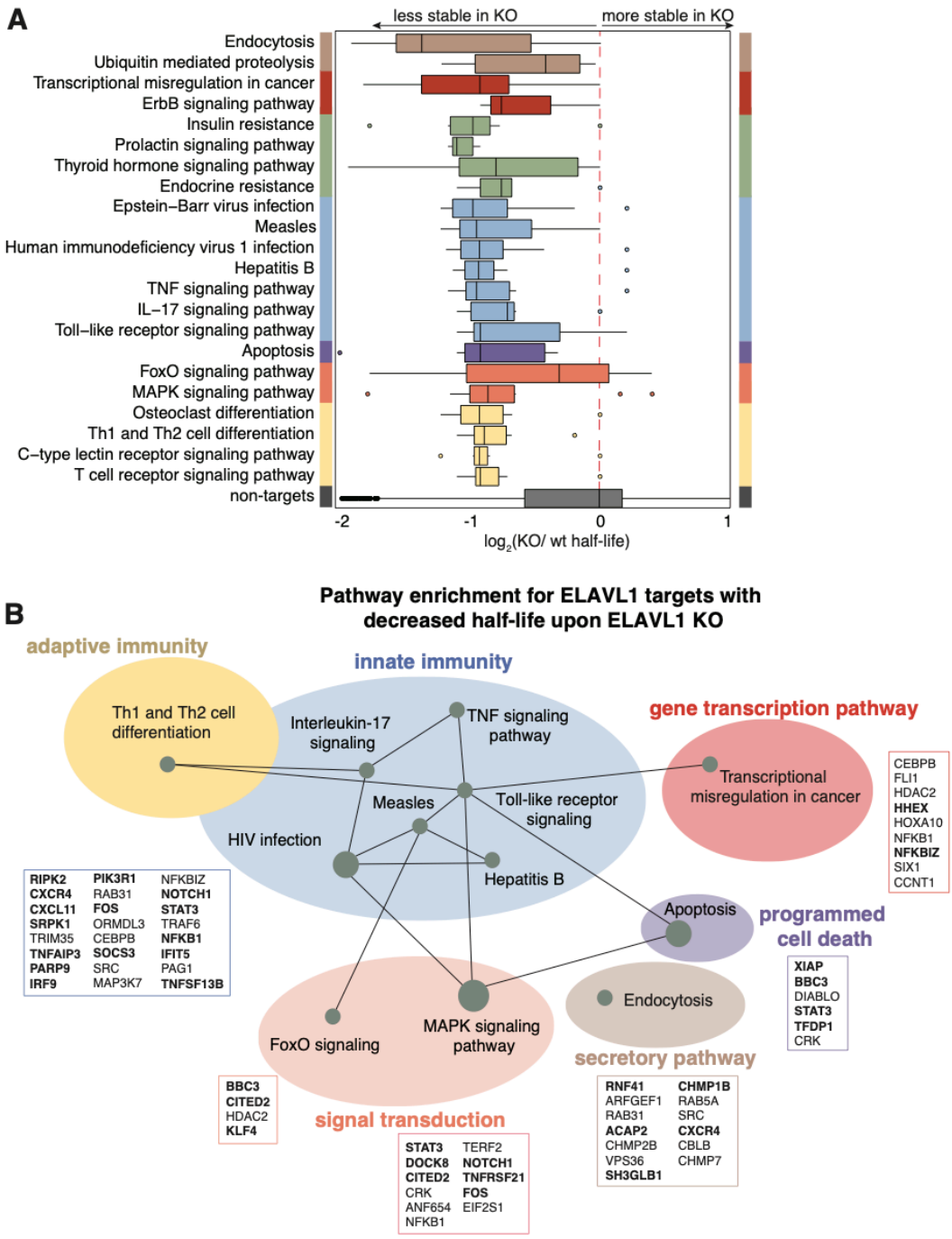

Figure 2.7 Canalization of ELAVL1 function towards the post-transcriptional regulation of immunologic pathways by IRF3 stimulation

(**A**) Box plot grouping transcripts based on the top enriched KEGG and Reactome pathway terms of the ELAVL-regulated targets protein components. Pathways were determined based on using the clusterProfiler R/Bioconductor package. Fisher's exact test using Benjamini-Hochberg FDR < 0.05. (**B**) Pathways of functional targets of ELAVL1. Each node represents a specific pathway, and colored circles represent closely related pathways. Connections represent shared genes between pathways. Boxes show specific mRNA transcripts and ISGs (bolded) in each pathway that are targeted by ELAVL1.

Discussion

We present a multi-layered analysis of high-throughput transcriptomics of the targeting and functional outcomes of the RBP ELAVL1 during an innate immune response. Using expression and PAR-CLIP data, we identified 98,689 naïve and 38,607 stimulated ELAVL1 RNA-binding sites. To date, this is the first report comparing how the binding properties and the targeting of an RBP change between steady-state and innate immune conditions. We find that ELAVL1 largely transitions to binding the 3'UTRs of mRNA transcripts during an innate immune response. 3'UTR binding is an absolute prerequisite for enrichment, and knockout of ELAVL1 led to widespread destabilization of its enriched transcripts. Specifically, we found that highly regulated targets had a three-fold average reduction in their stabilities, losing 30 to 80% of their original half-lives. Importantly, ELAVL1-regulated targets encode for ISGs and their transcriptional regulators, suggesting that ELAVL1 contributes at multiple levels of a pro-inflammatory response.

Two other ELAVL1 binding site reports performed in HeLa and BMDMs, show that ELAVL1 mostly binds the 3'UTR of mRNA targets (Lebedeva et al., 2011; Sedlyarov et al., 2016). In both of these reports, investigators immunoprecipitated ELAVL1 using endogenous antibodies for PAR-CLIP. In our hands, we found that endogenous antibodies obstructed RNA-protein interactions. Therefore, we used anti-Flag antibodies in this study and compared our results to the previous PAR-CLIP work performed in HEK293 cells, which used the same antibodies. Accordingly, we also observed a high proportion of ELAVL1 binding occurring at intronic sites, particularly during the naïve state. Nonetheless, our data did not show a link between ELAVL1 intronic sites and an increase in mature mRNA stability (Lebedeva et al., 2011; Mukherjee et al.,

2011). Those previous reports used microarrays that could detect introns and pre-mRNAs to discover an intron-dependent role of ELAVL1 for stabilizing pre-mRNAs. In contrast, our approach with SLAM-Seq was geared towards measuring the RNA decay rates of mature transcripts. While intuitively, changes in pre-mRNA levels would be predicted to contribute to the eventual levels of mature transcripts, we did not observe an intron-dependent effect on mature mRNAs. It is conceivable that our approach was insufficiently sensitive to detect intronic-dependent stability effects or that the two ELAVL1-dependent mechanisms are partially distinct.

One of the strongest signatures we were able to identify was a shift in the distribution of binding sites in favor of the 3'UTRs of mRNAs and speculate that this change is most likely due to the subcellular re-localization of ELAVL1 to the cytoplasm upon immune stimulation in THP-1 cells. As previously reported, ELAVL1 can be post-translationally modified by protein kinases and methylases, which can affect its nucleocytoplasmic localization and RNA-binding site distribution (Grammatikakis et al., 2016). Future studies using subcellular-restricted forms of ELAVL1 (e.g., phospho-ablated or phospho-mimetic) could add to the granularity of our understanding of how ELAVL1 transitions from binding intronic versus 3'UTR sites and its movement out of the nucleus. However, the subcellular localization of ELAVL1 can only partially explain our work since signal transduction and associated transcriptomic differences between naïve and stimulated states also play a role in defining the ELAVL1-regulated mRNA (Abe et al., 2012; Rabani et al., 2011). Given the presence of other post-transcriptional regulatory factors and elements, ELAVL1 likely competes with the actions of other RBPs, miRNA silencing machinery, and possibly viral RNAs that could act as competitors or sponges to titrate its activities away from cellular targets (Barnhart et al., 2013; Dassi, 2017; Hentze et al., 2018; B. Kim et al., 2020a; Lu et al., 2014). Therefore, when characterizing the function of a given RBP and its biological role, it is

important to consider how cellular context-specific factors can have a profound impact on how a target enriches with an RBP and the extent of its regulation.

Since transient associations can be identified between potential RNA targets and RBPs by CLIP methodologies, there is a need to quantify enrichment levels as a measure of interaction affinity. The stoichiometry of interactions between the limited number of RBP molecules and its changing RNA substrate pool makes it difficult to predict enrichment and post-transcriptional regulatory impact using information gleaned strictly from steady-state data, particularly for RBPs with a preference for highly redundant recognition sequences (Ascano et al., 2011). High throughput discovery methods, such as RNAcompete and RNA bind-n-Seq, show that most RBPs tested have convergent RNA recognition sequences (Dominguez et al., 2018a; Lambert et al., 2014; Ray et al., 2017). For 27 different RBPs (including ELAVL1), the preferred 6-mer binding site overlapped with the top-ranked 6-mer site of at least one other RBP, despite having distinct RNA-binding domains (Dominguez et al., 2018b). This observation underscores that many RBPs have similar and short binding-motif preferences of low-complexity (Adinolfi et al., 2019; Nussbacher and Yeo, 2018). Though these studies are valuable in discovering the primary and flanking sequence preferences of RBPs, these methods often analyze a single RBP in isolation and do not include competitor RBPs and miRNAs that will influence the RNA-substrate structure or the availability of a particular RNA binding site. Therefore, relying on sequence motifs and predicted RNA structure is insufficient to delineate the specific binding sites and the functional RNA targets of RBPs in specific cells and contexts. In recognizing these limitations, we integrated multiple high-throughput sequencing datasets to differentiate between RNA transcripts that are simply ‘sampled’ versus *bona fide* targets that are regulated during an immune signaling event.

For our functional analysis, we focused on the majority of targets, which exhibited a reduction in their half-lives in the absence of ELAVL1. We termed these mRNAs ELAVL1-regulated transcripts and performed pathway analysis to understand the cellular pathways that ELAVL1 could regulate during an immune response. Many of them (*NFKB1*, *IRF9*, *TAK1*, *STAT3*, *MAPK1*, and *MAPK*9) encode protein components involved in innate immune signaling that positively drive the expression of ISGs. These genes reinforce upstream signaling transduction events triggered by pathogen and nucleic-acid sensing, leading to enhanced cytokine and interleukin production and cellular differentiation. We speculate that ELAVL1 regulates these central signaling components to sensitize the cell for dealing with a pathogenic infection – allowing the cell to quickly integrate incoming pathogen- or damage-associated molecular pattern-triggered signaling. Furthermore, our data support the idea of an "RNA regulon" where an RBP can coordinate the expression of a group of functionally-related mRNAs (Keene, 2007; Simone and Keene, 2013). ELAVL1 regulates the mRNA of several biological processes within immune signal transduction pathways- from adaptor protein (TRAF6) to transcription factor (NF-kB, IRF9). ELAVL1 also regulates components of endocytosis, which plays a role in cytokine signaling and TLR receptor trafficking (Kurgonaite et al., 2015; Lund and DeLotto, 2014). Importantly, these transcripts were strongly regulated by ELAVL1 upon immune stimulation, despite many of these targets already being sampled by the RBP under naïve states.

Of note, we also observed that the half-lives of nearly 100 highly enriched transcripts increased in the absence of ELAVL1. Interestingly, these targets were associated with cell cycle pathways and were not associated with any innate immune terms. This observation suggests that ELAVL1 may also lead to target destabilization. It is conceivable that ELAVL1 could co-operate with distinct groups of other RBPs in a manner that allows it to regulate subsets of its targets as

functionally-related transcript groups, as has been previously postulated with the regulon hypothesis (Keene, 2007; Simone and Keene, 2013). When ELAVL1 interacts with trans-acting factors, it can form multiple RNPs that have distinct regulatory functions, and this may drive the stabilization fate of a subset of targets. Ultimately, the final regulatory effect that an mRNA is subject to will depend on the compendium of bound post-transcriptional factors.

With the increased interest in understanding the function of RBPs in gene regulation, numerous laboratories have undertaken essential and broad surveys of the target spectra of RBPs, largely under steady-state conditions (Castello et al., 2016; Darnell, 2010; Hafner et al., 2010; König et al., 2010; Nostrand et al., 2020; Ule et al., 2003; Van Nostrand et al., 2016). But it is important to recognize that RBPs represent a broad class of gene regulators that are post-translationally modified and are sensitive to cellular signaling events and changing transcriptomes. In examining the contribution of ELAVL1 to immune stimulation, we provide a general framework for studying other RBPs subject to analogous changes to a dynamic transcriptome or signal transduction event. This is especially relevant during host-pathogen interactions when substrate RNAs compete for post-transcriptional gene regulation by cellular proteins, leading to dramatic changes in the balance of host versus pathogenic transcript binding with limited trans-acting factors.

Table 2.1 RNA-Seq gene expression profiling

Example of DeSeq2 log^2 fold-change values between the IRF3 stimulated THP-1 cells and the naïve. The list shows the genes with the greatest upregulation due to innate immune stimulation.

Gene name	Base Mean	log^2 FoldChange	lfcSE	stat	p.value	p.adj
CCL8	22668.96	11.72	0.22	50.67	0.00	0.00
CXCL11	26035.54	11.44	0.19	57.70	0.00	0.00
CXCL10	66370.42	11.36	0.13	86.85	0.00	0.00
CCL4	5958.23	11.34	0.35	26.97	0.00	0.00
GBP1	15644.55	11.32	0.23	46.80	0.00	0.00
CCL4L2	9335.30	11.10	0.27	38.15	0.00	0.00
CCL4L1	9073.36	11.01	0.26	38.51	0.00	0.00
IDO1	7181.87	10.98	0.29	34.17	0.00	0.00
IL29	2408.89	10.88	0.45	16.62	0.00	0.00
IFI27	8862.53	10.80	0.25	39.83	0.00	0.00
CXCL9	4404.14	10.61	0.32	28.93	0.00	0.00
IFI44L	40317.64	10.60	0.13	78.95	0.00	0.00
CD80	4750.78	10.40	0.29	32.29	0.00	0.00
RGAG1	1190.49	9.93	0.46	15.18	0.00	0.00
IGFBP3	21105.25	9.92	0.14	71.71	0.00	0.00
CCL2	25900.33	9.91	0.28	35.15	0.00	0.00
SERPIND1	1532.03	9.87	0.41	19.22	0.00	0.00
CFH	2310.94	9.86	0.34	25.24	0.00	0.00
KDM6A	840.37	9.82	0.52	11.28	0.00	0.00
OASL	18325.48	9.82	0.14	67.70	0.00	0.00
IFNB1	1341.97	9.80	0.43	17.82	0.00	0.00
IFI44	20179.48	9.79	0.14	69.97	0.00	0.00
IFIT1	12602.80	9.79	0.16	59.38	0.00	0.00
CCR7	1920.51	9.77	0.36	23.21	0.00	0.00
CRLF2	6830.55	9.74	0.20	46.01	0.00	0.00
CCL7	907.13	9.73	0.49	13.22	0.00	0.00
IFIT2	32630.73	9.73	0.11	85.02	0.00	0.00
ISG20	8236.25	9.73	0.19	49.87	0.00	0.00
SLAMF7	4070.26	9.70	0.25	36.08	0.00	0.00
LAMP3	4619.18	9.65	0.24	38.73	0.00	0.00

Table 2.2 Summary of the PAR-CLIP called binding sites

Summary tables of the number of clusters and transcripts bound by ELAVL1 across naïve and innate immune stimulated conditions.

	naïve clusters	naïve RNA transcripts		IRF3 cluster	IRF3 RNA transcripts
PARalyzer*	133,742	9,854		50,074	7,563
RIP- and RNA-Seq data**	106,081	7,650		40,681	6,255
RNA-Seq > 5 CPM ***	99,461	6,465		39,021	5,596
mRNA ******	95,810	5,231 (mRNA transcripts)		38,473	5,381 (mRNA transcripts)

* (≥ 2 unique T-to-C sites, > 20% T-to-C ratio)

** clusters that had RIP- and RNA-Seq data

*** transcripts > 5 counts per million (CPM)

****clusters found in intron, 5'UTR, coding, 3'UTR

Table 2.3 PAR-CLIP cluster level meta-data

Example of PAR-pipe output file. Table shows the number of clusters for each transcript and also lists the number of binding sites per transcript feature, the genomic coordinates, sequence of the binding site, and the T-to-C fraction.

Gene name	5UTR	Intron	Exon	3UTR	Chr	Start	End	Cluster Sequence	Aligned to	T2C fraction	Strand
NOC2L	0	0	0	1	chr1	879638	879663	TCACATTTTCTTTTAAAATTTTTTGT	3'utr	0.92	-
SDF4	0	1	0	1	chr1	1152310	1152336	AATCACATACATTTACTTTAAATATAG	3'utr	1.00	-
UBE2J2	0	0	0	2	chr1	1189294	1189317	TCTTTCATTATATCTTTATTTCTG	3'utr	1.00	-
CPSF3L	0	2	0	0	chr1	1253660	1253685	TTTTATTTATATATTTATCCTTTTTG	intron	0.81	-
DVL1	0	0	0	1	chr1	1270675	1270695	CTTATTTTAAACACTAAAAAG	3'utr	1.00	-
CCNL2	0	3	0	1	chr1	1326459	1326483	CTTTTTTTTTTTCTAATAATTTCTG	intron	0.65	-
CCNL2	0	3	0	1	chr1	1330628	1330647	TTTCTATTTATAATCTCAAG	intron	1.00	-
MRPL20	0	0	0	1	chr1	1337374	1337395	TTTATCTACAACCCAATAACAG	3'utr	0.91	-
SSU72	0	4	0	5	chr1	1477205	1477226	TTTTTCTTCTTTAACCAAAAAG	3'utr	0.90	-
SSU72	0	4	0	5	chr1	1477248	1477273	TTTCTTCTTTTCCACTTTTACTTATG	3'utr	0.89	-
SSU72	0	4	0	5	chr1	1477385	1477404	TTCATACTTTTTCCTTCCTG	3'utr	0.94	-
SSU72	0	4	0	5	chr1	1504553	1504577	TTTTTTTCTTTTATTTTATTTTTTG	intron	0.71	-
SLC35E2B	0	0	0	2	chr1	1594382	1594402	ACATTTTTTAAAATAACTTTG	3'utr	1.00	-
SLC35E2B	0	0	0	2	chr1	1595230	1595250	ATTTCCATTTCTTTTTTTCTG	3'utr	0.81	-
SLC35E2	0	2	0	0	chr1	1660271	1660291	ACATTTTTTTAAATAACTTTG	intron	1.00	-
GNB1	0	16	0	9	chr1	1718004	1718027	CATTCATATTTCCTTTTTAAAATG	3'utr	0.91	-

Table 2.4 Combine RIP-Seq, RNA-Seq and PAR-CLIP data

Combined table of the RIP-Seq enrichment data for each condition and PAR-CLIP binding site date. Organized by transcript, each row contains the condition specific expression level, enrichment level, and binding site data.

gene short name	naive mean counts	IRF3 mean counts	normalized Flag naive	normalized Flag IRF3	naïve 5UTR	naive Intron	naive Exon	naive 3UTR	IRF3 5UTR	IRF3 Intron	IRF3 Exon	IRF3 3UTR
PDGFA	6.96	9.92	0.66	6.76	0	0	0	5	0	0	0	2
RND3	5.30	11.66	-0.73	6.55	0	3	0	4	0	1	0	4
UBE2E2	9.67	11.18	1.52	6.00	0	67	0	3	0	171	0	4
MARCKS	10.39	12.83	0.46	5.98	1	0	0	4	2	0	0	4
SDC4	8.22	11.95	1.48	5.94	0	0	0	6	0	0	0	5
OTUD1	7.20	10.74	0.37	5.77	0	0	0	9	0	0	0	6
PHLDA1	5.18	9.82	-1.32	5.58	0	0	0	9	0	0	0	10
MXD1	8.65	13.01	0.99	5.56	0	3	0	12	0	3	0	9
ADRB1	9.26	8.93	1.08	5.56	0	0	0	0	0	0	0	0
PABPN1	9.95	9.90	1.58	5.50	0	0	0	2	0	0	0	5
RAP2B	9.37	10.64	2.00	5.47	0	0	0	6	0	0	0	9
PAFAH1B2	10.96	10.95	1.90	5.44	0	0	0	9	0	4	0	12
LIN7C	9.14	9.83	1.96	5.35	0	1	0	17	0	0	0	22
SRSF6	12.93	12.57	2.20	5.29	0	1	0	2	0	2	0	4
C1orf55	10.16	10.72	1.68	5.27	0	0	0	0	0	0	0	0
PDIA4	12.28	13.06	1.74	5.23	0	0	0	4	0	0	0	4
CPEB4	8.55	10.75	0.27	5.21	1	3	0	17	1	4	1	17
TMOD3	10.32	11.41	1.38	5.21	0	1	0	12	0	3	0	18
TRPS1	9.94	11.40	0.65	5.21	0	26	0	14	0	121	0	19

Table 2.5 Reactome analysis for RIP-Seq enriched targets

Reactome pathway analysis for the enriched ELAVL1 targets in the stimulated condition.

ID	Description	GeneRatio	BgRatio	pvalue	p.adjust	qvalue
R-HSA-2029480	Fcgamma receptor (FCGR) dependent phagocytosis	20/701	86/10619	5E-07	6E-04	5E-04
R-HSA-9006934	Signaling by Receptor Tyrosine Kinases	58/701	458/10619	1E-06	6E-04	5E-04
R-HSA-983169	Class I MHC mediated antigen processing & presentation	48/701	371/10619	5E-06	1E-03	1E-03
R-HSA-166520	Signaling by NTRKs	20/701	99/10619	6E-06	1E-03	1E-03
R-HSA-975138	TRAF6 mediated induction of NFkB and MAP kinases upon TLR7/8 or 9 activation	19/701	92/10619	7E-06	1E-03	1E-03
R-HSA-3700989	Transcriptional Regulation by TP53	47/701	365/10619	7E-06	1E-03	1E-03
R-HSA-168181	Toll Like Receptor 7/8 (TLR7/8) Cascade	19/701	93/10619	8E-06	1E-03	1E-03
R-HSA-975155	MyD88 dependent cascade initiated on endosome	19/701	93/10619	8E-06	1E-03	1E-03
R-HSA-166016	Toll Like Receptor 4 (TLR4) Cascade	23/701	129/10619	1E-05	1E-03	1E-03
R-HSA-166058	MyD88:MAL(TIRAP) cascade initiated on plasma membrane	19/701	95/10619	1E-05	1E-03	1E-03
R-HSA-168188	Toll Like Receptor TLR6:TLR2 Cascade	19/701	95/10619	1E-05	1E-03	1E-03
R-HSA-450294	MAP kinase activation	15/701	64/10619	1E-05	1E-03	1E-03
R-HSA-168138	Toll Like Receptor 9 (TLR9) Cascade	19/701	97/10619	2E-05	1E-03	1E-03
R-HSA-168179	Toll Like Receptor TLR1:TLR2 Cascade	19/701	98/10619	2E-05	1E-03	1E-03
R-HSA-181438	Toll Like Receptor 2 (TLR2) Cascade	19/701	98/10619	2E-05	1E-03	1E-03

R-HSA-194138	Signaling by VEGF	20/701	107/10619	2E-05	1E-03	1E-03
R-HSA-2454202	Fc epsilon receptor (FCERI) signaling	23/701	134/10619	2E-05	1E-03	1E-03
R-HSA-166166	MyD88-independent TLR4 cascade	19/701	99/10619	2E-05	1E-03	1E-03
R-HSA-937061	TRIF(TICAM1)-mediated TLR4 signaling	19/701	99/10619	2E-05	1E-03	1E-03
R-HSA-168898	Toll-like Receptor Cascades	25/701	155/10619	3E-05	2E-03	1E-03
R-HSA-381340	Transcriptional regulation of white adipocyte differentiation	17/701	84/10619	3E-05	2E-03	1E-03
R-HSA-983168	Antigen processing: Ubiquitination & Proteasome degradation	40/701	309/10619	3E-05	2E-03	1E-03
R-HSA-168164	Toll Like Receptor 3 (TLR3) Cascade	18/701	94/10619	4E-05	2E-03	1E-03
R-HSA-187037	Signaling by NTRK1 (TRKA)	16/701	78/10619	4E-05	2E-03	2E-03
R-HSA-9006925	Intracellular signaling by second messengers	39/701	305/10619	5E-05	2E-03	2E-03
R-HSA-449147	Signaling by Interleukins	53/701	463/10619	5E-05	2E-03	2E-03
R-HSA-448424	Interleukin-17 signaling	15/701	72/10619	6E-05	2E-03	2E-03
R-HSA-114604	GPVI-mediated activation cascade	10/701	35/10619	6E-05	2E-03	2E-03
R-HSA-4420097	VEGFA-VEGFR2 Pathway	18/701	99/10619	7E-05	3E-03	2E-03
R-HSA-400206	Regulation of lipid metabolism by Peroxisome proliferator-activated receptor alpha (PPARalpha)	20/701	119/10619	9E-05	4E-03	3E-03
R-HSA-168142	Toll Like Receptor 10 (TLR10) Cascade	16/701	85/10619	1E-04	4E-03	3E-03
R-HSA-168176	Toll Like Receptor 5 (TLR5) Cascade	16/701	85/10619	1E-04	4E-03	3E-03
R-HSA-975871	MyD88 cascade initiated on plasma membrane	16/701	85/10619	1E-04	4E-03	3E-03

Table 2.6 SLAM-seq RNA half-lives
Representative table of the SLAM-seq calculated RNA half-lives for the transcripts listed.

geneId	SYMBOL	half-life
ENSG00000000971.11	CFH	1.38629436
ENSG00000001497.12	LAS1L	6.72746518
ENSG00000001561.6	ENPP4	0.44209335
ENSG00000001629.5	ANKIB1	24
ENSG00000001630.11	CYP51A1	7.07963664
ENSG00000001631.10	KRIT1	12.7292572
ENSG00000002016.12	RAD52	1.38629436
ENSG00000002549.8	LAP3	6.12471682
ENSG00000002822.11	MAD1L1	14.6452905
ENSG00000002834.13	LASP1	1.38629436
ENSG00000002919.10	SNX11	5.38575563
ENSG00000003393.10	ALS2	1.38629436
ENSG00000003402.15	CFLAR	1.38629436
ENSG00000003756.12	RBM5	1.38629436
ENSG00000004399.8	PLXND1	24
ENSG00000004487.11	KDM1A	12.0755553
ENSG00000004660.10	CAMKK1	6.60118104
ENSG00000004779.5	NDUFAB1	22.574241
ENSG00000004799.7	PDK4	1.38629436
ENSG00000004809.9	SLC22A16	8.3285124
ENSG00000004838.9	ZMYND10	1.38629436
ENSG00000004866.14	ST7	1.38629436
ENSG00000005007.8	UPF1	5.12124486
ENSG00000005022.5	SLC25A5	24
ENSG00000005175.5	RPAP3	10.6295034
ENSG00000005187.7	ACSM3	1.38629436
ENSG00000005189.15	REXO5	8.75672914
ENSG00000005302.13	MSL3	2.43995062
ENSG00000005379.11	TSPOAP1	1.38629436
ENSG00000005483.15	KMT2E	1.38629436
ENSG00000005486.12	RHBDD2	16.6314807

Table 2.7 Reactome pathway analysis of the functional targets of ELAVL1

Reactome pathway analysis of the functional targets of ELAVL1.

Enrichment FDR	Genes in list	Total genes	Functional Category	Genes
2E-05	17	163	Protein processing in endoplasmic reticulum	UBE4B MAN1A2 SEC31A UBQLN1 LMAN1 UBE2J1 DNAJB11 SEC61A2 MAPK9 MAP2K7 RAD23B SSR1 XBP1 EDEM3 SYVN1 HERPUD1 SEC24D
2E-04	19	244	Endocytosis	RNF41 ARFGEF1 RAB35 VPS37A RAB11FIP2 ACAP2 PSD4 CHMP2B VPS36 SH3GLB1 VPS29 CHMP1B RAB5A SRC TRAF6 RABEP1 CHMP7 VPS26A DNAJC6
2E-04	13	126	Osteoclast differentiation	IRF9 FOS JUND NFATC2 NFKB1 PIK3R1 PPP3CA MAPK1 MAPK9 MAP2K7 MAP3K7 TRAF6 SOCS3
2E-04	12	110	TNF signaling pathway	CEBPB FOS MMP14 NFKB1 PIK3R1 MAPK1 MAPK9 MAP2K7 MAP3K7 TNFAIP3 SOCS3 RPS6KA5
1E-03	10	92	IL-17 signaling pathway	CEBPB FOS USP25 JUND NFKB1 MAPK1 MAPK9 MAP3K7 TNFAIP3 TRAF6
2E-03	13	162	Hepatitis B	FOS NFATC2 NFKB1 PIK3R1 MAPK1 MAPK9 MAP2K7 BID SRC STAT3 MAP3K7 TRAF6 CCNE1
2E-03	12	138	Measles	IRF9 FOS RCHY1 NFKB1 PIK3R1 MAPK9 BID STAT3 MAP3K7 TNFAIP3 TRAF6 CCNE1
2E-03	10	101	T cell receptor signaling pathway	DLG1 FOS NFATC2 NFKB1 PIK3R1 PPP3CA MAPK1 MAPK9 MAP2K7 MAP3K7
2E-03	11	128	Autophagy	CTSB WIPI2 NRBF2 SH3GLB1 PIK3R1 PRKAA1 MAPK1 MAPK9 MAP3K7 TRAF6 ATG13
3E-03	8	70	Prolactin signaling pathway	FOS NFKB1 PIK3R1 MAPK1 MAPK9 SRC STAT3 SOCS3
3E-03	11	135	Ubiquitin mediated proteolysis	UBE4B UBE2C RCHY1 UBE2J1 UBE2W TRAF6 UBE2A UBE2H SYVN1 CUL4A SOCS3
4E-03	14	211	Human immunodeficiency virus 1 infection	FOS NFATC2 NFKB1 PIK3R1 PPP3CA MAPK1 MAPK9 MAP2K7 BID MAP3K7 TRAF6 CUL4A AP1S2 AP1M1
6E-03	9	103	Toll-like receptor signaling pathway	FOS NFKB1 PIK3R1 MAPK1 MAPK9 MAP2K7 CXCL11 MAP3K7 TRAF6

Table 2.8 Primers and gRNAs

Primer pairs used throughout Chapter II especially for the RIP RT-qPCR. Also, the guide RNAs used for the Cas9 KO of ELAVL1 in THP-1 cells.

Target	Name	Sequence
TUBA1A	TUBA1A qt F	GAGCGTCCAACCTATACTAACC
	TUBA1A qt F	GCAGCAAGCCATGTATTTACC
NFKB1	NFKB1 qt F 3226	AGACATCCTTCCGCAAACTC
	NFKB1 qt 3681	GGCGACCGTGATACCTTTAAT
MAPK1	MAPK1 qt F 3941	GGAACAGCACCTCCACTATTT
	MAPK1 qt R 4147	GCCACAATGTCTGCGTATCT
JUND	JUND qt F 1590	GAGTGTTCGATTCTGCCCTATT
	JUND qt R 1846	GCTGGCGTAACGAGACTTTA
IFIT5	IFIT5 qt F 787	CGGCTGGATGATTCTGATAGAG
	IFIT5 qt R1126	GTGTGTGGCCTTCTTGATTTG
TLR1	TLR1 qt F 1737	GCTTTAGCAGCCTTTCTGTATTG
	TLR1 qt R2007	GTGACGATCAGCAGAGTTATGT
TLR5	TLR5 qt F 2154	CCCTTCCACCAGGAGTATTTAG
	TLR5 qt R2465	TGGAAAGAGAGAAGAGGGAAAC
DGK2	DGK2 qt F 1107	CGAGCAGCTGGAGAAGATAAA
	DGK2 qt R1625	GGGATTGAGATACCAGAGGAAAG
PLCB2	PLCB2 qt F 1869	GTGACGGCTTATGAGGAGATG
	PLCB2 qt R2402	GGGTGACAGCTTAGTTCGATAG
IGBP1	IGBP1 qt F 184	GAGCTGTTCGAAACTGGTAGA
	IGBP1 qt R575	CCATAGCAACGAGACTAGGATAAG
XRN1	XRN1 qt F 3794	GCAACATTTGGCAGTCCTTAC
	XRN1 qt R4273	GGCTGAGAGGGTAATCCATATTC
IRF9	IRF 9 qt F 1431	CCACCTCACCTCTTTGTTCTT
	IRF 9 qt R1650	GGGTTCACACCATTTGGAATTT
XIAP	XIAP qt F 4401	ACTCAGCACTCCAACTTCTAATC
	XIAP qt R4837	TACCCTACCTTAGCCCGTAATC
IFITM3	IF ITM3 qt F 268	GCTTCATAGCATTCGCCTACT

	IF ITM3 qt R546	GTGTGAGGATAAAGGGCTGATAC
ILF2	ILF 2 qt F 1222	CCTCAAGGAGAGGAAGAAGAAAG
	ILF 2 qt R1418	GACTGGCAGCTAAGCCAATA
FireFly	FiReFly qt F 1000	CCAGGTATCAGGCAAGGATATG
	FiReFly qt R1271	GTTCGTCTTCGTCCCAGTAAG
DUSP10	DUSP10 qt F 1400	CACCATCGTCATCGCTTACT
	DUSP10 qt R1640	CATCCTCCTTCCTCATTGTCTC
TNFRSF21	TNFRSF 21 qt F 3114	CAAGCCATCAGGATTTGCTATT
	TNFRSF 21 qt R3451	CCTGGCAACTGAGCATTAGA
** for luciferase 3'UTR assay*	IRF9_3UTR_ELAVL1_specificsite1_R	GAAAGAGGGCGTATATCTCAAAATT
	IRF9_3UTR_ELAVL1_commonsite1_F	GATTGACCTGTCCTCTTTGTG
	IRF9_3UTR_ELAVL1_specificsite2_R	GTCCTTAGTGAATATCTAAGAGGAAA
	IRF9_3UTR_ELAVL1_commonsite1_R	TAGAGTTGGGAGGTCAGGG
	mutant_IRF9_3UTR_bindsite2_R	GTCCTTAGTGAATATTTTTTTTTTTTTTTT
	mutant_IRF9_bindsite1_R	GAAAGAGGGCGTATATCTTTTTTTTT
ELAVL1 F sgRNA1	sgRNA1	CACCgTGTGAACTACGTGACCGCGA
ELAVL1 R sgRNA1	sgRNA1	CACACTTGATGCACTGGCGCTCAAA
ELAVL1 F sgRNA2	sgRNA2	CACCgTATCCGGTTTGACAAACGGT
ELAVL1 R sgRNA2	sgRNA2	CATAGGCCAAACTGTTTGCCACAAA
ELAVL1 F sgRNA3	sgRNA3	CACCgTCGCCAGCGCGACGGTTCGG
ELAVL1 R sgRNA3	sgRNA3	CAGCGGTCGCGCTGCCAAGCCCAAA

CHAPTER III: IFIT1 BINDS HOST mRNA DURING AN INNATE IMMUNE RESPONSE

Introduction

The IFIT genes encode for a family of single-stranded RNA binding proteins (RBPs) that function as antiviral effectors by potentially inhibiting the translation of viral mRNA. The IFIT family's gene expression are tightly regulated and strongly induced in the presence of a virus and during a type-I interferon response. Recently, it was shown that one of the IFIT family members, IFIT1, could distinguish between different mRNAs based on the nature of the 5' untranslated region (UTR) (Johnson et al., 2018). IFIT1 could differentiate between 5'-triphosphorylated RNAs (PPP) RNAs, non-methyl guanosine-capped RNAs, and differentially 2'-O-methylated guanosine-capped mRNAs (Abbas et al., 2017). Given that these types of 5' UTR modifications also exist in cellular RNAs, it remains unclear how IFIT1 selectively associates with certain viral RNAs and not cellular RNA. An alternative hypothesis would predict that IFIT1 can associate with cellular RNA, but perhaps in a condition-dependent or topology-dependent fashion that has, as yet, prevented the identification and isolation of these host-encoded transcripts. Indeed, other IFIT protein family members (IFIT2 and IFIT5) have been shown to associate with host-encoded RNAs (Hubel et al., 2019). To date, no research has directly shown in vivo that IFIT1 binds to any viral RNA or cellular RNA.

IFIT1 binds host Pol II mRNAs

To test whether IFIT1 binds host mRNA, I performed PAR-CLIP with an additional step. In PAR-CLIP, RNA bound to the RBP of interest is 5' radiolabeled using CIP, T4-PNK, and ^{32}P-ATP. This step assumes that the 5' of the bound RNA has a monophosphate. Yet, if the bound RNA has a 5' 7-methylguanosine cap, the RNA cannot be labeled using this method. Therefore, when performing PAR-CLIP on IFIT1, I added an additional de-capping step using a pyrophosphatase before the CIP, T4-PNK, and ^{32}P-ATP radiolabeling step (Figure 3.1). When comparing the amount of radiolabeled bound RNA with and without decap, there is a greater amount of signal of radiolabeled RNA with the addition of the decapping step. This suggests that IFIT1 preferentially binds 7-methylguanosine cap RNAs. These observations also indicate that previous attempts at mapping IFIT1 binding sites can be missing a significant population of IFIT1 targets. This is because conventional cloning approaches for identifying RNA binding sites are not capable of capturing 5'-UTR termini, given the chemical nature of capped transcripts. To overcome this limitation, we are investigating approaches that allow this association to be identified by adding an m7G mRNA decapping step to our lab's well-established method of mapping RNA-binding protein-RNA interactions (PAR-CLIP protocol). This additional technique makes the 5' ends of capped RNA amenable to downstream cloning steps and eventual sequencing.

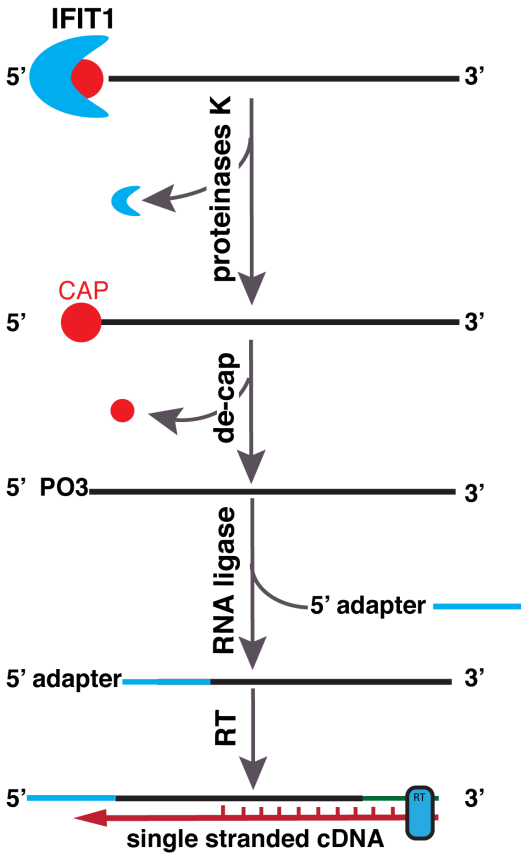

Figure 3.1 Experimental protocol of the removal of the 5' cap of IFIT1 bound mRNAs before adaptor ligation and library prep.
In order to sequence IFIT1 bound transcripts there is a new to remove the N7-methylguanosine cap before subsequent adaptor ligation steps. IFIT1 binds the 5' cap with high affinity; therefore, after the RBP has been immunoprecipitated and degraded by proteinase K there is a need to remove the 5' cap. Adaptor ligation allows for amplification and library prep of IFIT1-bound transcripts.

Through the use of biochemical methods, this data shows for the first time that IFIT1 binds cellular RNA and preferentially binds the m7G-cap of polymerase II mRNA transcripts in vivo (Figure 3.2). To control that the decapping step didn't cause an increase in ^{32}P signal in non-capped mRNAs, we performed the decapping protocol on ELAVL1 bound RNAs. ELAVL1 primarily binds introns and 3'UTR of mRNAs. Thus, the RNA bound would not contain 5' cap nor would there be an increase in signal due to the addition of a decapping step. ELAVL1 bound RNAs did not increase in signal with the addition of the decapping step, indicating that the decapping step is specific in the removal of 5' cap and not causing general RNA degradation.

This observation uncovers a potential new antiviral mechanism of IFIT1. However, what is unknown and needs further research are the identities of the mRNA targets of IFIT1 and how IFIT1-mRNA interactions impact the antiviral response of a cell. Our lab has shown that IFIT1 does not bind Chikungunya alphavirus genome despite being upregulated during infection, suggesting that IFIT1 has a host/cellular role in the innate immune response other than directly inhibiting the viral RNA. Given my preliminary data and established in vitro data of IFIT1, there is a clear need to comprehensively identify the RNA targets of IFIT1 in a whole transcriptome-wide manner during an innate immune response.

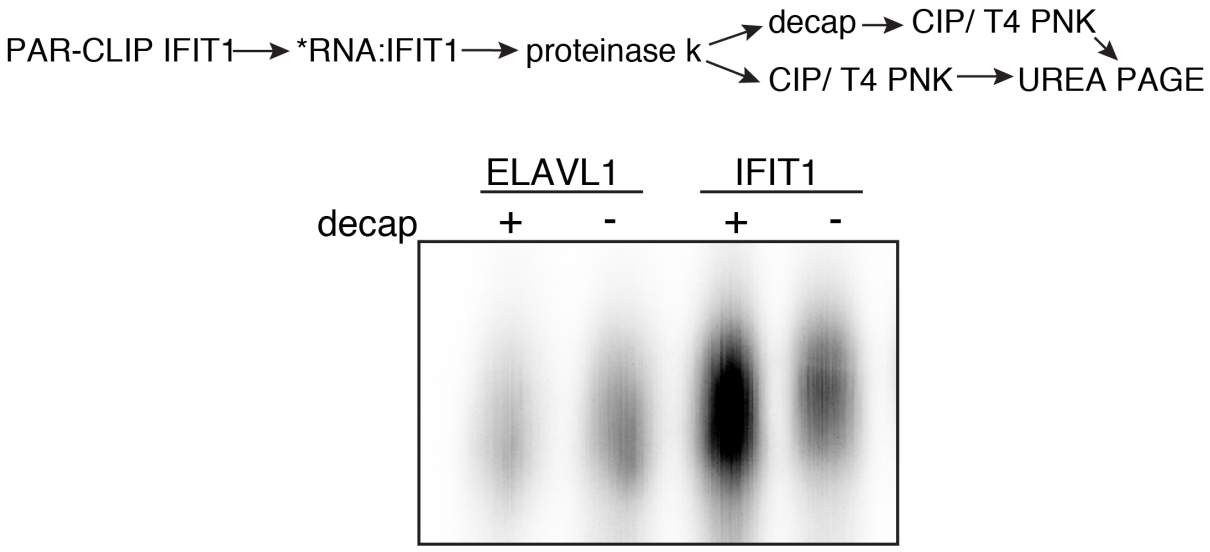

Figure 3.2 IFIT1 binds the 5' cap of cellular mRNAs in THP-1 cells.
In order to confirm that IFIT binds cellular RNA, PAR-CLIP was performed on Flag-HA tagged IFIT1 in THP-1 cells. Bound RNA proceeded through the indicated RNA labeling steps (either +/- decapping enzyme). De-capped IFIT1 bound RNA has a higher ^{32}P signal than non-decapped RNA, denoting that IFIT1 binds the 5'cap of cellular RNA. ELAVL1, which predominately binds introns and 3'UTRs, was used a negative control ensuring that decapping process does not increase ^{32}P signal of non-capped mRNAs.

CHAPTER IV: DISCUSSION and OUTLOOK

In the past few years, there has been a rapid increase in the number of methods to probe RNA-protein interactions (Figure 4.1). The strategies of capturing the RNA-protein interactions range from identifying a particular gene's RNA interactome (RAP, ChIRP, RaPID) to unbiased capture that identifies all mRBPs or RBPs within a specific cell type (RIC, CLASP) (Engreitz, Lander, and Guttman 2015; Kim et al. 2020; Licatalosi, Ye, and Jankowsky 2020; Ramanathan, Porter, and Khavari 2019). The final steps of these protocols are the identification of bound RBPs via mass spectrometry. RNA-antisense purification (RAP) and Chromatin isolation by RNA purification (ChIRP) both use UV crosslinking along with anti-sense oligos to enrich for a sequence specific RNA of interest (Chu, Quinn, and Chang 2012). RNA-protein interaction detection (RaPID) uses newer techniques through the combination of an RNA component, such as BoxB stem-loop or MS2, with proximity labeling. The RNA stem-loop component allows picomolar affinity with the RaPID fusion protein that contains a biotin-ligase. Thus, when the RaPID fusion protein binds the RNA stem-loop, the biotin-ligase biotinylates proteins proximal to the stem-loop. Streptavidin beads can then be used to capture biotinylated proteins. There are also numerous approaches to sequence the RNA targets and binding sites of a specific RBP in a whole transcriptomic manner. These RBP-centric approaches are dominated by numerous CLIP methodologies such as, eCLIP, iCLIP, HITS-CLIP, PAR-CLIP

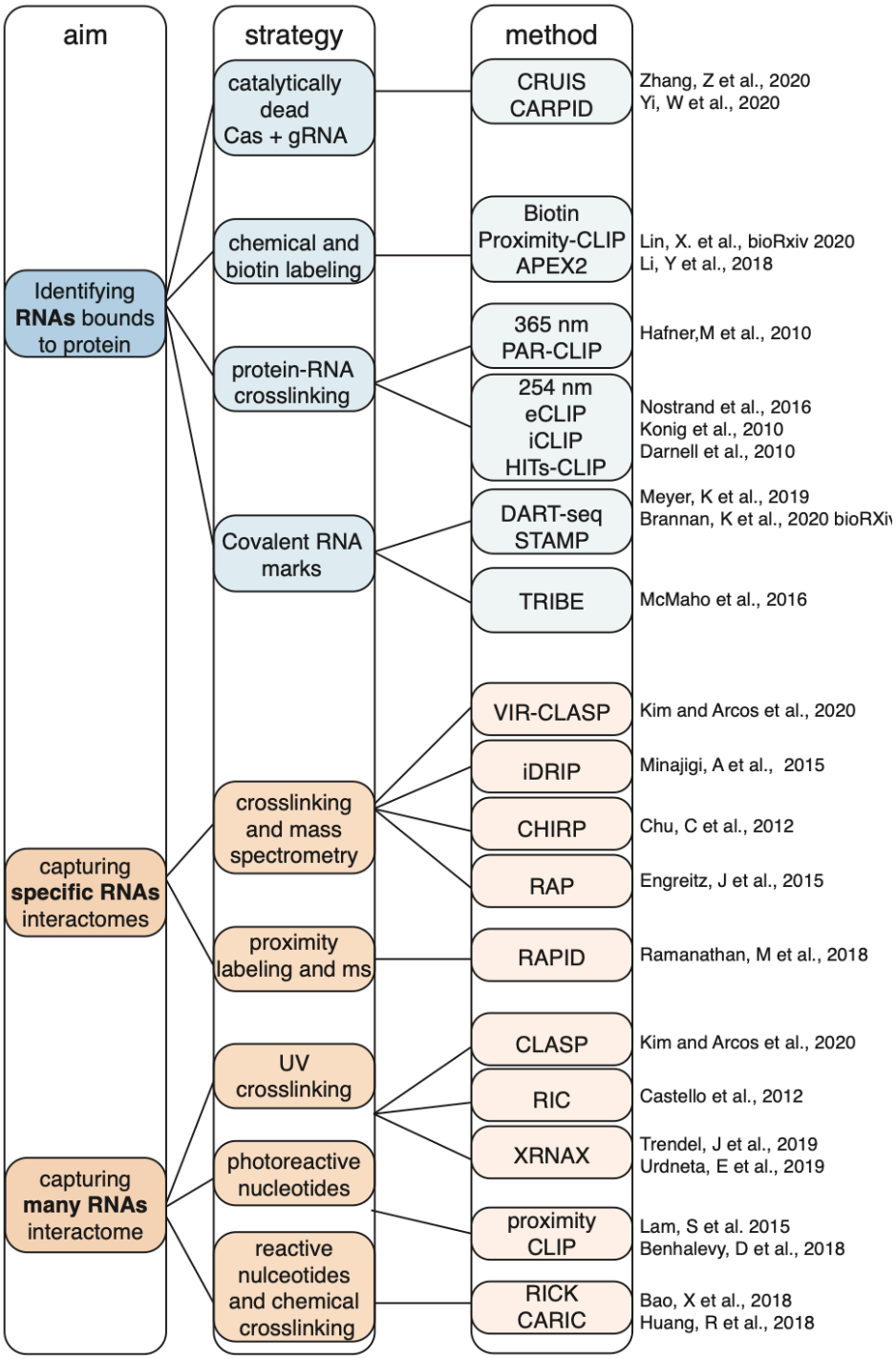

*****inspired from Liscatalosi et al., 2020*

Figure 4.1 Methods to capture RNA-protein interactions
A list of the major methods that capture RNA-protein interactions. The nodes highlighted in blue are RBP-centric whereas the orange nodes are RNA-centric.

(Darnell 2010; Van Nostrand et al. 2016; König et al. 2010; Hafner et al. 2010). These methods are all variations off of the core steps of covalent protein-RNA crosslinking with immunoprecipitation followed by subsequent cDNA library sequencing and analysis (reviewed in (Hafner et al. 2021)). CLIP methodologies are limited by the effectiveness and the background signal of the antibody used to IP for the RBP of interests –especially when using endogenous antibodies are used. Endogenous antibodies may block RNA-binding domains or enrich for RBPs not bound to RNA. Newer approaches such as Targets of RBPs Identified By Editing (TRIBE), Deamination Adjacent to RNA modification Target (DART-Seq), and APOBEC-mediated profiling (STAMP) use enzymatic tagging approaches that allow for transcriptome wide identification of RBP binding-sites without crosslinking, immunoprecipitation, or cDNA library synthesis. TRIBE, DART-Seq, and STAMP use the transgenic expression of an RBP of interest fused to the catalytic domain of ADAR or APOBEC, which causes RNA edited sites near the RBP interaction site (A-to-I in dsRNA or C-to-U in ssRNA, respectively) (Meyer 2019; McMahon et al. 2016). These methods are advantageous due to the few handling steps of the RNA, allowing for a much smaller amount of input material needed. Once sequenced, the RNA edited reads are then compiled and used to call binding sites of the RBP. STAMP enzymatically labels ssRNA enabling the method to use for single-cell analysis of RBP's RNA targets (Brannan et al. 2020).

With the plethora of different methods, the field is better able to capture the precise binding sites of RBPs in cells or even a single cell. However, many of the RNA-protein interaction experiments are carried out under steady-state conditions and cell types, HEK293 or HeLa, that do not reflect the biological process being examined. Therefore, when considering the function of an RBP and its biological role, it is important to consider the context-specific factors that determine the RNA targets of that RBP: (i) Many RBPs have a wide domain of expression (expressed in

numerous cell types and cellular compartments), and each domain of expression has a distinct transcriptome that can interact with the RBPs. (ii) Changes in the cellular environments (i.e., differentiation, immune response) affect the transcriptome. (iii) Levels and the post-translation states of competing RBPs are specific for each domain of expression and cellular environment. (iv) viral-RNA can interact and usurp host RBPs affecting PTGR and the immune fitness of a cell. Therefore, there is a need to integrate the different components of the post-transcriptional landscape listed above, through both biochemical and high-throughput analyses in order to drill down the exact binding properties and functional outcome of a particular RBP.

Though there are numerous screens to identify new RBPs and their cognate targets, an area of the PTGR that is anemic is how post-translational modifications affect an RBP's function and binding affinity. Recently, in an unbiased systematic identification of protein phosphorylation-mediated interactions, the GO terms for the top hits were RNA binding proteins (Floyd et al., 2021). This observation suggests phosphorylation plays a significant role in RNA binding. We know that ELAVL1 can be post-translational modified at numerous sites, but what much more is needed to parse out how these modifications affect RNA targeting. Another area of PTGR that is not well understood and would add a lot of depth to the post-transcriptional field is to study the stoichiometry of binding between ELAVL1, or any RBP, and its RNA-targets during an immune response. For example, within the nucleus how many ELAVL1 molecules are actively bound to RNA at a particular time. This analysis can be extended to look at the different cellular compartments and examine if the stoichiometry between ELAVL1 and RNA differs due to the cellular location. This type of quantitative approach would give insight into RNA-protein dynamics.

In part, this dissertation highlights the experimental and resource limitations on the ability to comprehensively identify the cell-type or tissue-type specific targets of a given RBP for all areas that it is expressed. However, this dissertation also provides an example of a strategy for how to study RBPs that are subject to a dynamic transcriptome or signal transduction event. The integration of biochemical and multiple high throughput functional assays will best discern the how an RBP affects gene expression within a cell. The increase in the understandings of the molecular mechanisms that govern an RBP will give insight into development of potential therapies to target the list of RBPs that are associated with human disease.

CHAPTER V: MATERIALS and METHODS

Cell lines and culture

Human THP-1s monocytes (male) were cultured in RPMI (Gibco) with 10% fetal bovine serum (FBS from Peal Serum), 100 μg/ml streptomycin (Gibco), 100 U/ml penicillin (Gibco), 25 μg/ml blasticidin, and 100 μg/ml hygromycin (Invivogen).

Plasmid construction

For the cloning of the lentiviral expression construct, the coding sequence of ELAVL1 was PCR amplified from THP-1 cDNA, introducing *attB*-sites for the Flip-IN-recombinase system. The PCR product was gel purified and then recombined (LR clonase) into the pLenti-CMVtight-Flag-HA-DEST-Blast plasmid. The Flag-HA-tag lentiviral inducible expression vector pLenti CMVtight Blast Flag-HA-DEST was constructed by insertion of Flag-HA-tag from pFRT_TO_DEST Flag-HA (#26361, Addgene) into the plasmid pLenti CMVtight Blast DEST (w762-1) (#26434, Addgene).

For the luciferase reporter plasmid, the wt and mutant 3'UTRs of *IRF9* were custom-ordered from IDT (MiniGene) and cloned into the firefly luciferase 3'UTR (#12178, Addgene) with SacI (5' end) and XbaI (3'end) and T4 DNA ligation (NEB).

Lentiviral Production and generation of Inducible expressing Flag-HA ELAVL1

For lentiviral production, HEK293T cells were first cultured in 15 cm plates in high glucose DMEM (Gibco) supplemented with 10% FBS. They were then transfected using Lipofectamine

2000 (Invitrogen) according to manufacture suggestion with 9 μgs of lentiviral vector and 9 μg viral particle packaging vectors, 6.75 μg psPAX2 (12260, Addgene) and 2.25 μg pMD2.G(12259, Addgene). 48 hours after transfection, the viral particle-containing supernatant was collected and spun-down at 3000 g for 15 mins. The supernatant was then concentrated and purified by layering the supernatant over a 20% sucrose cushion in TNE buffer (50 mM Tris-HCl [pH 7.2], 0.1 M NaCl, and 1 mM EDTA) and ultra-centrifuged at 25,000 g for 4 hours in a Beckman SW32Ti rotor. Viral pellets were then resuspended in fresh DMEM media and filtered through a 0.45 μm syringe filter unit (Millex-HV). For viral transduction, THP-1-rtTA cells were spun-inoculated (800 g for 2 hours at 32°C) with an MOI ~100. Two days after viral inoculation, cells were moved into selection media 25 μgs/ml blasticidin and 100 μg/ml hygromycin. Expression of ELAVL1 was then verified via immunoblot using both ELAVL1 endogenous antibody or anti-HA antibody.

RNA-Sequencing and Library Prep

RNA from 1 x 10^6 THP-1s were collected at the indicated timepoint and were washed with 1 x PBS. For stimulated samples, we activated cells for 16 hours with the EC50 of encapsulated cGAMP (Shae et al., 2019). Cells were then resuspended in 1 mL of TRizol. RNA was extracted following the manufacture's protocol. Total RNA was converted into cDNA and sequenced using NEBNext DNA Library Prep Kit for Illumina on the Illumina NovaSeq6000 platform using PE150 at the Vanderbilt Technologies for Advanced Genomics (VUMC VANTAGE). Fastq files were pre-processed with trim-galore with the default settings (http://www.bioinformatics.babraham.ac.uk/projects/trim_galore/) to remove any adapter contamination and then aligned to the human genome (Genocode, hg19) with STAR mapper (Dobin et al., 2012). DeSeq2 (Love et al., 2014) was used to calculate differential expressed genes.

PAR-CLIP

PAR-CLIP was performed as previously described (Garzia et al., 2016; Hafner et al., 2010) with minor adjustments. In brief, 3-5 x 10^9 THP-1 cells were doxycycline induced and labeled with 100 μM 4SU 24 hours before harvesting and UV_{365nm} irradiation. Stimulated THP-1 cells were additionally treated with 70 nM (EC50) cyclic GMP-AMP 16 hours before harvest. After crosslinking, THP-1s were lysed using NP-40 lysis buffer (50 mM HEPES [pH 7.5], 150 mM KCl, 2 mM EDTA, 1 mM NaF, 2% (v/v) NP40, 0.5 mM DTT, Roche EDTA-free protease inhibitor) and incubated with Dyna-protein G beads (Invitrogen) coupled with anti-FLAG M2 antibody (Sigma) for ~ 2 hours at 4°C. Beads were washed with high-salt buffer and then underwent CIP and T4 PNK mediated 5'-end RNA radiolabeling with [γ-^{32}P]-ATP. Flag-tagged ELAVL1 crosslinked to RNA was then was resolved on a 4-20% Bis-Tris, NuPage gradient gel (Invitrogen). The band corresponding to ELAVL1 protein was cut out. The protein: RNA complex was then electroeluted out of the gel and treated with proteinase K (Roche). RNA was then size-selected and underwent both 3' (MultiplexDX Inc.) and 5' adapter (Illumina compatible) ligation and was reverse transcribed into cDNA. cDNA library was sequenced on the NextSeq Illumina platform at Hudson Alpha.

Defining binding sites

PARpipe (https://github.com/ohlerlab/PARpipe) (Mukherjee et al., 2018) with PARalyzer (Corcoran et al., 2011; Mukherjee et al., 2014) was used to define crosslinking sites from the PAR-CLIP data. PARalyzer calculates the T-to-C fraction, which serves as a quality index that is calculated based on the frequency of a given uracil (thymidine) to be substituted with a cytosine.

For groups of reads (> 5 unique reads), kernel density estimates were calculated for both reads with and without T-to-C conversions. Clusters (i.e., binding sites) were defined as a group of transcripts that had a higher kernel density for T-to-C converted reads over unmodified reads.

Motif Analysis

For the 6-mer analysis, we counted the most frequent 6-mers from each unique PAR-pipe called clusters annotated as either intron or 3'UTR using BioStrings R/Bioconductor (Pages et al., 2020). To calculate the top enriched 6-mers for ELAVL1, we regressed the 6-mer frequency relative to a reference library of annotated 3'UTRs or introns (Mukherjee et al., 2018).

RIP-Sequencing

Immunoprecipitation was performed as previously described in the PAR-CLIP method section without UV crosslinking or RNAse treatment. An anti-IgG immunoprecipitation (IP) was used to subtract background RNA expression that is intrinsic of IPs. Following anti-FLAG and anti-IgG IP, beads were added to 1 ml TRizol (Ambion), and RNA was extracted following the manufacture's protocol, and total RNA was submitted to the Vantage sequencing core.

Statistical Analysis

The significant differences between cumulative distribution fractions were calculated using Wilcoxon.Test, and *P*.values were adjusted using the Bonferroni method to the number of observations. The student's t-test was calculated to compare the means of different categories (e.g., the difference in the number of binding sites between two conditions).

Reactome and KEGG analysis

Reactome and KEGG analysis was performed using R/Bioconductor packages clusterProfiler with default settings. (Yu et al., 2012).

RT-qPCR

RNA collected and extracted using Trizol (Ambion). The concentration of total RNA was determined using NanoDrop 2000 (ThermoFisher). Equal amounts of total RNA for each sample were reverse transcribed using SuperScript III (ThermoFisher) with random hexamer. Real-time PCR reactions were done with FastSYBR Green Plus Master Mix (Applied Biosystems) and a StepOnePlus qPCR machine (Applied Biosystems). Target Ct values were normalized to *TUBA1A* Ct values and used to calculate ΔCt. Relative mRNA expression of target genes was then calculated using the ΔΔCt method ($2^{\Delta\Delta Ct}$).

Nucleo-cytoplasmic Fractionation

Harvested cells were washed with 1 x PBS and resuspended in hypotonic lysis buffer (10 mM HEPES, 60 mM KCl, 1 mM EDTA, 0.075% (v/v) NP40, 1 mM DTT, and 1 mM EDTA-free Roche PMSF) and incubated on ice for 10 minutes. Cell lysis was then centrifuged at 4°C (15,000 g, 5 minutes) to pellet the nuclear fraction. The top cytoplasmic fraction was removed and placed into a new tube. Nuclear fraction pellet was washed twice in hypotonic lysis buffer without NP40 and then lysed with hypertonic lysis buffer (20 mM Tris-Cl, 420 mM NaCl, 1.5 $MgCl_2$, 0.2 mM EDTA, 1 mM EDTA-free PMSF (Roche), and 25% (v/v) glycerol). Nuclear lysis was then centrifuged at 4°C (20,000 g, 5 minutes), and the supernatant was collected as the nuclear fraction.

Antibodies and immunoblotting

The antibodies anti-ELAVL1 (ab170193) and anti-TUBA4A (ab7291) are from Abcam; anti-Histone 2A (JBW301) and anti-phospho HuR (Ser 221) (ABE265) are from Sigma. anti-GM130 (12480) is from Cell Signaling.

Samples were separated by SDS-PAGE. After electrophoresis, proteins were semi-dry transferred (Bio-Rad) to nitrocellulose membranes (Hybond-ECL, GE Life Science). Protein membranes were processed via a standard immunoblot protocol followed by enhanced chemiluminescent detection (Luminata Forte ECL, Millipore) using a chemiluminescence imaging system (ChemiDoc MP, Bio-Rad).

Generations of Cas9 sgRNA knockout in THP-1 monocytes

crRNAs were designed using the CRISPR design tool in Benchling [Biology Software] (2019) retrieved from https://www.benchling.com/crispr/ and ordered from IDT. To assemble Cas9/sgRNA RBPs, first Alt-R crRNAs and trcRNAs were first reconstituted in Nuclease Free Duplex buffer (IDT). An equimolar ratio of crRNA and trcRNA were added to a nuclease-free tube and denatured by heating at 95 °C for 5 minutes. The oligo duplex was then cooled at room temperature for 10 minutes prior to adding Cas 9 nuclease enzyme (IDT) to assemble RNPs (Vakulskas et al., 2018). Duplexed oligos and Cas9 were then incubated at room temperature for 20 minutes prior to THP-1 electroporation.

For electroporation, 2 x 10^6 THP-1 cells per sample were counted and washed twice with 1 x PBS. Assembled Cas9 RNPs and washed cells were then suspended in 100 µl of R buffer (NeonTransfection) and electroporated in 100 µl tip with the NeonTransfection unit (1600V, 10 ms, 2 pulses). Electroporate cells were then added to pre-warmed THP-1 media (RPMI + 10%

FBS) without antibiotics and cultured in an incubator 37 C + 5% CO_2 for 48 hours before changing the media.

SLAM-Seq

THP-1 (ELAVL1-wt and ELAVL1-KO) cells were seeded the day before the experiment at a density of 2 x 10^6 cells/ ml. For the pulse, cells were labeled with 100 μM 4SU and stimulated with 70 nM (EC50) cyclic GMP-AMP 16 hours before harvest. For the chase, cells were washed twice in 1x PBS and then incubated with RPMI + 10% FBS supplemented with 10 mM of uridine (Sigma). Cells were harvested, washed in 1x PBS, and added to TRIzol at the respective time points (0, 1, 3, 6, and 8 hours after the chase). Total RNA (~5 μgs per sample) was extracted and then treated with 10 mM iodoacetamide (Sigma) as described in Herzog et .al, 2017 in *Protocol Exchange* (DOI: 10.1038/protex.2017.105). SLAM-Seq libraries were prepared using the Lexogen QuantSeq 3' mRNA-Seq Library Prep Kit FWD for Illumina (Cat. No. 015.24) following the manufacturer's instructions. Libraries were sequenced using Illumina NextSeq 550 in a 75 bp single-end mode. SLAM-Seq libraries were analyzed as previously described in (Herzog et al., 2017) and (Neumann et al., 2019). Briefly, read converged normalized T-to-C conversion rates were generated using the SLAM-DUNK pipeline.

To calculate RNA half-lives, T-to-C conversion rates were normalized to chase onset (0-hour timepoint) and used to fit a first-order decay reaction in R using the min-pack. lm package (Elzhov et al., 2016).

Calculating RNA half-life with Actinomycin D

THP-1 cells (ELAVL1-wt and ELAVL1-KO) were seeded the day before the experiment at a density of 1 x 10^6 cells/ ml and stimulated with 70 nM cyclic GMP-AMP 16 hours before

polymerase II inhibition with actinomycin D (5 μg/ mL). Cells were harvested, washed in 1x PBS, and added to TRIzol at the respective time points (0, 1, 2, 3, 4, and 5 hours after transcription inhibition). The concentration of total RNA was determined using NanoDrop 2000 (ThermoFisher). Equal amounts of total RNA for each sample were reverse transcribed using SuperScript III (ThermoFisher) with random hexamer. Real-time PCR reactions were done with FastSYBR Green Plus Master Mix (Applied Biosystems) and a StepOnePlus qPCR machine (Applied Biosystems). Target Ct values were normalized to *18S* Ct values and used to calculate ΔCt. Relative mRNA abundance was calculated to the start of transcription inhibition (0-hour timepoint*) ($2^{-(\Delta Ct - \Delta Ct^*)}$) for each gene. RNA half-lives were calculated using first-order decay in Prism 9.

For the luciferase-3'UTR half-life reporter, THP-1 cells (1 x 10^6 cells/ ml) were seeded in a 6-well plate and transfected with wt and mutant 3'UTR luciferase plasmids using Lipofectamine LTX PLUS following the manufacture's protocol. After 24-hour transfection, cells were stimulated with 70 nM cyclic GMP-AMP 16 hours before actinomycin D (5 μg/ mL) treatment.

VIR-CLASP

For VIR-CLASP, cells were infected with 1000 MOI of non-labeled or 4SU-labeled virus for 1 hr at 4°C, and uninfected virus was washed away with cold PBS. The infected cells were incubated for the indicated times at 37°C, prior to 365 nm ultraviolet irradiation. For pretreatment with interferon, IFN was added to the media 16 hr before viral infection.

After irradiation, U2OS cells were lysed in denaturation buffer (50 mM Tris–HCl, pH 6.8, 10% glycerol, 2.5% SDS, 0.66% NP-40), incubated for 10 min at 95 °C and subsequently slowly cooled to 25°C. Crosslinked RNA-protein complexes were purified by Solid-Phase Reversible

Immobilization (SPRI) (Hawkins et al., 1994) beads (GE Healthcare, cat# 65152105050250) under denaturing SPRI buffer (30 mM Tris–HCl, pH 6.8, 6% glycerol, 1.5% SDS, 0.4% NP-40, 1 M NaCl, 8% PEG-8000). To each sample, 0.66× (e.g., 660 µl of beads for 1ml of sample) of SPRI beads (1mg/ml SPRI beads in 10 mM Tris-HCl, pH 8.0, 1 M NaCl, 18% PEG-8000, 1 mM EDTA and 0.055% Tween 20) were added, and samples were incubated at room temperature for 10 minutes. The SPRI beads and complexes were washed 5 times with denaturing SPRI buffer. The crosslinked RNA-protein complexes were eluted for 5min at 37 °C in denaturation buffer (lysis buffer).

REFERENCES

Abbas, Y.M., Laudenbach, B.T., Martínez-Montero, S., Cencic, R., Habjan, M., Pichlmair, A., Damha, M.J., Pelletier, J., Nagar, B., 2017. Structure of human IFIT1 with capped RNA reveals adaptable mRNA binding and mechanisms for sensing N1 and N2 ribose 2′-O methylations. Proc Natl Acad Sci USA 114, E2106–E2115. doi:10.1073/pnas.1612444114

Abe, K., Ishigami, T., Shyu, A.-B., Ohno, S., Umemura, S., Yamashita, A., 2012. Analysis of interferon-beta mRNA stability control after poly(I:C) stimulation using RNA metabolic labeling by ethynyluridine. Biochemical and Biophysical Research Communications 428, 44–49. doi:10.1016/j.bbrc.2012.09.144

Ablasser, A., Goldeck, M., Cavlar, T., Deimling, T., Witte, G., Röhl, I., Hopfner, K.P., Ludwig, J., Hornung, V., 2013. cGAS produces a 2′-5′-linked cyclic dinucleotide second messenger that activates STING. Nature 1–6. doi:10.1038/nature12306

Adinolfi, M., Pietrosanto, M., Parca, L., Ausiello, G., Ferrè, F., Helmer-Citterich, M., 2019. Discovering sequence and structure landscapes in RNA interaction motifs. Nucleic Acids Research 47, 4958–4969. doi:10.1093/nar/gkz250

Anderson, P., 2009. Post-transcriptional regulons coordinate the initiation and resolution of inflammation. Nat Rev Immunol 1–12. doi:10.1038/nri2685

Anderson, P., 2008. Post-transcriptional control of cytokine production. Nat Immunol 9, 353–359. doi:10.1038/ni1584

Arthur, J.S.C., Ley, S.C., 2013. Mitogen-activated protein kinases in innate immunity. Nat Rev Immunol 13, 1–14. doi:10.1038/nri3495

Ascano, M., Hafner, M., Cekan, P., Gerstberger, S., Tuschl, T., 2011. Identification of RNA-protein interaction networks using PAR-CLIP. WIREs RNA 3, 159–177. doi:10.1002/wrna.1103

Bakheet, T., Hitti, E., Khabar, K.S.A., 2017. ARED-Plus: an updated and expanded database of AU-rich element-containing mRNAs and pre-mRNAs. Nucleic Acids Research 46, D218–D220. doi:10.1093/nar/gkx975

Barnhart, M.D., Moon, S.L., Emch, A.W., Wilusz, C.J., Wilusz, J., 2013. Changes in Cellular mRNA Stability, Splicing, and Polyadenylation through HuR Protein Sequestration by a Cytoplasmic RNA Virus. Cell Reports 5, 909–917. doi:10.1016/j.celrep.2013.10.012

Bartel, D.P., 2018. Metazoan MicroRNAs. CELL 173, 20–51. doi:10.1016/j.cell.2018.03.006

Berkovits, B.D., Mayr, C., 2015. Alternative 3′ UTRs act as scaffolds to regulate membrane protein localization. Nature 522, 363–367. doi:10.1038/nature14321

Bhattacharyya, S.N., Habermacher, R., Martine, U., Closs, E.I., Filipowicz, W., 2006. Relief of microRNA-mediated translational repression in human cells subjected to stress. CELL 125, 1111–1124. doi:10.1016/j.cell.2006.04.031

Bidet, K., Garcia-Blanco, M.A., 2014. Flaviviral RNAs: weapons and targets in the war between virus and host. Biochem. J. 462, 215–230. doi:10.1042/BJ20140456

Bonenfant, G., Williams, N., Netzband, R., Schwarz, M.C., Evans, M.J., Pager, C.T., 2019. Zika Virus Subverts Stress Granules To Promote and Restrict Viral Gene Expression. Journal of Virology 93. doi:10.1128/JVI.00520-19

Brannan, K, I Chaim, B Yee, R Marina, and D Lorenz. 2020. “Robust Single-Cell Discovery of RNA Targets of RNA Binding Proteins and Ribosomes.”

Buchan, J.R., 2014. mRNP granules. Assembly, function, and connections with disease. RNA Biology 11, 1019–1030. doi:10.4161/15476286.2014.972208

Buchan, J.R., Muhlrad, D., Parker, R., 2008. P bodies promote stress granule assembly in Saccharomyces cerevisiae. J Cell Biol 183, 441–455. doi:10.1083/jcb.200807043

Burdette, D.L., Monroe, K.M., Sotelo-Troha, K., Iwig, J.S., Eckert, B., Hyodo, M., Hayakawa, Y., Vance, R.E., 2011. STING is a direct innate immune sensor of cyclic di-GMP. Nature 478, 515–518. doi:10.1038/nature10429

Cai, X., Chiu, Y.-H., Chen, Z.J., 2014. The cGAS-cGAMP-STING Pathway of Cytosolic DNA Sensing and Signaling. Molecular Cell 54, 289–296. doi:10.1016/j.molcel.2014.03.040

Carpenter, S., Ricci, E.P., Mercier, B.C., Moore, M.J., Fitzgerald, K.A., 2014. Post-transcriptional regulation of gene expression in innate immunity. Nature Publishing Group 14, 361–376. doi:10.1038/nri3682

Castello, A., Fischer, B., Frese, C.K., Horos, R., Alleaume, A.-M., Foehr, S., Curk, T., Krijgsveld, J., Hentze, M.W., 2016. Comprehensive Identification of RNA-Binding Domains in Human Cells. Molecular Cell 63, 696–710. doi:10.1016/j.molcel.2016.06.029

Castello, A., Hentze, M.W., Preiss, T., 2015. Metabolic Enzymes Enjoying New Partnerships as RNA-Binding Proteins. Trends in Endocrinology \& Metabolism 26, 746–757. doi:10.1016/j.tem.2015.09.012

Chen, C.-Y.A., Shyu, A.-B., 2011. Mechanisms of deadenylation-dependent decay. WIREs RNA 2, 167–183. doi:10.1002/wrna.40

Chen, C.Y., Shyu, A.B., 1995. AU-rich elements: characterization and importance in mRNA degradation. Trends in Biochemical Sciences 20, 465–470. doi:10.1016/s0968-0004(00)89102-1

Christodoulou-Vafeiadou, E., Ioakeimidis, F., Andreadou, M., Giagkas, G., Stamatakis, G., Reczko, M., Samiotaki, M., Papanastasiou, A.D., Karakasiliotis, I., Kontoyiannis, D.L., 2018. Divergent Innate and Epithelial Functions of the RNA-Binding Protein HuR in Intestinal Inflammation. Front. Immunol. 9, 490–19. doi:10.3389/fimmu.2018.02732

Corcoran, D.L., Georgiev, S., Mukherjee, N., Gottwein, E., Skalsky, R.L., Keene, J.D., Ohler, U., 2011. PARalyzer: definition of RNA binding sites from PAR-CLIP short-read sequence data. Genome Biol. 12, 1–16. doi:10.1186/gb-2011-12-8-r79

Corley, M., Burns, M.C., Yeo, G.W., 2020. How RNA-Binding Proteins Interact with RNA: Molecules and Mechanisms. Molecular Cell 78, 9–29. doi:10.1016/j.molcel.2020.03.011

Cowling, V.H., 2009. Regulation of mRNA cap methylation. Biochem. J. 425, 295–302. doi:10.1042/BJ20091352

Crow, Y.J., 2015. ScienceDirect Type I interferonopathies: Mendelian type I interferon up-regulation. Current Opinion in Immunology 32, 7–12. doi:10.1016/j.coi.2014.10.005

Curtale, G., Mirolo, M., Renzi, T.A., Rossato, M., Bazzoni, F., Locati, M., 2013. Negative regulation of Toll-like receptor 4 signaling by IL-10-dependent microRNA-146b. Proc. Natl. Acad. Sci. U.S.A. 110, 11499–11504. doi:10.1073/pnas.1219852110

Darnell, R.B., 2010. HITS-CLIP: panoramic views of protein–RNA regulation in living cells. WIREs RNA 1, 266–286. doi:10.1002/wrna.31

Dassi, E., 2017. Handshakes and Fights: The Regulatory Interplay of RNA-Binding Proteins. Front. Mol. Biosci. 4, 2890–8. doi:10.3389/fmolb.2017.00067

Deragon, J.-M., Bousquet-Antonelli, C., 2015. The role of LARP1 in translation and beyond. WIREs RNA 6, 399–417. doi:10.1002/wrna.1282

Diaz-Quintana, A.D., García-Mauriño, S.M., Díaz-Moreno, I., 2015. Dimerization model of the C-terminal RNA Recognition Motif of HuR. FEBS Letters 589, 1059–1066. doi:10.1016/j.febslet.2015.03.013

Dickson, A.M., Anderson, J.R., Barnhart, M.D., Sokoloski, K.J., Oko, L., Opyrchal, M., Galanis, E., Wilusz, C.J., Morrison, T.E., Wilusz, J., 2012. Dephosphorylation of HuR Protein during Alphavirus Infection Is Associated with HuR Relocalization to the Cytoplasm. J. Biol. Chem. 287, 36229–36238. doi:10.1074/jbc.M112.371203

Dobin, A., Davis, C.A., Schlesinger, F., Drenkow, J., Zaleski, C., Jha, S., Batut, P., Chaisson, M., Gingeras, T.R., 2012. STAR: ultrafast universal RNA-seq aligner. Bioinformatics 29, 15–21. doi:10.1093/bioinformatics/bts635

Dominguez, D., Freese, P., Alexis, M.S., Su, A., Hochman, M., Palden, T., Bazile, C., Lambert, N.J., Van Nostrand, E.L., Pratt, G.A., Yeo, G.W., Graveley, B.R., Burge, C.B., 2018a. Sequence, Structure, and Context Preferences of Human RNA Binding Proteins. Molecular Cell 70, 854–867.e9. doi:10.1016/j.molcel.2018.05.001

Dominguez, D., Freese, P., Alexis, M.S., Su, A., Hochman, M., Palden, T., Bazile, C., Lambert, N.J., Van Nostrand, E.L., Pratt, G.A., Yeo, G.W., Graveley, B.R., Burge, C.B., 2018b. Sequence, Structure, and Context Preferences of Human RNA Binding Proteins. Molecular Cell 70, 854–867.e9. doi:10.1016/j.molcel.2018.05.001

Dreyfuss, G., Kim, V.N., Kataoka, N., 2002. Messenger-RNA-binding proteins and the messages they carry. Nat Rev Mol Cell Biol 3, 195–205. doi:10.1038/nrm760

Engreitz, Jesse, Eric S Lander, and Mitchell Guttman. 2015. "RNA Antisense Purification (RAP) for Mapping RNA Interactions with Chromatin.." *Methods in Molecular Biology (Clifton, N.J.)* 1262. Humana Press, New York, NY: 183–97. doi:10.1007/978-1-4939-2253-6_11.

Fan, J., Ishmael, F.T., Fang, X., Myers, A., Cheadle, C., Huang, S.-K., Atasoy, U., Gorospe, M., Stellato, C., 2011. Chemokine Transcripts as Targets of the RNA-Binding Protein HuR in Human Airway Epithelium. The Journal of Immunology 186, 2482–2494. doi:10.4049/jimmunol.0903634

Fan, X.C., Steitz, J.A., 1998. HNS, a nuclear-cytoplasmic shuttling sequence in HuR. Proc Natl Acad Sci USA 95, 15293–15298. doi:10.1073/pnas.95.26.15293

Fleith, R.C., Mears, H.V., Emmott, E., Graham, S.C., Mansur, D.S., Sweeney, T.R., 2018. IFIT3 and IFIT2/3 promote IFIT1-mediated translation inhibition by enhancing binding to non-self RNA. 1–25. doi:10.1101/261776

Frangou, E.A., Bertsias, G.K., Boumpas, D.T., 2013. Gene expression and regulation in systemic lupus erythematosus. Eur J Clin Invest 43, 1084–1096. doi:10.1111/eci.12130

Fros, J.J., Pijlman, G.P., 2016. Alphavirus Infection: Host Cell Shut-Off and Inhibition of Antiviral Responses. Viruses 8, 166. doi:10.3390/v8060166

Fu, M., Blackshear, P.J., 2016. RNA-binding proteins in immune regulation: a focus on CCCH zinc finger proteins. Nature Publishing Group 17, 130–143. doi:10.1038/nri.2016.129

Gallouzi, I.-E., Brennan, C.M., Stenberg, M.G., Swanson, M.S., Eversole, A., Maizels, N., Steitz, J.A., 2000. HuR binding to cytoplasmic mRNA is perturbed by heat shock. Proc Natl Acad Sci USA 97, 3073–3078. doi:10.1073/pnas.97.7.3073

Gao, P., Ascano, M., Wu, Y., Barchet, W., Gaffney, B.L., Zillinger, T., Serganov, A.A., Liu, Y., Jones, R.A., Hartmann, G., Tuschl, T., Patel, D.J., 2013a. Cyclic [G(2′,5′)pA(3′,5′)p] Is the Metazoan Second Messenger Produced by DNA-Activated Cyclic GMP-AMP Synthase. CELL 153, 1094–1107. doi:10.1016/j.cell.2013.04.046

Gao, P., Ascano, M., Zillinger, T., Wang, W., Dai, P., Serganov, A.A., Gaffney, B.L., Shuman, S., Jones, R.A., Deng, L., Hartmann, G., Barchet, W., Tuschl, T., Patel, D.J., 2013b. Structure-Function Analysis of STING Activation by c[G(2′,5′)pA(3′,5′)p] and Targeting by Antiviral DMXAA. CELL 154, 748–762. doi:10.1016/j.cell.2013.07.023

García-Mauriño, S.M., Rivero-Rodríguez, F., Velázquez-Cruz, A., Hernández-Vellisca, M., Díaz-Quintana, A., la Rosa, De, M.A., Díaz-Moreno, I., 2017. RNA Binding Protein Regulation and Cross-Talk in the Control of AU-rich mRNA Fate. Front. Mol. Biosci. 4, 1271–9. doi:10.3389/fmolb.2017.00071

Garzia, A., Meyer, C., Morozov, P., Sajek, M., Tuschl, T., 2016. Optimization of PAR-CLIP for transcriptome-wide identification of binding sites of RNA-binding proteins. Methods 1–17. doi:10.1016/j.ymeth.2016.10.007

Gebauer, F., Preiss, T., Hentze, M.W., 2012. From Cis-Regulatory Elements to Complex RNPs and Back. Cold Spring Harbor Perspectives in Biology 4, a012245–a012245. doi:10.1101/cshperspect.a012245

Gebauer, F.X.T., Schwarzl, T., rcel, J.V.X., Hentze, M.W., 2020. RNA-binding proteins in human genetic disease. Nat Rev Genet 1–14. doi:10.1038/s41576-020-00302-y

Gerstberger, S., Hafner, M., Tuschl, T., 2014. A census of human RNA-binding proteins. Nature Publishing Group 15, 829–845. doi:10.1038/nrg3813

Gilchrist, D.A., Fromm, G., Santos, dos, G., Pham, L.N., McDaniel, I.E., Burkholder, A., Fargo, D.C., Adelman, K., 2012. Regulating the regulators: the pervasive effects of Pol II pausing on stimulus-responsive gene networks. Genes Dev. 26, 933–944. doi:10.1101/gad.187781.112

Grammatikakis, I., Abdelmohsen, K., Gorospe, M., 2016. Posttranslational control of HuR function. WIREs RNA 8, e1372–11. doi:10.1002/wrna.1372

Hafner, M., Landthaler, M., Burger, L., Khorshid, M., Hausser, J., Berninger, P., Rothballer, A., Ascano, M., Jr, Jungkamp, A.-C., Munschauer, M., Ulrich, A., Wardle, G.S., Dewell, S., Zavolan, M., Tuschl, T., 2010. Transcriptome-wide Identification of RNA-Binding Protein and MicroRNA Target Sites by PAR-CLIP. CELL 141, 129–141. doi:10.1016/j.cell.2010.03.009

Hao, S., Baltimore, D., 2009. The stability of mRNA influences the temporal order of the induction of genes encoding inflammatory molecules. Nat Immunol 10, 281–288. doi:10.1038/ni.1699

Hentze, M.W., Castello, A., Schwarzl, T., Preiss, T., 2018. A brave new world of RNA-binding proteins. Nature Publishing Group 1–15. doi:10.1038/nrm.2017.130

Herdy, B., Karonitsch, T., Vladimer, G.I., Tan, C.S.H., Stukalov, A., Trefzer, C., Bigenzahn, J.W., Theil, T., Holinka, J., Kiener, H.P., Colinge, J., Bennett, K.L., Superti-Furga, G., 2015. The RNA-binding protein HuR/ELAVL1 regulates IFN-β mRNA abundance and the type I IFN response. Eur. J. Immunol. 45, 1500–1511. doi:10.1002/eji.201444979

Herman, A.B., Vrakas, C.N., Ray, M., Kelemen, S.E., Sweredoski, M.J., Moradian, A., Haines, D.S., Autieri, M.V., 2018. FXR1 Is an IL-19-Responsive RNA-Binding Protein that Destabilizes Pro-inflammatory Transcripts in Vascular Smooth Muscle Cells. Cell Reports 24, 1176–1189. doi:10.1016/j.celrep.2018.07.002

Herzog, V.A., Reichholf, B., Neumann, T., Rescheneder, P., Bhat, P., Burkard, T.R., Wlotzka, W., Haeseler, von, A., Zuber, J., Ameres, S.L., 2017. Thiol-linked alkylation of RNA to assess expression dynamics. Nat Methods 14, 1198–1204. doi:10.1038/nmeth.4435

Honda, K., Takaoka, A., Taniguchi, T., 2006. Type I Inteferon Gene Induction by the Interferon Regulatory Factor Family of Transcription Factors. Immunity 25, 349–360. doi:10.1016/j.immuni.2006.08.009

Hubel, P., Urban, C., Bergant, V., Schneider, W.M., Knauer, B., Stukalov, A., Pietro Scaturro, Mann, A., Brunotte, L., Hoffmann, H.H., Schoggins, J.W., Schwemmle, M., Mann, M., Rice, C.M., Pichlmair, A., 2019. A protein-interaction network of interferon- stimulated genes extends the innate immune system landscape. Nat Immunol 1–18. doi:10.1038/s41590-019-0323-3

Ingolia, N.T., Ghaemmaghami, S., Newman, J.R.S., Weissman, J.S., 2009. Genome-wide analysis in vivo of translation with nucleotide resolution using ribosome profiling. Science 324, 218–223. doi:10.1126/science.1168978

Ishikawa, H., Barber, G.N., 2008. STING is an endoplasmic reticulum adaptor that facilitates innate immune signalling. Nature 455, 674–678. doi:10.1038/nature07317

Ishikawa, H., Ma, Z., Barber, G.N., 2009. STING regulates intracellular DNA-mediated, type I interferon-dependent innate immunity. Nature 1–6. doi:10.1038/nature08476

Johnson, B., VanBlargan, L.A., Xu, W., White, J.P., Shan, C., Shi, P.-Y., Zhang, R., Adhikari, J., Gross, M.L., Leung, D.W., Diamond, M.S., Amarasinghe, G.K., 2018. Human IFIT3 Modulates IFIT1 RNA Binding Specificity and Protein Stability. Immunity 1–31. doi:10.1016/j.immuni.2018.01.014

Kafasla, P., Karakasiliotis, I., Kontoyiannis, D.L., 2012. Decoding the functions of post-transcriptional regulators in the determination of inflammatory states: focus on macrophage activation. WIREs Syst Biol Med 4, 509–523. doi:10.1002/wsbm.1179

Kafasla, P., Skliris, A., Kontoyiannis, D.L., 2014. Post-transcriptional coordination of immunological responses by RNA-binding proteins. Nat Immunol 15, 492–502. doi:10.1038/ni.2884

Katsanou, V., Papadaki, O., Milatos, S., Blackshear, P.J., Anderson, P., Kollias, G., Kontoyiannis, D.L., 2005a. HuR as a Negative Posttranscriptional Modulator in Inflammation. Molecular Cell 19, 777–789. doi:10.1016/j.molcel.2005.08.007

Katsanou, V., Papadaki, O., Milatos, S., Blackshear, P.J., Anderson, P., Kollias, G., Kontoyiannis, D.L., 2005b. HuR as a Negative Posttranscriptional Modulator in Inflammation. Molecular Cell 19, 777–789. doi:10.1016/j.molcel.2005.08.007

Keene, J.D., 2007. RNA regulons: coordination of post-transcriptional events. Nat Rev Genet 8, 533–543. doi:10.1038/nrg2111

Keene, J.D., Komisarow, J.M., Friedersdorf, M.B., 2006. RIP-Chip: the isolation and identification of mRNAs, microRNAs and protein components of ribonucleoprotein complexes from cell extracts. Nat Protoc 1, 302–307. doi:10.1038/nprot.2006.47

Khabar, K.S.A., Young, H.A., 2007. Post-transcriptional control of the interferon system. Biochimie 89, 761–769. doi:10.1016/j.biochi.2007.02.008

Kim, B., Arcos, S., Rothamel, K., Jian, J., Rose, K.L., McDonald, W.H., Bian, Y., Reasoner, S., Barrows, N.J., Bradrick, S., Garcia-Blanco, M.A., Ascano, M., 2020a. Discovery of Widespread Host Protein Interactions with the Pre-replicated Genome of CHIKV Using VIR-CLASP. Molecular Cell 1–25. doi:10.1016/j.molcel.2020.04.013

Kim, B., Arcos, S.E., Rothamel, K.L., Ascano, M., 2020b. Viral cross-linking and solid-phase purification enables discovery of ribonucleoprotein complexes on incoming RNA virus genomes. bioRxiv.

Kim, H.H., Kuwano, Y., Srikantan, S., Lee, E.K., Martindale, J.L., Gorospe, M., 2009. HuR recruits let-7/RISC to repress c-Myc expression. Genes Dev. 23, 1743–1748. doi:10.1101/gad.1812509

Kim, Y., Noren Hooten, N., Dluzen, D.F., Martindale, J.L., Gorospe, M., Evans, M.K., 2015. Posttranscriptional Regulation of the Inflammatory Marker C-Reactive Protein by the RNA-Binding Protein HuR and MicroRNA 637. Mol. Cell. Biol. 35, 4212–4221. doi:10.1128/MCB.00645-15

Kleaveland, B., Shi, C.Y., Stefano, J., Bartel, D.P., 2018. A Network of Noncoding Regulatory RNAs Acts in the Mammalian Brain. CELL 1–31. doi:10.1016/j.cell.2018.05.022

Kontoyiannis, D., Pasparakis, M., Pizarro, T.T., Cominelli, F., Kollias, G., 1999. Impaired on/off regulation of TNF biosynthesis in mice lacking TNF AU-rich elements: implications for joint and gut-associated immunopathologies. Immunity 10, 387–398. doi:10.1016/s1074-7613(00)80038-2

König, J., Zarnack, K., Rot, G., Curk, T., Kayikci, M., Zupan, B., Turner, D.J., Luscombe, N.M., Ule, J., 2010. iCLIP reveals the function of hnRNP particles in splicing at individual nucleotide resolution. Nature Publishing Group 17, 1–8. doi:10.1038/nsmb.1838

Kurgonaite, K., Gandhi, H., Kurth, T., Pautot, S., Schwille, P., Weidemann, T., Bokel, C., 2015. Essential role of endocytosis for interleukin-4-receptor-mediated JAK/STAT signalling. Journal of Cell Science 128, 3781–3795. doi:10.1242/jcs.170969

Lambert, N., Robertson, A., Jangi, M., McGeary, S., Sharp, P.A., Burge, C.B., 2014. RNA Bind-n-Seq: Quantitative Assessment of the Sequence and Structural Binding Specificity of RNA Binding Proteins. Molecular Cell 54, 887–900. doi:10.1016/j.molcel.2014.04.016

Lebedeva, S., Jens, M., Theil, K., Schwanhäusser, B., Selbach, M., Landthaler, M., Rajewsky, N., 2011. Transcriptome-wide Analysis of Regulatory Interactions of the RNA-Binding Protein HuR. Molecular Cell 43, 340–352. doi:10.1016/j.molcel.2011.06.008

Li, C., Jiang, J.-Y., Wang, J.-M., Sun, J., An, M.-X., Li, S., Yan, J., Wang, H.-Q., 2018. BAG3 regulates stability of IL-8 mRNA via interplay between HuR and miR-4312 in PDACs. Cell Death and Disease 1–15. doi:10.1038/s41419-018-0874-5

Li, Y., Shi, X., 2019. MicroRNAs in the regulation of TLR and RIG-I pathways. Cellular and Molecular Immunology 1–7. doi:10.1038/cmi.2012.55

Licatalosi, Donny D, Xuan Ye, and Eckhard Jankowsky. 2020. “Approaches for Measuring the Dynamics of RNA-Protein Interactions..” *Wiley Interdisciplinary Reviews: RNA* 11 (1). John Wiley & Sons, Ltd: e1565. doi:10.1002/wrna.1565.

Liu, B., Qian, S.-B., 2013. Translational reprogramming in cellular stress response. WIREs RNA 5, 301–305. doi:10.1002/wrna.1212

Louis, I.V.-S., Bohjanen, P.R., 2016. Post-transcriptional regulation of cytokine and growth factor signaling in cancer. Cytokine and Growth Factor Reviews 1–11. doi:10.1016/j.cytogfr.2016.11.004

Lourou, N., Gavriilidis, M., Kontoyiannis, D.L., 2019. Lessons from studying the AU-rich elements in chronic inflammation and autoimmunity. Journal of Autoimmunity 104, 102334. doi:10.1016/j.jaut.2019.102334

Love, M.I., Huber, W., Anders, S., 2014. Moderated estimation of fold change and dispersion for RNA-seq data with DESeq2. Genome Biol. 15, 31–21. doi:10.1186/s13059-014-0550-8

López de Silanes, I., Zhan, M., Lal, A., Yang, X., Gorospe, M., 2004. Identification of a target RNA motif for RNA-binding protein HuR. Proc Natl Acad Sci USA 101, 2987–2992. doi:10.1073/pnas.0306453101

Lu, Y.-C., Chang, S.-H., Hafner, M., Li, X., Tuschl, T., Elemento, O., Hla, T., 2014. ELAVL1 Modulates Transcriptome-wide miRNA Binding in Murine Macrophages. CellReports 9, 2330–2343. doi:10.1016/j.celrep.2014.11.030

Lukong, K.E., Chang, K.-W., Khandjian, E.W., Richard, S., 2008. RNA-binding proteins in human genetic disease. Trends Genet 24, 416–425. doi:10.1016/j.tig.2008.05.004

Lund, V.K., DeLotto, R., 2014. Regulation of Toll and Toll-like receptor signaling by the endocytic pathway. Small GTPases 2, 95–98. doi:10.4161/sgtp.2.2.15378

Lunde, B.M., Moore, C., Varani, G., 2007. RNA-binding proteins: modular design for efficient function. Nature Publishing Group 8, 479–490. doi:10.1038/nrm2178

Machkovech, H.M., Bloom, J.D., Subramaniam, A.R., 2019. Comprehensive profiling of translation initiation in influenza virus infected cells. PLoS Pathog 15, e1007518–40. doi:10.1371/journal.ppat.1007518

Madhani, H.D., 2013. The Frustrated Gene: Origins of Eukaryotic Gene Expression. CELL 155, 744–749. doi:10.1016/j.cell.2013.10.003

Marceau, C.D., Puschnik, A.S., Majzoub, K., Ooi, Y.S., Brewer, S.M., Fuchs, G., Swaminathan, K., Mata, M.A., Elias, J.E., Sarnow, P., Carette, J.E., 2016. Genetic dissection of Flaviviridae host factors through genome-scale CRISPR screens. Nature 535, 159–163. doi:10.1038/nature18631

McMahon, Aoife C, Reazur Rahman, Hua Jin, James L Shen, Allegra Fieldsend, Weifei Luo, and Michael Rosbash. 2016. "TRIBE: Hijacking an RNA-Editing Enzyme to Identify Cell-Specific Targets of RNA-Binding Proteins." *Cell* 165 (3). Elsevier Inc.: 742–53. doi:10.1016/j.cell.2016.03.007.

McManus, J., Cheng, Z., Vogel, C., 2015. Next-generation analysis of gene expression regulation – comparing the roles of synthesis and degradation. Mol. BioSyst. 11, 2680–2689. doi:10.1039/C5MB00310E

Meyer, C., Garzia, A., Mazzola, M., Gerstberger, S., Molina, H., Tuschl, T., 2018. The TIA1 RNA-Binding Protein Family Regulates EIF2AK2-Mediated Stress Response and Cell Cycle Progression. Molecular Cell 69, 622–635.e6. doi:10.1016/j.molcel.2018.01.011

Meyer, Kate D. 2019. "DART-Seq: an Antibody-Free Method for Global m6A Detection." *Nature Methods*, November. Springer US, 1–11. doi:10.1038/s41592-019-0570-0.

Mino, T., Takeuchi, O., 2013. Post-transcriptional regulation of cytokine mRNA controls the initiation and resolution of inflammation. Biotechnology and Genetic Engineering Reviews 29, 49–60. doi:10.1080/02648725.2013.801236

Momen-Heravi, F., Bala, S., 2018. miRNA regulation of innate immunity. J Leukoc Biol 103, 1205–1217. doi:10.1002/JLB.3MIR1117-459R

Moore, M.J., 2005. From birth to death: the complex lives of eukaryotic mRNAs. Science 309, 1514–1518. doi:10.1126/science.1111443

Mostafavi, S., Yoshida, H., Moodley, D., LeBoité, H., Rothamel, K., Raj, T., Ye, C.J., Chevrier, N., Zhang, S.-Y., Feng, T., Lee, M., Casanova, J.-L., Clark, J.D., Hegen, M., Telliez, J.-B., Hacohen, N., De Jager, P.L., Regev, A., Mathis, D., Benoist, C., Consortium, T.I.G.P., 2016. Parsing the Interferon Transcriptional Network and Its Disease Associations. CELL 164, 564–578. doi:10.1016/j.cell.2015.12.032

Mukherjee, N., Corcoran, D.L., Nusbaum, J.D., Reid, D.W., Georgiev, S., Hafner, M., Ascano, M., Jr, Tuschl, T., Ohler, U., Keene, J.D., 2011. Integrative Regulatory Mapping Indicates that the RNA-Binding Protein HuR Couples Pre-mRNA Processing and mRNA Stability. Molecular Cell 43, 327–339. doi:10.1016/j.molcel.2011.06.007

Mukherjee, N., Jacobs, N.C., Hafner, M., Kennington, E.A., Nusbaum, J.D., Tuschl, T., Blackshear, P.J., Ohler, U., 2014. Global target mRNA specification and regulation by the RNA-binding protein ZFP36. Genome Biol. 15, R12–16. doi:10.1186/gb-2014-15-1-r12

Mukherjee, N., Wessels, H.-H., Lebedeva, S., Sajek, M., Ghanbari, M., Garzia, A., Munteanu, A., Yusuf, D., Farazi, T., Hoell, J.I., Akat, K.M., Akalin, A., Tuschl, T., Ohler, U., 2018. Deciphering human ribonucleoprotein regulatory networks. Nucleic Acids Research 47, 570–581. doi:10.1093/nar/gky1185

Munroe, D., Gene, A.J., 1990, n.d. Tales of poly (A): a review. Elsevier
. doi:10.1016/0378-1119(90)90082-3

Nabors, L.B., Gillespie, G.Y., Harkins, L., King, P.H., 2001. HuR, a RNA stability factor, is expressed in malignant brain tumors and binds to adenine- and uridine-rich elements within the 3' untranslated regions of cytokine and angiogenic factor mRNAs. Cancer Res 61, 2154–2161.

Neumann, T., Herzog, V.A., Muhar, M., Haeseler, A., Zuber, J., Ameres, S.L., Rescheneder, P., 2019. Quantification of experimentally induced nucleotide conversions in high-throughput sequencing datasets 1–16. doi:10.1186/s12859-019-2849-7

Nostrand, E.L., Freese, P., Pratt, G.A., Wang, X., Wei, X., Xiao, R., Blue, S.M., Chen, J.-Y., Cody, N.A.L., Dominguez, D., Olson, S., Sundararaman, B., Zhan, L., Bazile, C., Bouvrette, L.P.B., Bergalet, J., Duff, M.O., Garcia, K.E., Gelboin-Burkhart, C., Hochman, M., Lambert, N.J., Li, H., McGurk, M.P., Nguyen, T.B., Palden, T., Rabano, I., Sathe, S., Stanton, R., Su, A., Wang, R., Yee, B.A., Zhou, B., Louie, A.L., Aigner, S., Fu, X.-D., Lécuyer, E., Burge, C.B., Graveley, B.R., Yeo, G.W., 2020. A large-scale binding and functional map of human RNA-binding proteins. Nature 583, 1–39. doi:10.1038/s41586-020-2077-3

Nussbacher, J.K., Yeo, G.W., 2018. Systematic Discovery of RNA Binding Proteins that Regulate MicroRNA Levels. Molecular Cell 69, 1005–1016.e7. doi:10.1016/j.molcel.2018.02.012

Pager, C.T., Schütz, S., Abraham, T.M., Luo, G., Sarnow, P., 2013. Modulation of hepatitis C virus RNA abundance and virus release by dispersion of processing bodies and enrichment of stress granules. Virology 435, 472–484. doi:10.1016/j.virol.2012.10.027

Pai, A.A., Baharian, G., Pagé Sabourin, A., Brinkworth, J.F., Nédélec, Y., Foley, J.W., Grenier, J.-C., Siddle, K.J., Dumaine, A., Yotova, V., Johnson, Z.P., Lanford, R.E., Burge, C.B., Barreiro, L.B., 2016. Widespread Shortening of 3' Untranslated Regions and Increased Exon Inclusion Are Evolutionarily Conserved Features of Innate Immune Responses to Infection. PLoS Genet 12, e1006338–24. doi:10.1371/journal.pgen.1006338

Perez-Perri, J.I., Rogell, B., Schwarzl, T., Stein, F., Zhou, Y., Rettel, M., Brosig, A., Hentze, M.W., 2018. Discovery of RNA-binding proteins and characterization of their dynamic responses by enhanced RNA interactome capture. Nature Communications 1–13. doi:10.1038/s41467-018-06557-8

Piccirillo, C.A., Bjur, E., Topisirovic, I., Sonenberg, N., Larsson, O., 2014. Translational control of immune responses: from transcripts to translatomes. Nat Immunol 15, 503–511. doi:10.1038/ni.2891

Protter, D.S.W., Parker, R., 2016. Principles and Properties of Stress Granules. Trends in Cell Biology 26, 668–679. doi:10.1016/j.tcb.2016.05.004

Rabani, M., Levin, J.Z., Fan, L., Adiconis, X., Raychowdhury, R., Garber, M., Gnirke, A., Nusbaum, C., Hacohen, N., Friedman, N., Amit, I., Regev, A., 2011. Metabolic labeling of RNA uncovers principles of RNA production and degradation dynamics in mammalian cells. Nat Biotechnol 29, 436–442. doi:10.1038/nbt.1861

Ramanathan, Muthukumar, Douglas F Porter, and Paul A Khavari. 2019. "Methods to Study RNA–Protein Interactions." *Nature Methods*, March. Springer US, 1–10. doi:10.1038/s41592-019-0330-1.

Ray, D., Ha, K.C.H., Nie, K., Zheng, H., Hughes, T.R., Morris, Q.D., 2017. RNAcompete methodology and application to determine sequence preferences of unconventional RNA-binding proteins. Methods 118-119, 3–15. doi:10.1016/j.ymeth.2016.12.003

Reder, A.T., 2013. Aberrant type I interferon regulation in autoimmunity: opposite directions in MS and SLE, shaped by evolution and body ecology 1–13. doi:10.3389/fimmu.2013.00281/abstract

Rigby, R.E., Rehwinkel, J., 2015. RNA degradation in antiviral immunity and autoimmunity. Trends in Immunology 36, 179–188. doi:10.1016/j.it.2015.02.001

Ripin, N., Boudet, J., Duszczyk, M.M., Hinniger, A., Faller, M., Krepl, M., Gadi, A., Schneider, R.J., Šponer, J., Meisner-Kober, N.C., Allain, F.H.-T., 2019. Molecular basis for AU-rich element recognition and dimerization by the HuR C-terminal RRM. Proc. Natl. Acad. Sci. U.S.A. 116, 2935–2944. doi:10.1073/pnas.1808696116

Rusinova, I., Forster, S., Yu, S., Kannan, A., Masse, M., Cumming, H., Chapman, R., Hertzog, P.J., 2012. INTERFEROME v2.0: an updated database of annotated interferon-regulated genes. Nucleic Acids Research 41, D1040–D1046. doi:10.1093/nar/gks1215

Sato, M., Tanaka, N., Hata, N., Oda, E., Taniguchi, T., 1998. Involvement of the IRF family transcription factor IRF-3 in virus-induced activation of the IFN-beta gene. FEBS Letters 425, 112–116. doi:10.1016/s0014-5793(98)00210-5

Savan, R., 2014. Post-Transcriptional Regulation of Interferons and Their Signaling Pathways. Journal of Interferon & Cytokine Research 34, 318–329. doi:10.1089/jir.2013.0117

Schneider, W.M., Chevillotte, M.D., Rice, C.M., 2014. Interferon-Stimulated Genes: A Complex Web of Host Defenses. Annu. Rev. Immunol. 32, 513–545. doi:10.1146/annurev-immunol-032713-120231

Schoggins, J.W., Wilson, S.J., Panis, M., Murphy, M.Y., Jones, C.T., Bieniasz, P., Rice, C.M., 2011. A diverse range of gene products are effectors of the type I interferon antiviral response. Nature 472, 481–485. doi:10.1038/nature09907

Sedlyarov, V., Fallmann, J., Ebner, F., Huemer, J., Sneezum, L., Ivin, M., Kreiner, K., Tanzer, A., Vogl, C., Hofacker, I., Kovarik, P., 2016. Tristetraprolin binding site atlas in the

macrophage transcriptome reveals a switch for inflammation resolution. Molecular Systems Biology 12, 868–21. doi:10.15252/msb.20156628

Shae, D., Becker, K.W., Christov, P., Yun, D.S., Lytton-Jean, A.K.R., Sevimli, S., Ascano, M., Kelley, M., Johnson, D.B., Balko, J.M., Wilson, J.T., 2019. Endosomolytic polymersomes increase the activity of cyclic dinucleotide STING agonists to enhance cancer immunotherapy. Nature Nanotechnology 1–16. doi:10.1038/s41565-018-0342-5

Shatkin, A.J., 1976. Capping of eucaryotic mRNAs. CELL 9, 645–653. doi:10.1016/0092-8674(76)90128-8

Shwetha, S., Kumar, A., Mullick, R., Vasudevan, D., Mukherjee, N., Das, S., 2015. HuR Displaces Polypyrimidine Tract Binding Protein To Facilitate La Binding to the 3' Untranslated Region and Enhances Hepatitis C Virus Replication. Journal of Virology 89, 11356–11371. doi:10.1128/JVI.01714-15

Simone, L.E., Keene, J.D., 2013. Mechanisms coordinating ELAV/Hu mRNA regulons. Current Opinion in Genetics & Development 23, 35–43. doi:10.1016/j.gde.2012.12.006

Sokoloski, K.J., Dickson, A.M., Chaskey, E.L., Garneau, N.L., Wilusz, C.J., Wilusz, J., 2010. Sindbis virus usurps the cellular HuR protein to stabilize its transcripts and promote productive infections in mammalian and mosquito cells. Cell Host and Microbe 8, 196–207. doi:10.1016/j.chom.2010.07.003

Srikantan, S., Tominaga, K., Gorospe, M., 2012. Functional Interplay between RNA-Binding Protein HuR and microRNAs. CPPS 13, 372–379. doi:10.2174/138920312801619394

STRAUSS, J.H., STRAUSS, E.G., n.d. The Alphaviruses: Gene Expression, Replication, and Evolution, europepmc.org

Sueyoshi, T., Kawasaki, T., Kitai, Y., Ori, D., Akira, S., Kawai, T., 2018. Hu Antigen R Regulates Antiviral Innate Immune Responses through the Stabilization of mRNA for Polo-like Kinase 2. J. Immunol. 200, 3814–3824. doi:10.4049/jimmunol.1701282

Sun, L., Wu, J., Du, F., Chen, X., Chen, Z.J., 2013. Cyclic GMP-AMP Synthase Is a Cytosolic DNA Sensor That Activates the Type I Interferon Pathway. Science 339, 786–791. doi:10.1126/science.1232458

Szabo, A., Dalmau, J., Manley, G., Rosenfeld, M., Wong, E., Henson, J., Posner, J.B., Furneaux, H.M., 1991. HuD, a paraneoplastic encephalomyelitis antigen, contains RNA-binding domains and is homologous to Elav and Sex-lethal. CELL 67, 325–333. doi:10.1016/0092-8674(91)90184-z

Takeuchi, O., 2015. HuR keeps interferon-β mRNA stable. Eur. J. Immunol. 45, 1296–1299. doi:10.1002/eji.201545616

Tcherkezian, J., Cargnello, M., Romeo, Y., Huttlin, E.L., Lavoie, G., Gygi, S.P., Roux, P.P., 2014. Proteomic analysis of cap-dependent translation identifies LARP1 as a key regulator of 5'TOP mRNA translation. Genes Dev. 28, 357–371. doi:10.1101/gad.231407.113

Techasintana, P., Davis, J.W., Gubin, M.M., Magee, J.D., Atasoy, U., 2015. Transcriptomic-Wide Discovery of Direct and Indirect HuR RNA Targets in Activated CD4+ T Cells. PLoS ONE 10, e0129321–20. doi:10.1371/journal.pone.0129321

Tenenbaum, S.A., Carson, C.C., Lager, P.J., Keene, J.D., 2000. Identifying mRNA subsets in messenger ribonucleoprotein complexes by using cDNA arrays. Proc Natl Acad Sci USA 97, 14085–14090. doi:10.1073/pnas.97.26.14085

Tiedje, C., Díaz-Muñoz, M.D., Trulley, P., Ahlfors, H., Laaß, K., Blackshear, P.J., Turner, M., Gaestel, M., 2016. The RNA-binding protein TTP is a global post-transcriptional regulator of feedback control in inflammation. Nucleic Acids Research 7, gkw474–23. doi:10.1093/nar/gkw474

Treiber, T., Treiber, N., Meister, G., 2019. Regulation of microRNA biogenesis and its crosstalk with other cellular pathways. Nature Publishing Group 1–16. doi:10.1038/s41580-018-0059-1

Turner, M., Díaz-Muñoz, M.D., 2018. RNA-binding proteins control gene expression and cell fate in the immune system. Nat Immunol 1–10. doi:10.1038/s41590-017-0028-4

Ule, J., Jensen, K.B., Ruggiu, M., Mele, A., Ule, A., Darnell, R.B., 2003. CLIP identifies Nova-regulated RNA networks in the brain. Science 302, 1212–1215. doi:10.1126/science.1090095

Vakulskas, C.A., Dever, D.P., Rettig, G.R., Turk, R., Jacobi, A.M., Collingwood, M.A., Bode, N.M., McNeill, M.S., Yan, S., Camarena, J., Lee, C.M., Park, S.H., Wiebking, V., Bak, R.O., Gomez-Ospina, N., Pavel-Dinu, M., Sun, W., Bao, G., Porteus, M.H., Behlke, M.A., 2018. A high-fidelity Cas9 mutant delivered as a ribonucleoprotein complex enables efficient gene editing in human hematopoietic stem and progenitor cells. Nat Med 24, 1216–1224. doi:10.1038/s41591-018-0137-0

Van Nostrand, E.L., Pratt, G.A., Shishkin, A.A., Gelboin-Burkhart, C., Fang, M.Y., Sundararaman, B., Blue, S.M., Nguyen, T.B., Surka, C., Elkins, K., Stanton, R., Rigo, F., Guttman, M., Yeo, G.W., 2016. Robust transcriptome-wide discovery of RNA-binding protein binding sites with enhanced CLIP (eCLIP). Nat Methods 13, 508–514. doi:10.1038/nmeth.3810

Wang, T., Xiao, G., Chu, Y., Zhang, M.Q., Corey, D.R., Xie, Y., 2015. Design and bioinformatics analysis of genome-wide CLIP experiments. Nucleic Acids Research 43, 5263–5274. doi:10.1093/nar/gkv439

Wu, J., Sun, L., Chen, X., Du, F., Shi, H., Chen, C., Chen, Z.J., 2013. Cyclic GMP-AMP is an endogenous second messenger in innate immune signaling by cytosolic DNA. Science 339, 826–830. doi:10.1126/science.1229963

Yiakouvaki, A., Dimitriou, M., Karakasiliotis, I., Eftychi, C., Theocharis, S., Kontoyiannis, D.L., 2012. Myeloid cell expression of the RNA-binding protein HuR protects mice from pathologic inflammation and colorectal carcinogenesis. J. Clin. Invest. 122, 48–61. doi:10.1172/JCI45021

Young, D.F., Andrejeva, J., Li, X., Inesta-Vaquera, F., Dong, C., Cowling, V.H., Goodbourn, S., Randall, R.E., 2016. Human IFIT1 Inhibits mRNA Translation of Rubulaviruses but Not Other Members of the Paramyxoviridae Family. Journal of Virology 90, 9446–9456. doi:10.1128/JVI.01056-16

Young, L.E., Moore, A.E., Sokol, L., Meisner-Kober, N., Dixon, D.A., 2012. The mRNA stability factor HuR inhibits microRNA-16 targeting of COX-2. Mol. Cancer Res. 10, 167–180. doi:10.1158/1541-7786.MCR-11-0337

Yu, G., Wang, L.-G., Han, Y., He, Q.-Y., 2012. clusterProfiler: an R Package for Comparing Biological Themes Among Gene Clusters. OMICS: A Journal of Integrative Biology 16, 284–287. doi:10.1089/omi.2011.0118

Zhang, J., Kong, L., Guo, S., Bu, M., Guo, Q., Xiong, Y., Zhu, N., Qiu, C., Yan, X., Chen, Q., Zhang, H., Zhuang, J., Wang, Q., Zhang, S.S., Shen, Y., Chen, M., 2016. hnRNPs and ELAVL1 cooperate with uORFs to inhibit protein translation. Nucleic Acids Research 63, gkw991–16. doi:10.1093/nar/gkw991

Zhao, J., Ohsumi, T.K., Kung, J.T., Ogawa, Y., Grau, D.J., Sarma, K., Song, J.J., Kingston, R.E., Borowsky, M., Lee, J.T., 2010. Genome-wide Identification of Polycomb-Associated RNAs by RIP-seq. Molecular Cell 40, 939–953. doi:10.1016/j.molcel.2010.12.011

Zhao, J., Sun, B.K., Erwin, J.A., Song, J.J., Lee, J.T., 2008. Polycomb Proteins Targeted by a Short Repeat RNA to the Mouse X Chromosome. Science 322, 750–756. doi:10.1126/science.1163045